5

EVALUATION OF THE SAG PROPERTIES IN A DUAL STABILIZED FERRITIC STAINLESS STEEL

By

Bruce Walter Muller

A thesis submitted to the Faculty of Engineering, University of Cape Town, in fulfilment of the degree of Master of Science in Applied Science.

CENTRE FOR MATERIALS ENGINEERING
DEPARTMENT OF MECHANICAL ENGINEERING
UNIVERSITY OF CAPE TOWN

SEPTEMBER 2002

SYNOPSIS

The dual stabilised type 441 (DIN 1.4509) ferritic stainless steel is primarily used in the automotive industry for catalytic converters. The steel, in addition to oxidation and corrosion resistance, is required to have a certain degree of creep resistance in the operating environment. The customer, by means of a modified creep test known as the sag test, usually specifies this requirement. This requirement is attained in most cases; however, in certain instances the customer places a severe requirement on the material, which exceeds the normal capabilities of type 441 material for sag resistance. There appears to be a lack of understanding of the mechanisms that facilitate creep (sag) resistance and how these can be applied to the steel.

The stabilisation of stainless steels with titanium and niobium is primarily to inhibit sensitisation after welding. In certain ferritic grades the niobium is added in excess in order to improve the creep resistance of the material. The literature has shown that a certain degree of over stabilisation is required to improve the creep resistance of the material (greater than 0.3 per cent niobium). In addition, the niobium needs to be in solution to obtain the maximum benefit for sag (creep) resistance. The thermo-mechanical processing of the material thus becomes critical in optimising the amount of niobium in solution.

This work indicates that a longer annealing time improves the sag resistance of the cold rolled material. The combination of longer higher temperatures on the hot band and on the final anneals appears to be beneficial to the sag resistance of the material. This translates directly into a grain size and niobium in solution relationship with the sag resistance of the material. This relationship with grain size on the final cold rolled material has been proven via experimental and plant results. Detailed statistical analysis has indicated that the sag resistance is conclusively related to the final grain size in the material on final annealing.

It was found that with production material the effect of grain size is only significant up to a grain size ASTM number of approximately 6.5 (mean linear intercept length of 0.034mm). The contribution to the sag value from a modelling perspective flattens

out at a coarser grain size (smaller ASTM number). This, therefore, appears to be a critical grain size should the present processing parameters be adhered to in order to obtain a significant increase in sag resistance.

Experimental work on final cold rolled material has shown that there appears to be a change in the "bulk" activation energy (recovery, recrystallization and grain growth) from below approximately 1000°C to that above this temperature. The values were 1114 kJ/mol and 113 kJ/mol respectively for below and above 1000 °C. The "bulk" activation energy was determined as material is generally annealed in production plants from cold rolled material to obtain a final grain size. The annealing speed would thus be significantly slower at temperatures below 1000°C if a specific grain size is required than it would be above 1000°C.

The sag resistance of type 441 material does not appear to be significantly increased by ageing heat treatments on final annealed material.

The sag resistance of the material can be significantly increased with a hot band anneal temperature of 1150°C and above. It appears that this is due; to a greater degree of solid solution strengthening by the niobium. The elongation of the material, however, annealed at these higher temperatures, is negatively affected. The optimum results as far as sag and elongation properties is concerned is to anneal the hot band between 1000°C and 1100°C followed by a similar heat treatment at 1050 °C on the cold band material to obtain an ASTM grain size of approximately 6.5 or less.

The as-cast material had a similar increase in the sag resistance at temperatures below and above the reheat temperature of approximately 1100°C. It would appear at this stage from a processing perspective that the material should be reheated at a temperature of approximately 1150°C. The temperature should be sufficient to cause the maximum amount of niobium to go in to solution. This temperature is also not significantly higher than the present practice of reheating at approximately 1100 °C. The formation of laves phase should thus be avoided by the fast laminar cooling after hot rolling to below approximately 600°C. The processing parameters would, however, need some modification to take account of the higher mass percent niobium in solution. The sag values should not, however, be significantly altered by the

slightly larger grain size, but could be improved upon (by assuming that the same model would apply to final annealed material with a higher niobium content) should the grain size be limited to a maximum ASTM number of 6.5. The longer anneal on the final material may be critical to ensure that maximum dissolution of the niobium has occurred both from an elongation and sag resistance perspective.

The optimum processing parameters for maximum sag resistance, with some consideration of the final elongation, could thus be determined.

DECLARATION

I, Bruce Muller, hereby declare that the work in this thesis project is essentially my own work and that no part of it has been submitted for a degree at any other university.

I further declare that this work is presented with full integrity with regard to the presentation of its results and that values obtained have not been altered in any way.

Signed ..Signed by candidate

Date.....22/09/2002.....

ACKNOWLEDGMENTS

I would like to express my appreciation to all the people who have assisted me during the course of these studies. I am particularly grateful to:

Professor Rob Knutsen for all the assistance during the three years of study and for affording me the opportunity to study further within this field.

Lucien Matthews for the discussions during the period of study and Columbus Stainless for the use of various resources and for sponsoring my studies for the first two years.

Dave Smith for the hours of proof reading this document, your command of the English language coupled with a vast knowledge of metallurgy has made your inputs invaluable.

Mr. Allan Meyer for his time and invaluable corrections during the final compilation of the thesis.

My friends and colleagues for all their support in assisting me in completing the task at hand.

To my mom and sister for their unwavering words of encouragement and support.

To my wife Sharon and sons Aidan and Kieran, for their love, patience and understanding when the midnight oil was being burnt.

Dedicated to Allan

Frater vale

24th July 1957- 20th July 2000
Scientia longa, vita brevis

CONTENTS

CHAPTER 1 INTRODUCTION

1.1 Project background 1

1.2 Ferritic strategy and the automotive industry 2

1.3 Aims of Project 2

CHAPTER 2 LITERATURE REVIEW

2.1 Short history of stainless steel development 4

2.2 Stainless steels types and general characteristics 5

2.2.1 Creep in austenitic stainless steels 8

2.2.2 Creep in martensitic stainless steels 10

2.2.3 Creep in precipitation hardened steels 11

2.3 Ferritic stainless steels 12

2.4 Stabilisation in ferritic stainless steels 14

2.4.1 Production considerations 15

2.4.2 Weldability 18

2.4.3 High temperature strength and creep resistance 18

2.4.4 Oxidation and corrosion resistance 23

2.4.5 Laves phase 26

2.4.6 Ridging 27

2.4.7 Niobium and titanium stabilised ferritic steels used in the automotive industry 28

2.4.8 Conclusion of literature search 28

CHAPTER 3 EXPERIMENTAL PROCEEDURE 30

3.1 Metallographic procedure 32

3.1.1 Statistical analysis of grain size measurement 33

3.1.2 Statistical analysis of second phase fraction 36

3.2 Sag test –alternative creep test 37

3.2.1 Effect of gauge on sag 40

3.2.2 Effect of grain size on the sag test 41

3.2.3 Effect of chemistry on the sag test 42

3.2.3 Verification of sag test 42
3.3 Deep etching SEM and EDS analysis 45
3.4 Statistical methods 46
3.5 Heat treatment, hot and cold rolling 46

CHAPTER 4 ANALYSIS OF PRODUCTION MATERIAL

4.1 Statistical analysis of production material 49
4.1.1 Determination of niobium in solution 50
4.1.2 Correlation analysis 53
4.2 Precipitate morphology and composition at the various production stages 58
4.2.1 Tundish sample 59
4.2.2 As-cast sample 60
4.2.3 Transfer bar sample 63
4.2.4 Hot band sample 63
4.2.5 Hot rolled and annealed sample 67
4.2.6 Cold rolled material 67

CHAPTER 5 EXPERIMENTAL RESULTS

5.1 Experimental heat treatment of cold band material 70
5.1.1 Effect of annealing temperature on the percent precipitates present 70
5.1.2 Grain growthin cold rolled material 72
5.1.3 Sag resistance of material after various experimental heat treatments on cold rolled material 76
5.1.4 Statistical analysis of experimentally annealed cold band material 77
5.1.5 Secondary ageing treatments applied to cold rolled material 78
5.1.6 Dissolution of precipitates after sag test 81
5.2 Experimental heat treatment of hot band material 83
5.2.1 Effect of annealing temperature on the second phase area fraction and grain size after hot rolling 83

5.2.2 Sag resistance of material after various experimental heat treatments on hot rolled material 85
5.2.3 Effect of various hot band annealing temperatures on the final mechanical properties 86
5.3 Experimental heat treatment of as-cast material 87
5.3.1 Analysis of the area fraction after various reheat treatments 88
5.3.2 Morphological examination of precipitates 88
5.3.3 Sag resistance of as-cast annealed material after final cold rolling and annealing 92
5.3.4 Effect of various as-cast reheat temperatures on the final mechanical properties 92

CHAPTER 6 DISCUSSION 94
6.1 Statistical analysis of plant material 95
6.2 Morphological development of precipitates during production 96
6.3 Experimental heat treatments 97
6.3.1 Cold band material 97
6.3.2 Hot band material 99
6.3.3 As cast material 102

CHAPTER 7 CONCLUSIONS 104

BIBLIOGRAPHY 107

APPENDIX 1 113

APPENDIX 2 125

APPENDIX 3 127

APPENDIX 4 129

APPENDIX 5 131

Chapter 1 Introduction

1.1 Project background

Columbus stainless is the only primary manufacturer of flat cast and wrought stainless steel products in Southern Africa. The plant produces approximately 430000 tons of stainless steel per annum. The local market consumes approximately 100000 tons per annum with the remainder being exported. It is strategically important that Columbus grows the local market. One of the growth sectors is the automotive component industry and more particularly the catalytic converter industry. The primary steel used in this application is type 441, which is equivalent to the DIN 1.4509 and Euronorm specification X2 CrTiNb18 contained in the British standard BS EN 10088-2: 1995.

Type 441 is a dual stabilized (titanium and niobium) ferritic stainless steel with approximately 17% chromium. The dual stabilization imparts beneficial corrosion, oxidation, elevated temperature and thermo-mechanical processing improvements to the standard 17% chromium steel. Of particular interest as far as a customer requirement is concerned is the creep or sag resistance of the material during operation at temperatures in excess of 800°C. It was identified, as is the case with many of the inherent properties of ferritic stainless steels, that the thermo-mechanical history of the material may play a role in determining the degree of sag resistance that the material is capable of.

The thermo-mechanical history would affect the morphology and distribution of precipitates and thus impact on the sag (creep) resistance of the material. This would be directly influenced by the distribution of the niobium prior to creep. It was further identified that solid solution strengthening from the niobium may also play a role. Research was thus undertaken to identify the role that the thermo-mechanical history plays in determining the degree of sag resistance of the material.

1.2 Ferritic strategy and the automotive industry

The development of ferritic stainless steels is of strategic importance to most stainless steel producers as approximately 40 per cent of the operating cost to produce austenitic stainless steels can be attributed to the nickel content in the stainless steels produced. The ferritics are thus seen as a low cost alternative to austenitic stainless steels from a customer and particularly a manufacturers perspective. The early 1930's saw the first commercial use of stainless steel in an automotive application, as the radiator of a Rolls-Royce [1] motor vehicle. The first exhaust application was of a Type 409 (Allegheny type MF - 1) used in 1960 for the mufflers in the Thunderbird exhaust system [2].

The automotive component industry is one of the major growth areas in the local South African market. The general properties of stainless steels; recyclability, relative weight to strength ratio and high temperature properties make them ideally suited to certain applications in the automotive industry, notably the exhaust and structural applications.

1.3 Project aim

The primary focus of the research was to improve the sag resistance of type 441 material via improvements to the thermo-mechanical processing route to which the material is subjected. Type 441 ferritic stainless steel is produced via a conventional continuous casting, hot rolling and final cold rolling process. Several heat treatment stages are integrated into the process to ensure appropriate microstructure and property evolution. This rather broad aim can be subcategorized as follows:

- An analysis to identify any trends from historical processing data as related to the sag resistance of the material.
- Investigate the morphology of the precipitates after each thermal cycle in the processing of the material.
- To quantitatively determine the minimum and rate of precipitate dissolution at critical thermal cycles in the processing route.

- To determine the effect of various times and temperatures at final annealing on the sag resistance of the material
- To determine the effect of various times and temperatures at hot band annealing on the sag resistance of the material.
- To determine the effect of various temperatures at slab reheating on the sag resistance of the material.
- Determine if there is a processing route that gives the optimum sag resistance.

Chapter 2 Literature review

2.1 Short history of stainless steel development

This short history focuses mainly on the commercial development of stainless steel. Monnartz in Germany discovered and thoroughly investigated the improvement in corrosion imparted to a steel with more than 10% chromium [1,3,4]. This laid the foundation for the commercial exploitation of stainless steel by Harry Brearley who produced the first commercial ingots (50 cwt) on the 20th of August 1913[1] in Sheffield, England. The steel contained 0.24%C, 0.2%Si, 0.44%Mn and 12.86%Cr. The first commercial application was for gun barrels, which was not very successful. Material from the same heat was subsequently used to make cutlery blades. The Krupp Research Department in Germany patented the first austenitic stainless steel containing about 20% chromium and 7% nickel in 1912. Maurer and Strauss from Krupp developed these steels in the period from 1909 to 1914[4]. This austenitic grade expedited the large-scale production of flat rolled products originating from mills for further fabrication. The first commercial use of this steel occurred in about 1914. Dantsizen and Becket were responsible for the development of the ferritic stainless steels and their commercial use [4]. The commercial production of stainless steel in the United States of America occurred in the 1920's[5]. In March 1925 William Hatfield presented data on the new "Firth Staybrite" steel; this was the now well known 18-8 steel. In the 1920's originally tungsten, then tungsten and titanium, and finally only titanium were added to the 18-8 steel to prevent inter-granular corrosion. This steel was eventually known as type 321. Krupp patented a steel for higher oxidation resistance in 1927[3]. This steel contained 25% chromium and 20% nickel and this steel eventually became known as Type 310. The main three groups of stainless steel, namely austenitic, ferritic and martensitic were established within 20 years of Brearley's first commercial heat. Duplex stainless steels were already produced in the 1930's at Avesta Ironworks [6]. The precipitation hardenable steels were produced in 1945 by U.S. Steel [5]. In 1950 the nickel shortage caused many manufactures to look for substitutes. Manganese, copper and nitrogen were evaluated as suitable and the 200 series of stainless steels were designed. Duplex stainless steels (only appear in production figures from 1987[4]) and high nitrogen stainless steels (Cromanite, first

produced by continuous casting in South Africa in November, 1994[7]) are the latest viable production additions to stainless steels, although these steels were produced in small batches and on an experimental base much earlier. Fifty three years passed after the first commercial heat by Brearley before a commercial stainless steel production heat was made in South Africa on the 28th of October 1966[8] in Middelburg, Transvaal (Mpumalanga).

2.2 Stainless steels types and general characteristics

Stainless steels have been defined as any steel containing at least 12% chromium to impart a certain degree of corrosion and oxidation resistance to the environment by the development of a passive film on the surface of the material. Stainless steels generally do not contain more than 30 per cent chromium. The iron-chromium phase diagram [9] shows that the steels in the composition range 12-30 percent chromium can exist in predominantly two phases: ferritic (α) and austenitic (γ) (figure 2.1). The addition of austenite stabilisers (nickel, carbon, nitrogen, copper and manganese) increases the size of the gamma loop. This ensures that austenite, after solution annealing at approximately 1100°C, is generally stable at room temperature.

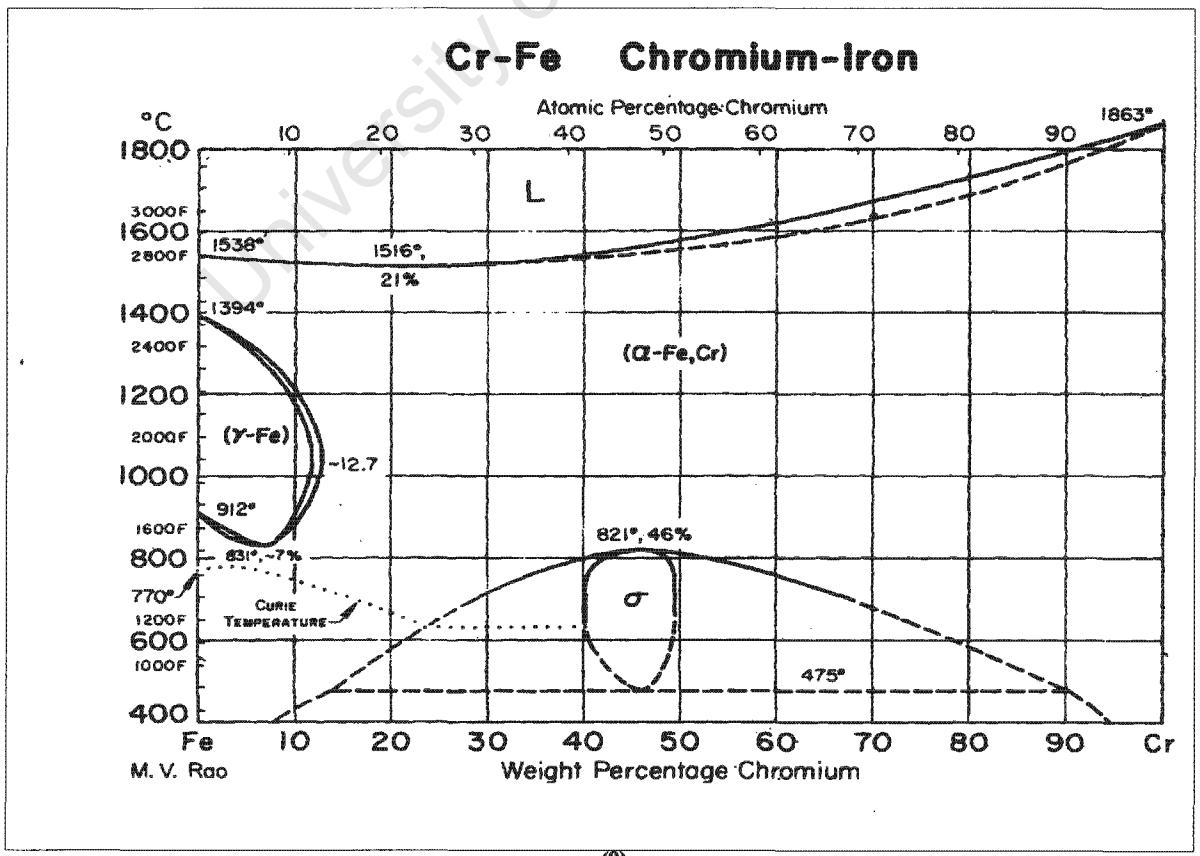

Figure 2.1: Iron chromium phase diagram [9].

Martensitic stainless steels are formed in a similar manner; however, the material contains insufficient austenite stabilising elements. In this case the material has a martensite start and martensite finish transformation temperature, in which the austenite present on quenching or rapid cooling from within the γ loop transforms to martensite. The major groups of stainless steels generally consist of ferrite, austenite, martensite or a combination of the above. Each of these phases has a unique crystallographic structure (Table 2.1) which imparts certain basic metallurgical characteristics. The most obvious is the mechanical properties and it can be seen that the austenitic structure imparts excellent mechanical properties to the material. (Table 2.2).

Table 2.1

General crystal lattice parameters for some of the more common phases found in stainless steels [10].

Phase	Lattice	n= number of atoms per unit lattice cell	N_c = Co-ordination Number – max no of atoms in contact with one atom	r= Atomic radius	d= Density
Ferrite (α)	BCC	2	8	$a\sqrt{3}/4$	$2.A/(a^3_{b.c.c}N_a)$
Austenite (γ)	FCC	4	12	$a\sqrt{2}/4$	$4.A/(a^3_{f.c.c}N_a)$
Martensite (γ')	CPH	6	12 or 6	a/2	$6.A/(3/2c_h\, a^2_h \sqrt{3}\, N_a)$

*BCC= Body Centered Cubic, FCC= Face Centered Cubic, CPH= Close Packed Hexagonal

Stainless steels can be categorised into the three original major groups [5]:

- Martensitic
- Austenitic
- Ferritic

A number of further classifications of stainless steels have been developed and can be classified as [3]:

- Super ferritic
- High strength austenitic stainless steels
- Duplex
- Precipitation hardenable

The general metallurgical aspects of each of these groups will be briefly discussed with some focus on the effect of niobium and the creep resistance of that group.

Table 2.2

Typical mechanical properties for each group of stainless steels.

Type	Mechanical properties		
	Yield strength (MPa)	Tensile strength (MPa)	Total elongation 50mm (%)
Ferritic			
409	255	440	32
430	343	511	27
441	316	486	28
Austenitic			
304	308	642	52
316	351	641	48
321	249	611	54
Martensitic (tempered at 700)			
410	525	725	26
420	550	750	21
431	600	850	25
Precipitation hardening			
17-4PH annealed	758	1034	10
17-4PH Precipitation Hardened	1227	1379	12
15- 5 Annealed	586	862	10
15-5 Precipitation Hardened	1275	1379	14
Super ferritic			
E-Brite	345	480	30
29-4-2	515	655	25
Duplex			
SAF2205	430	790	25
7Mo	565	683	31
3RE60	450	800	30
Super austenitic (high nitrogen)			
Cromanite	592	885	40
Tenelon	480	860	40
Nitronic 32	380	690	30

2.2.1 Creep in austenitic stainless steels.

Nickel is the most important alloying addition in these stainless steels. Nickel expands the gamma (γ - austenite) loop in the iron-chromium phase diagram. This increases the amount of austenite present during solution treatment. In addition it also suppresses the M_s temperature to below room temperature in an 8% nickel alloy. The structure thus remains fully austenitic on cooling to room temperature.

2.2.1.2 Creep resistance

In austenitic stainless steels carbon, nitrogen, chromium, molybdenum, tungsten, vanadium, boron, titanium and niobium increase the creep resistance [10,13]. Austenitic steels have an inherently higher creep resistance than ferritic stainless steels (figure 2.4). The increase in creep resistance by the addition of molybdenum is due to solid solution strengthening. The interstitial elements, particularly boron and nitrogen, improve the creep strength at low temperatures (<700^{O}C). The carbide and nitride formers, particularly titanium, vanadium and niobium, strengthen the matrix when precipitated as fine particles in the matrix. The rate of secondary creep is dependent on the amount of precipitation during service to lock dislocations. If the precipitates are too stable they will not go into solution and secondary creep increases (figure 2.2). Alternatively if the affinity to form nitrides or carbides is too weak, insufficient precipitation could occur with no benefits [10].

It was found that for niobium alloyed steels the maximum amount of carbide precipitation occurs at the stiochiometric level. At small deviations from the stiochiometric value (Nb:C=10.32:1 for Nb_4C_3), for both NbC and Nb_4C_3, there is rapid reduction in the amount of niobium carbide available for precipitation [18]. This reduction is greater for an excess of niobium than for carbon. The niobium carbide reportedly precipitates at the grain boundaries restricting slip, which reduces cavitation (creep damage – lowest at stiochiometric value) and improves creep resistance.

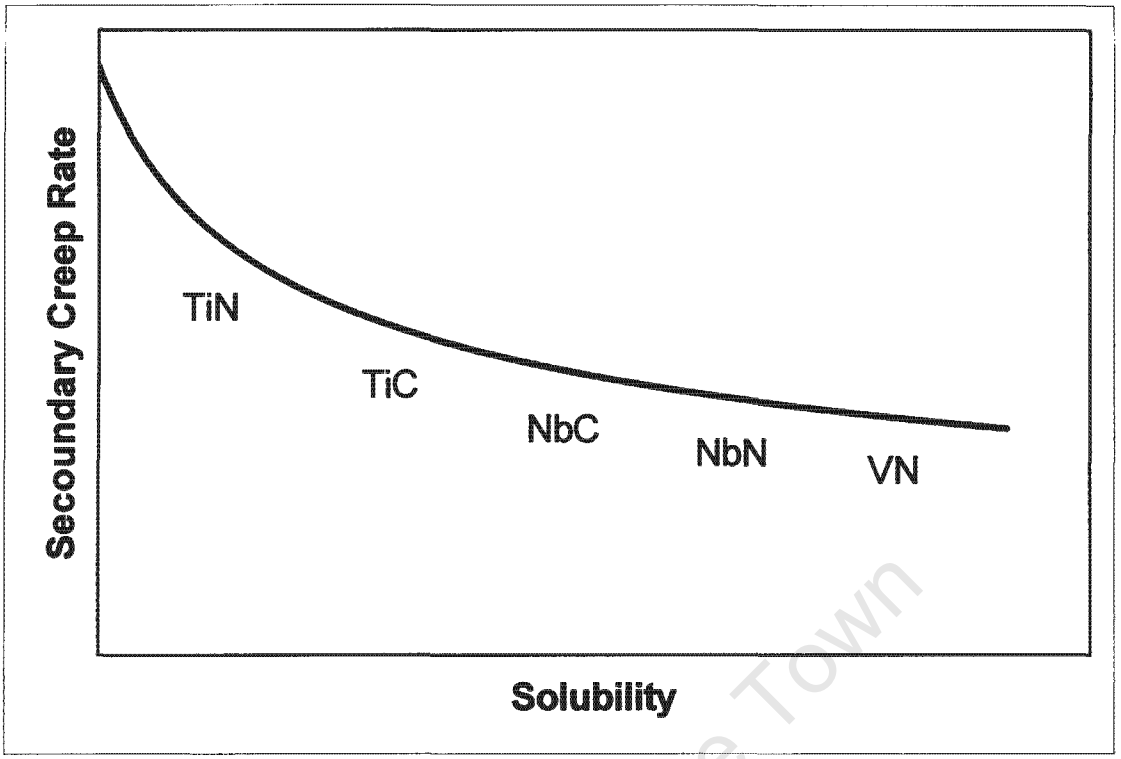

Figure 2.2: Variation in secondary creep at 650°C after a solution anneal at 1050°C for various carbides and nitrides in an austenitic stainless steel [10].

Earlier researches have shown that the grain size does not have a significant effect on the creep resistance of the material [19] and it was shown that solid solution hardening or the subsequent precipitation (high degrees of solid solution hardening) has a far greater effect. It was argued that in a niobium stabilised austenitic (Type 347) stainless steel the niobium going into solution plays a major part in improving the creep resistance of the material (figure 2.3). It was further indicated that the increase in creep resistance was mainly confined to primary creep (see section 4.2) rather than secondary creep.

It has, also been shown that "normal" residual elements such as phosphorus are important in increasing the creep resistance of the steel. Phosphorus reportedly decreases the stacking fault energy of the steel and in turn decreases the creep rate [15].

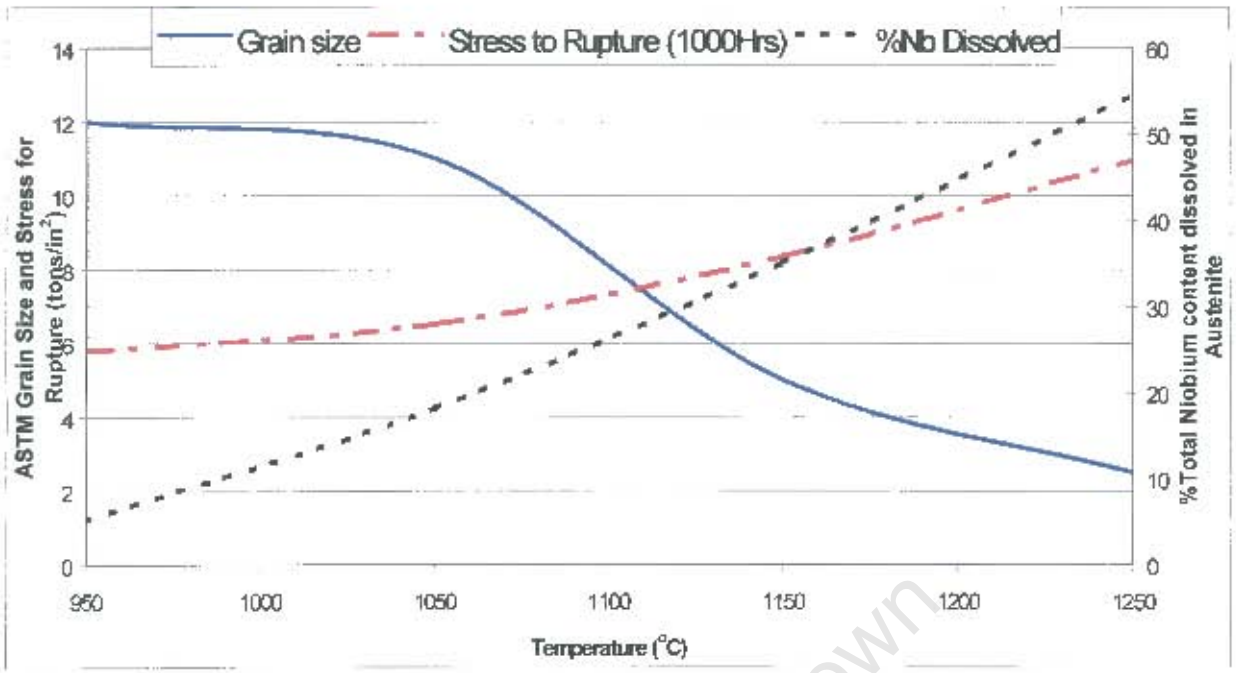

Figure 2.3: Effect of solution temperature on solubility of niobium, grain size and rupture strength of a 18%Cr-12%Ni-1%Nb steel [19].

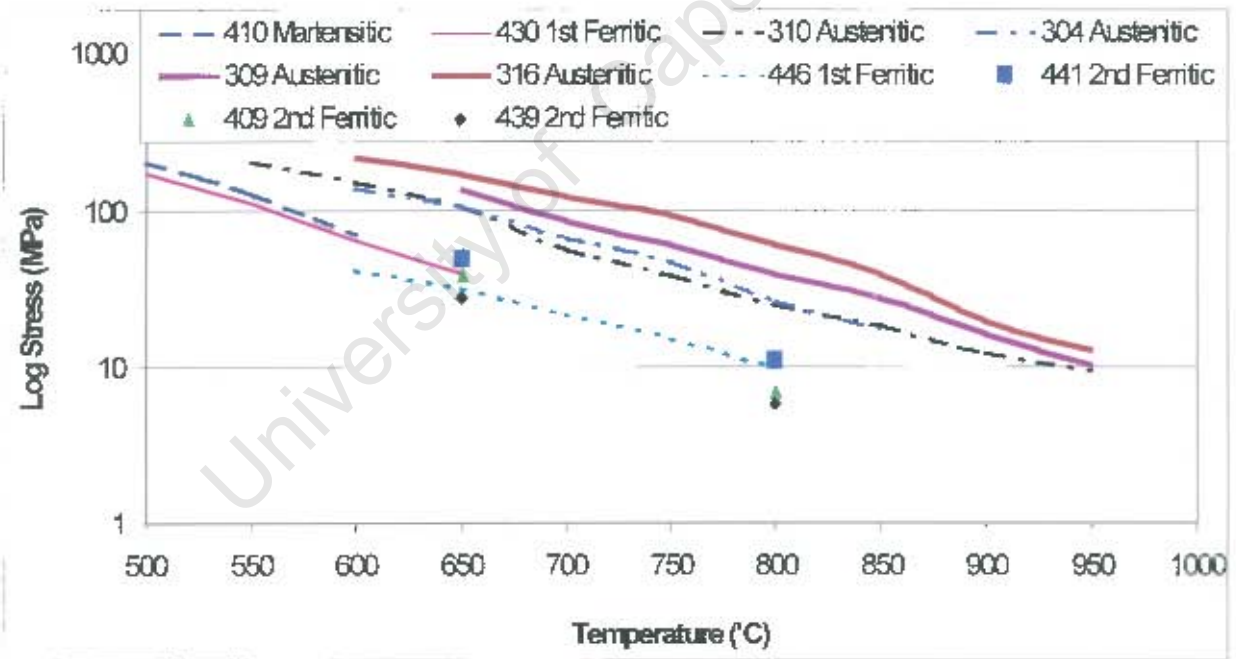

Figure 2.4: Stress rupture data (1000 hrs) of various stainless steels [4, 16]

2.2.2 Creep in martensitic stainless steels

These alloys have sufficient carbon in solution to make them fully austenitic at annealing temperatures. On cooling they pass through the M_s temperature that is above room temperature to produce a martensitic structure. The chemical composition

of these steels is generally between 12-17% chromium, 0-4% nickel and 0.1-1.0% carbon with additions of molybdenum, vanadium, niobium, aluminium, titanium and copper [3, 11]. The hardness in these steels is principally obtained from the carbon and the hardenability is influenced by all the alloying additions notably chromium [4]. These steels suffer from temper and hydrogen embrittlement.

The creep resistance in these steels is primarily attributed to the formation of plate like precipitates particularly in the vanadium alloyed steels. The ideal precipitate size to increase creep resistance has been calculated to be 8.5-15nm in diameter and 0.7-1.2nm in thickness. Laves phase precipitates during long service periods at high temperature, increasing the creep resistance further in that this more than compensates for the decrease in solid solution strengthening [21].

2.2.3 Creep in precipitation hardened steels.

In general terms the hardening of a material involves impeding the movement of dislocations [10]. In a solid solution the interstitial elements are normally the most effective in locking the dislocations. These form a stable atmosphere around the dislocation known as Lomer-Cottrell atmospheres. The dislocations need to be torn from these atmospheres and this causes the well-known phenomenon of Lüder Bands. Alternatively, precipitates can act as barriers to dislocation movement. In general terms three stages of precipitate development have been identified [10]:

- Pre-precipitation; formation of Guinier-Preston G.P. Zones

  These can only be detected by x-ray diffraction techniques. They represent the pre-alignment of clustered elements ready for precipitation.
- Formation of coherent precipitates

  At this stage the atomic groupings of atoms are visible under an electron microscope. The atoms and the lattice planes of these atoms remain coherent with the matrix material.
- Formation of incoherent precipitates.

  Precipitates form that are in equilibrium with the matrix, with a clearly defined chemical composition.

The first two stages above lead to the strongest strengthening since they act over a longer distance and are commonly known as "age hardening". When precipitates are present the dislocations overcome the barrier by means of the Orowan mechanism. The strengthening in this instance is localised at the precipitate.

There are generally three categories [4, 14] of precipitation hardened steels:

- Martensitic

  The martensite in these steels on cooling in air is weaker than conventional martensitic steels. The martensite is then aged to strengthen the material.
- Austenitic

  The strength due to precipitation is not significantly increased in these steels.
- Semi-austenitic

  Martensite is formed in these steels by cold working or subzero cooling. The steel is conditioned at about 750^{O}C to form chromium carbides. The material forms martensite on subsequent cooling and is then aged as in the martensitic precipitation hardened steels.

Precipitation hardened steels appear to be extensively used for creep resistant applications up to approximately 600^{o}C[13]. The effect of niobium in these steels appears to be mainly beneficial as a grain growth inhibitor and facilitating the maximum amount of nitrogen being present to combine with other elements such as vanadium [17]. It was also found that when the steel was alloyed close to the stiochiometric ratio (VN) the steel had the highest creep resistance. This effect was reported in the austenitic steels above.

2.3 Ferritic stainless steels

The pure iron-chromium phase diagram (figure 2.1) indicates that a steel with 12 to 13 percent chromium does not pass through the γ (gamma –austenite) loop on the left. This is not true of most ferritic stainless steels as they contain some residual austenitising elements notably carbon and nitrogen that increases the γ loop substantially. The common AISI type 430 stainless steel with 17 percent chromium

content will form martensite on quenching from the γ region. The dual stabilised (titanium and niobium) 441 material with approximately 18 percent chromium does not go through the γ phase. This is due to the titanium and niobium taking carbon and nitrogen out of solution and thus decreasing the size of the γ loop. Ferritic stainless steels range in composition from about 17 to 26 percent and contain no nickel.

Mechanical and formability properties.

The mechanical properties when compared to the other grades of stainless steel are (Table 2.2) generally acceptable with lower elongation than the austenitics but significantly higher than the precipitation hardened steels and the martensitic steels. These materials tend to have the lowest tensile strength of all the stainless steels. In addition they exhibit impact transition strength at a given temperature known as a ductile to brittle transition temperature (DBTT). The DBTT is primarily dependent on grain size in these steels, decreasing as the grain size number increases [12] (figure 2.5). The gauge of the material also plays a significant role and the DBTT increases as the gauge of the material increases. This is due to the fact that the stresses change from biaxial in thin gauge to triaxial in thicker gauges [2. 3].

A measure of the stretchability of a steel is determined by obtaining the gradient of the log stress versus log strain after the onset of plastic deformation and prior to necking. This value is known as the plastic strain ratio and is denoted by the letter n. The n-value appears to be adversely affected by most interstitial or substitutional elements in a steel [20]. It has been shown that for titanium stabilised 13 percent chromium ferritic stainless steel the n- value can be determined mathematically:

$$n = 0.327 - (0.015*Si + 0.003*Mn + 0.560*P + 0.004*Cr + 0.050*Al + 0.069*[Ti] + 0.094*[C+N]^{1/2})$$

Where; $[Ti] = 0$ and $[C+N] = [C+N] - Ti/10$, for $Ti/(C+N)<10$

$[Ti] = Ti - 10*(C+N)$ and $(C+N)=0$, for $Ti/(C+N)\geq 10$

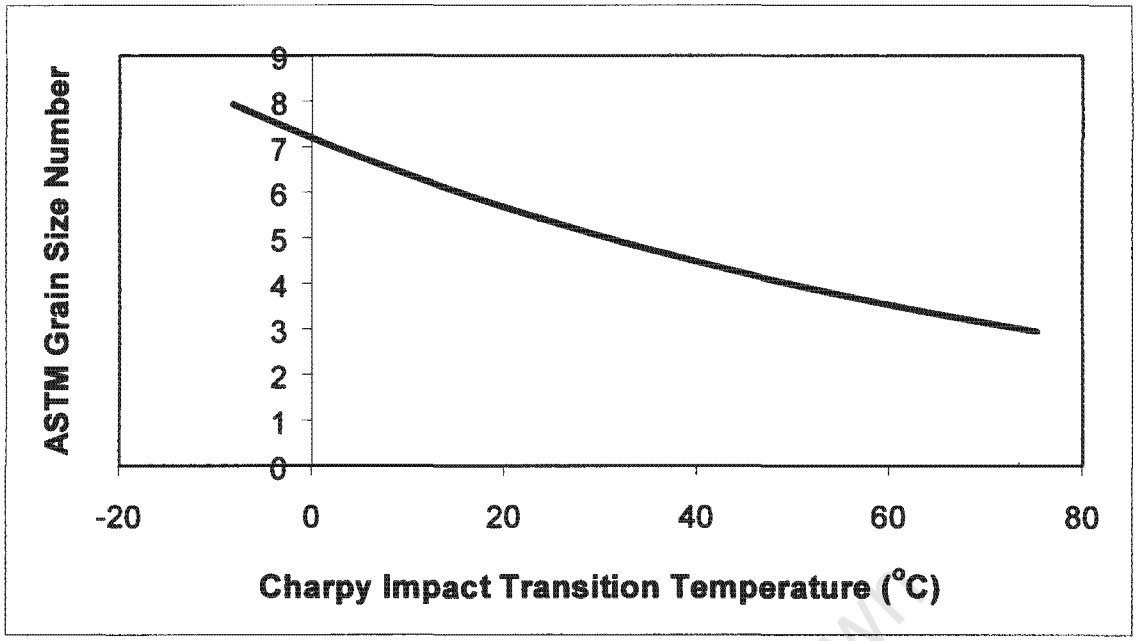

Figure 2.5: Decrease in DBTT with increasing grain size [12]

Creep resistance

Ferritic steels generally have higher stacking fault energy than austenitic stainless steels. This causes the ferritics to have a higher secondary creep rate and accounts for the fact the ferritics have lower stress rupture strength (figure 2.4) than the austenitic.

Super ferritics

These steels can be seen as a sub category of ferritics, however, these steels are guaranteed to be ferritic at all temperatures due to their high chromium content [4]. Their interstitial contents (carbon and nitrogen) are normally below 0.02 weight percent for increased corrosion resistance [3]. These steels are also termed the third generation ferritics [4].

2.4 Stabilisation in ferritic stainless steels

The literature search will be focused to gain some insight as to the impact that stabilisation and more specifically niobium has on the metallurgical properties of ferritic stainless steels. The focus will be on the high temperature properties and in particularly the creep (sag resistance) of the material. Ferritic stainless steels are

stabilised with niobium to improve their high temperature strength for use in automotive exhaust systems. The exhaust gasses should be above 700°C for the optimal performance of the catalytic converter. The temperature to which the material is usually exposed can be in excess of 950°C. The material should thus exhibit excellent high temperature properties (creep, thermal fatigue and oxidation resistance). In addition the material should also be resistant to high temperature corrosion in chloride solutions (salt used for ice melting on roads in colder climates).

2.4.1 Production Considerations

2.4.1.1 Steel plant practice

The solubility of titanium nitrides in a liquid ferritic stainless steel increases as the chromium increases and as the nitrogen level decreases for any given titanium level (figure 2.6)[22]. Thermo-calc (computer software package that uses a data base containing thermodynamic data to predict the stable phases present in a multi-component system) has been used to calculate the phases present at equilibrium on cooling of a 14%Cr, 1%Si, 0.4%Cu, 0.15%Ti, 0.38%Nb steel [23]. Primary ferrite solidifies first followed by the precipitation of carbo-nitrides at about 1500°C. The laves phase starts to precipitate out at about 700°C (figure 2.7).

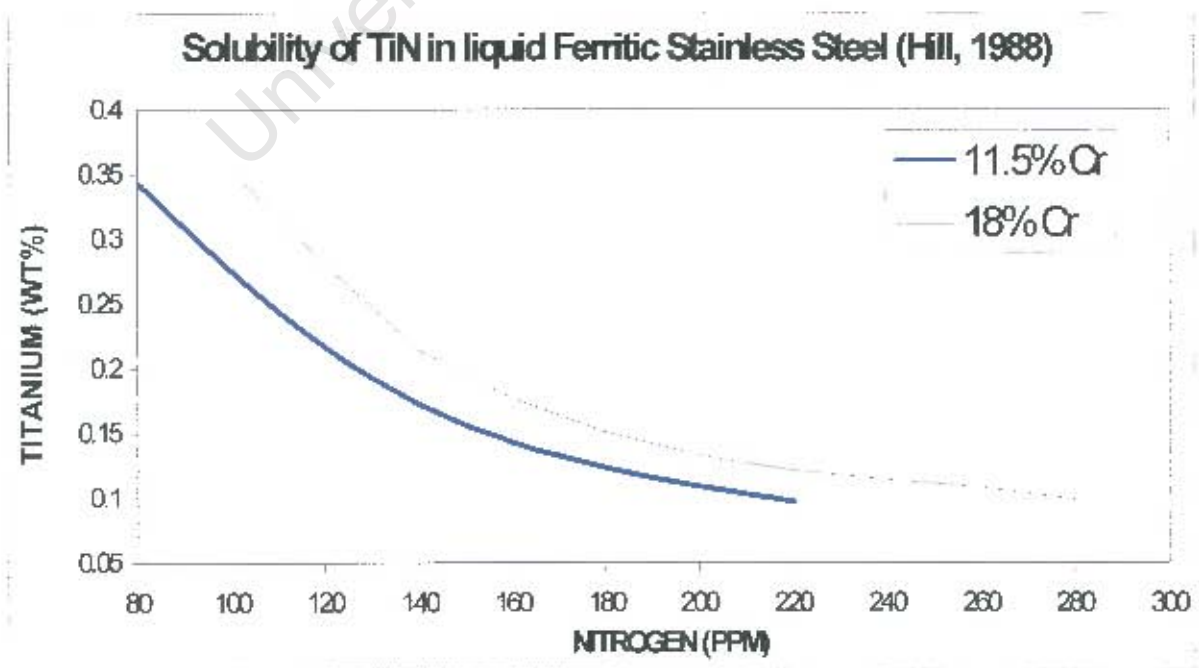

Figure 2.6: Solubility of TiN in liquid ferritic stainless steel (Hill, 1988)

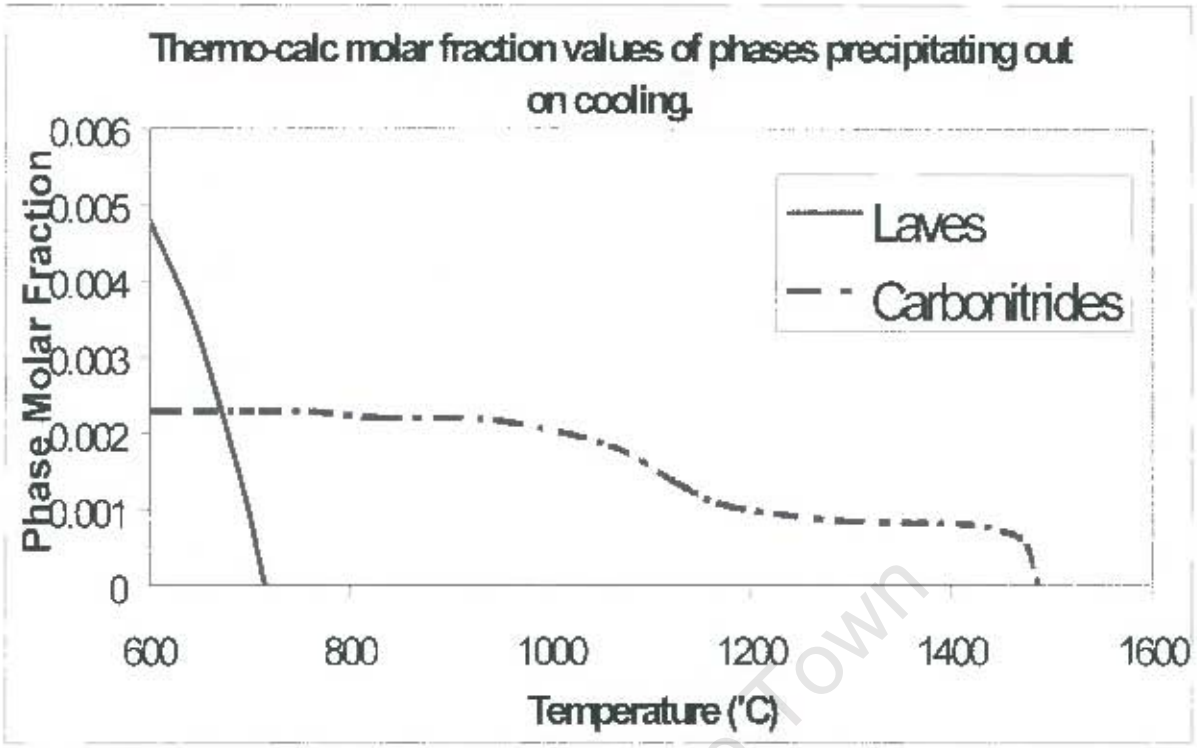

Figure 2.7: Equilibrium molar fraction of phases represented at various temperatures on cooling of a 14%Cr, 1%Si, 0.4%Cu, 0.15%Ti, 0.38%Nb alloy.

2.4.1.2 Hot and cold mill processing – effect on surface quality and formability.

Generally no indication of the solution temperature prior to hot rolling is given, it was, however noted that for 14% Cr-0.3Nb-0.1Ti-0.5Mo steel [24] the reheat temperature was quoted as 1250°C. This is rather high and experience with a walking beam furnace is that the slabs tend to bow between the beams making them impossible to hot roll. In addition, the high drop out temperature causes the material to finish at too high a temperature and can cause embrittlement problems due to either the precipitation of the laves phase (due to slow cooling in the range [25] 700 – 900°C)) or the formation of excessive amount of nitrides [26]. The hot rolling practice thus needs to be optimised along with the quenching obtained via laminar cooling with water to avoid these precipitation phenomenon.

An accelerated degree of recrystallization is required to reduce the severity of ridging and roping in a niobium stabilised steel (17%Cr and 0.44% Nb)[27]. This is generally

achieved by finishing rather cold on the Steckel mill (less than 700°C) and using a high temperature anneal of the hot and cold band at approximately 950°C. Alternatively it has been suggested that finishing at 800°C is just as favourable [28], however, a minimum reduction of 30% is required followed by a similar anneal as above.

A 17%Cr – 0.44%Nb steel appears to exhibit a maximum rate of recrystallization at about 950°C for various reductions during hot rolling. The material reportedly has 70% recrystallization at 40% hot reduction at 950°C. The original as-cast structure appears under these conditions to have been replaced by a new recrystallised, homogeneous structure [28].

The plastic strain ratio (R-value), which is a measure of the deep drawability of steel, generally increases as the amount of cold reduction increases. The addition of niobium to 12% chromium steel in addition appears to increase the materials affinity to form a more favourable crystallographic texture and subsequently a higher R-value is obtained [29], (figure 2.8).

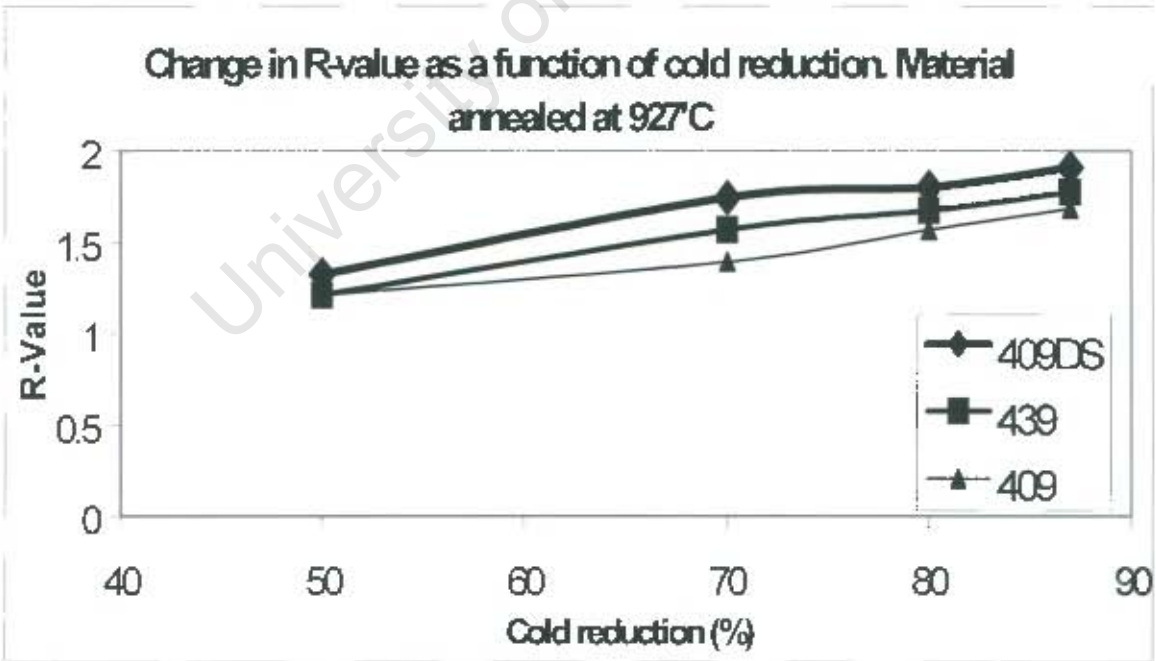

Figure 2.8: The influence of cold reduction on the R-value.

Various ideal annealing temperatures after cold rolling are discussed in the proceeding sections related to the precipitation of the laves phase and increasing the degree of creep resistance in the material.

2.4.2 Weldability

The principal effect that welding has on ferritic stainless steels is two fold:

- It decreases the impact strength and ductile to brittle transition temperature of the material due to grain growth and
- It sensitises the steel if it is not stabilised with titanium or niobium.

The first issue is discussed here while the latter is discussed in section 2.2.5.5 – Oxidation and corrosion resistance. It has been shown that the addition of niobium to titanium stabilised steel does not adversely affect the weldability of the steel [30]. The addition may in fact increase the toughness of the titanium stabilised steel [31]. In addition dual stabilisation was found to produce tough, clean weld lines after high frequency welding when compared to titanium stabilised steels [32]. A balance or ratio normally exists between the titanium and niobium (with the niobium being the greater i.e. Nb:Ti shown to be 2:1 for a 17 % chromium ferritic steel) for optimum toughness and ductility of weldments [33, 34]. Finally it has been shown that dual stabilised steels can be susceptible to intergranular hot cracking in the fusion and heat affected zones [35]. It has further been shown that in this respect niobium is in fact the more deleterious element and care should be taken to minimise this stabilising element [35].

2.4.3 High temperature strength and creep resistance

Creep in a material appears to be governed by three factors [36, 37, 19, 38] ((figure2.9); these are;

- Temperature
- Applied stress or strain
- Internal structure (grain size, dislocations, vacancies, precipitates and substitutional and interstitial elements to mention a few)

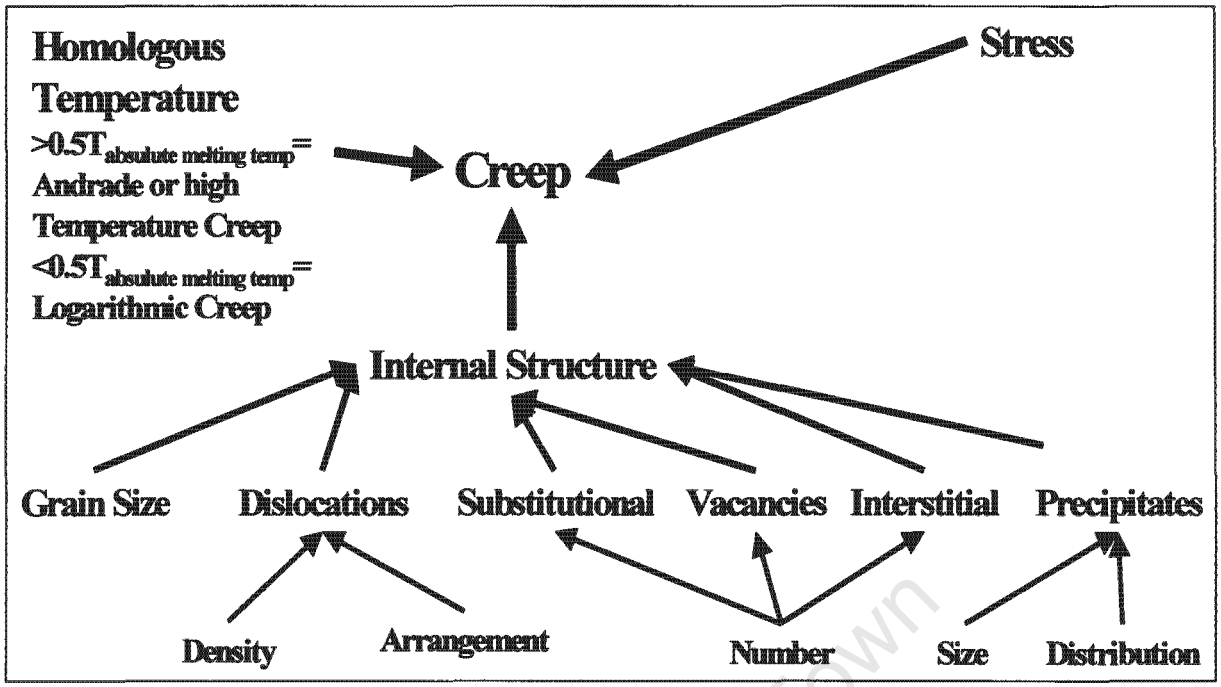

Figure 2.9: Factors influencing the rate of creep in a material.

The creep resistance of steel has been further categorised into two components [39] namely:

- Inherent creep resistance and
- Latent creep resistance.

The inherent creep resistance is dependent on the initial internal structure as mentioned above while the latent creep resistance is seen to depend on one or more precipitation processes [39].

The high temperature tensile strength was found to increase with the addition of an excess of niobium in ferritic stainless steels alloyed with Molybdenum [40]. The minimum excess niobium required for achieving a strengthening benefit, at 900 °C, was 0.2, as determined by the equation:

$Nb_{excess} = Nb - 8*(C+N) = 0.2$ minimum

Where:

Nb = Niobium in weight percentage

N = Nitrogen in weight percentage

C = Carbon in weight percentage

The strengthening or increase in proof stress depends on the heat treatment and the amount of niobium present in the steel [41] (figure 2.10). The amount of niobium in solution or solid solution strengthening is the primary source of the strengthening observed in these steels at high temperatures.

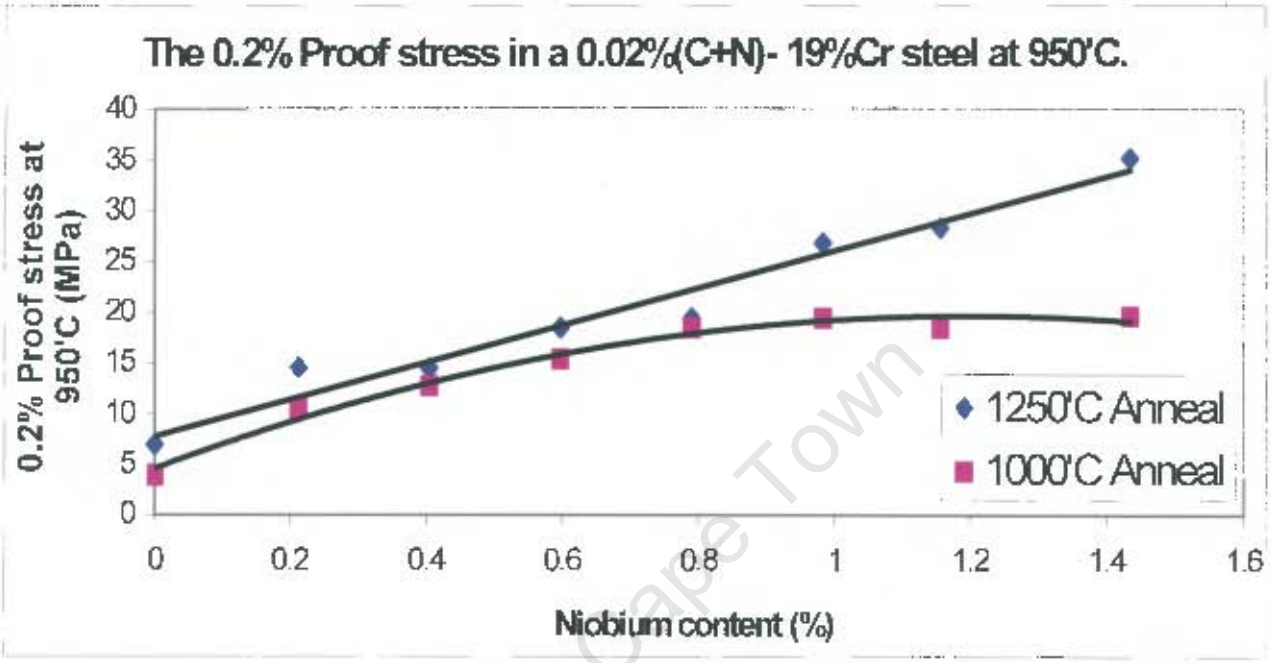

Figure 2.10: The increase in 0.2% proof stress in a 0.02%(C+N) – 19%Cr steel at 950°C as a function of niobium content and annealing temperature [41].

There appears to be an upper limit of niobium, beyond which the creep resistance of the material drops to the levels which were experienced prior to alloying (figure 2.11)[42]. The ideal range of niobium content, after stabilisation issues have been accounted for, appears to be approximately 0.6 to 1.00 per cent by weight (this ferritic stainless steel contained about 16%Cr and 0.3%Ti). The annealing temperature also appeared to affect the degree of creep particularly at the lower niobium contents, where the higher annealing temperature decreases the materials resistance to creep (sagging).

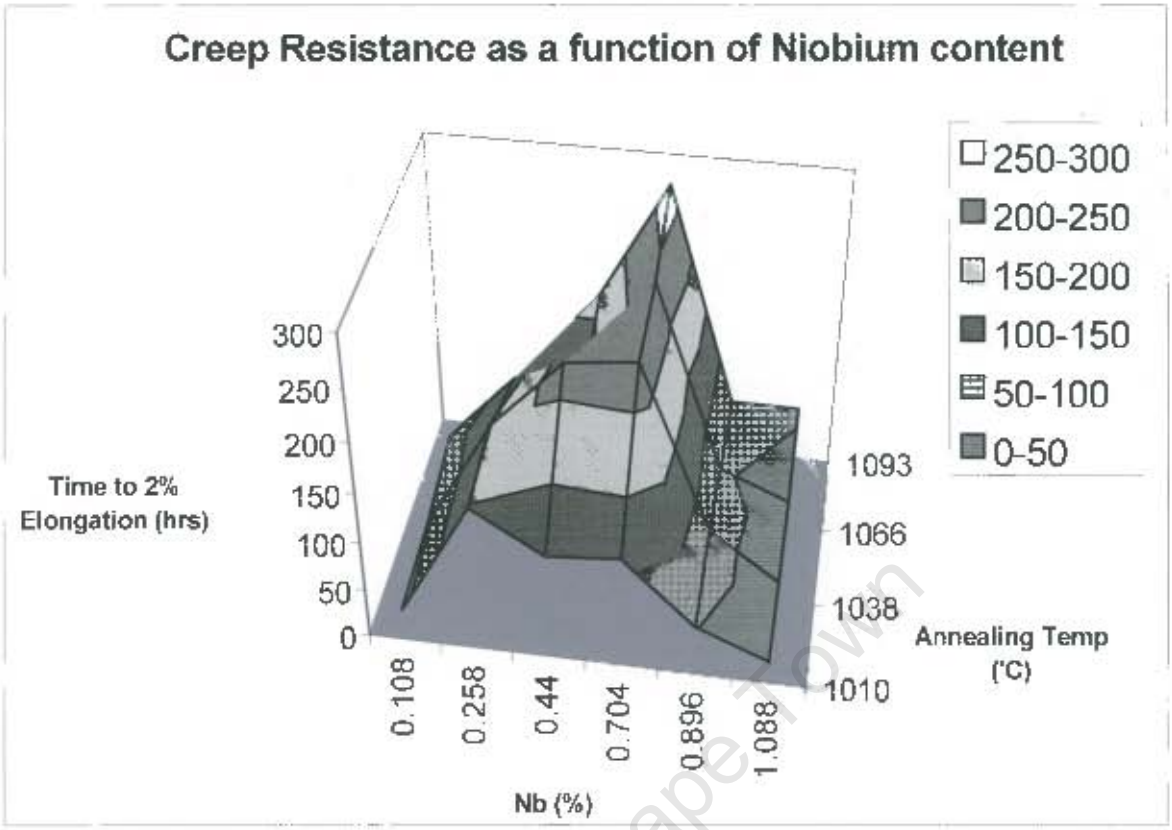

Figure 2.11: The creep life of a 16%Cr-0.3%Ti alloy at 871°C and an applied stress of 8.274MPa as a function of niobium content [42].

The amount of niobium in solid solution prior to testing the material appears to be the critical factor in determining the creep resistance of the material. In the range of 700°C to 1000°C the solid solubility of niobium in a 14%Cr, 0.15%Ti, 0.38%Nb appears to be approximately 0.34% by weight [23]. In addition the creep resistance was found to increase with the dissolution of intra-granular precipitates that could form in this steel on final processing. The steel should be annealed above 1040°C for complete dissolution of the precipitates [43].

2.4.3.1 Titanium and niobium carbides.

Titanium carbides (TiC) are a class one carbide (cubic type). Niobium carbides can exist as a class one (NbC) or a class two carbide (close-packed hexagonal Nb_2C)[44]. The cubic niobium carbide exists over a range of compositions from NbC to Nb_4C_3. The latter composition is due to the formation of a lattice defect in the carbide [44]. In addition there is also a high degree of solubility of nitrogen in both these types of

carbides. The carbides are generally not a pure binary system and some alloying of the surrounding matrix material occurs.

Generally steels which rely on carbides for their creep resistance have between 0.1 and 0.2 percent carbon. This is obviously not the case in the present steel, as this would adversely affect the already low mechanical properties, particularly elongation, of this material. These steels are also generally tempered to obtain the greatest benefit from carbide formation. There is normally a sequence (with time and dependent on chemistry) in which carbides would precipitate ($Fe_3C \rightarrow Mo_2C \rightarrow M_{23}C_6 \rightarrow M_aC_b \rightarrow M_6C$) and can be broadly described by use of the Hollomon-Jaffe tempering parameter (figure 2.12)[44]. These carbides either form by two methods:

- "In situ" when the existing carbide is transformed into another
- Nucleation and growth at new sites within the matrix material.

Cold deformation prior to the tempering treatment reportedly increases the rate of precipitation from the matrix that is supersaturated in the elements necessary for carbide formation. In supersaturated steels (martensitic) the precipitates form by a sequence of reactions involving:

1. The formation of zones rich in the elements to form the precipitates (embryonic phase).
2. The formation of an intermediate precipitate (M_3C)
3. The formation of the equilibrium precipitates ($M_{23}C_6$ and M_6C)

The transitions of the various reactions above from 1 to 2 and 2 to 3 generally occur at a reasonable rate at 0.4 to 0.5Tm and above 0.5 Tm respectively (Tm = absolute melting temperature). In low supersaturated solutions (non-martensitic) precipitate nucleation is difficult and only occurs at favourable sites such as dislocations. Deformation during precipitation increases the dislocation density producing a more uniform dispersion and finer precipitate[44].

Most creep resistant steels derive their superior creep properties from a fine dispersion of particles[44]. Inter-particle spacing is an important factor. These act as barriers to

dislocation movement. There is a critical spacing above which the creep resistance decreases [44]. The effect of particle shape is not known, however, it is generally perceived that this is overshadowed by the affects of size and spacing [44]. More stable carbides (cubic carbides -V_4C_3, NbC) are preferential, as these should theoretically not grow as rapidly, thus, maintaining a maximum dispersion of fine carbides the longest at elevated temperatures.

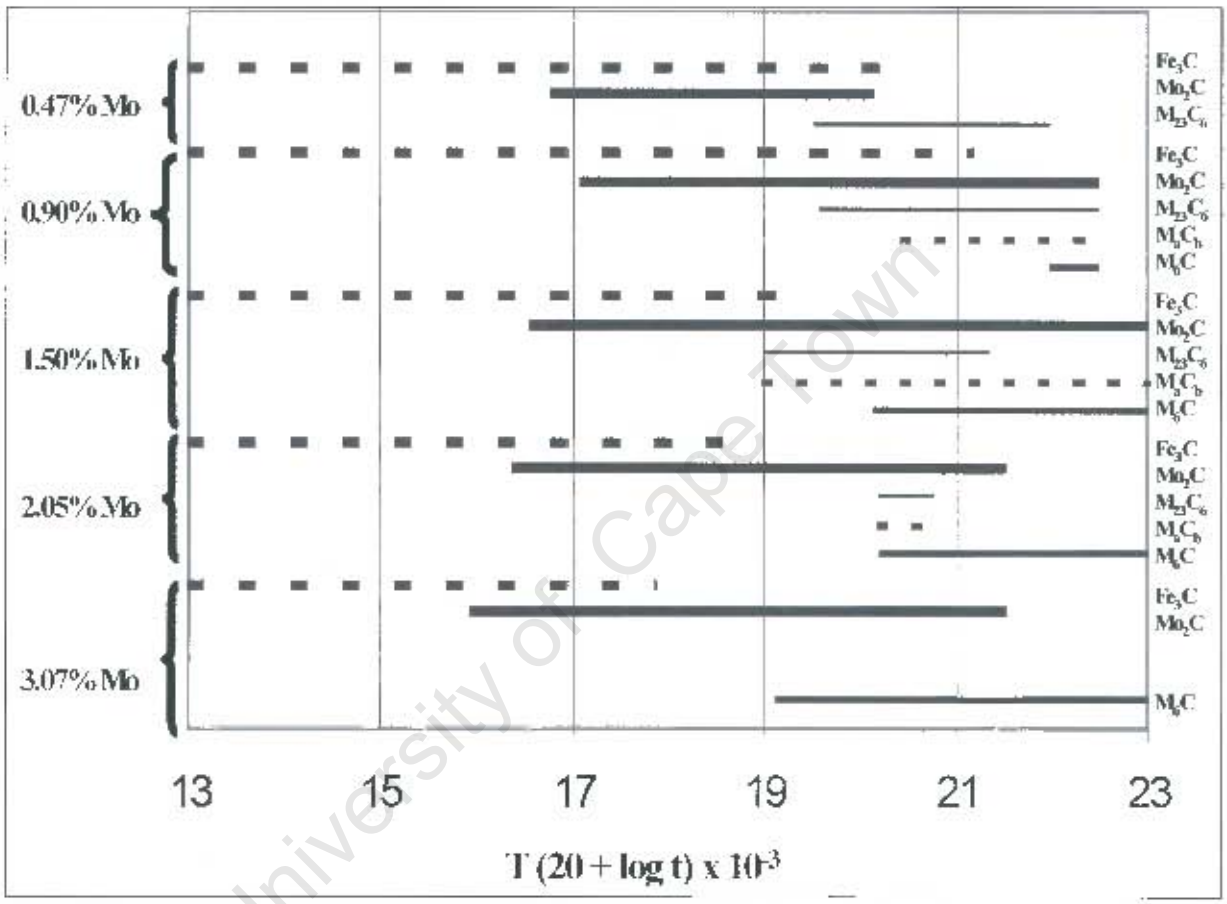

Figure 2.12: The effect of time, temperature and composition on the precipitation of carbides in a 0.1% carbon molybdenum steel [44].

2.4.4 Oxidation resistance and corrosion resistance.

Niobium additions to stainless steels appear to increase the oxidation resistance of the material to both continuous and cyclic oxidation [32]. The spalling resistance of a ferritic stainless steel with a basic composition of 18% Cr and 0.45%Nb exhibited a significant reduction in mass loss due to spalling if the manganese content in the steel exceeded 0.6 percent [40](figure 2.13).

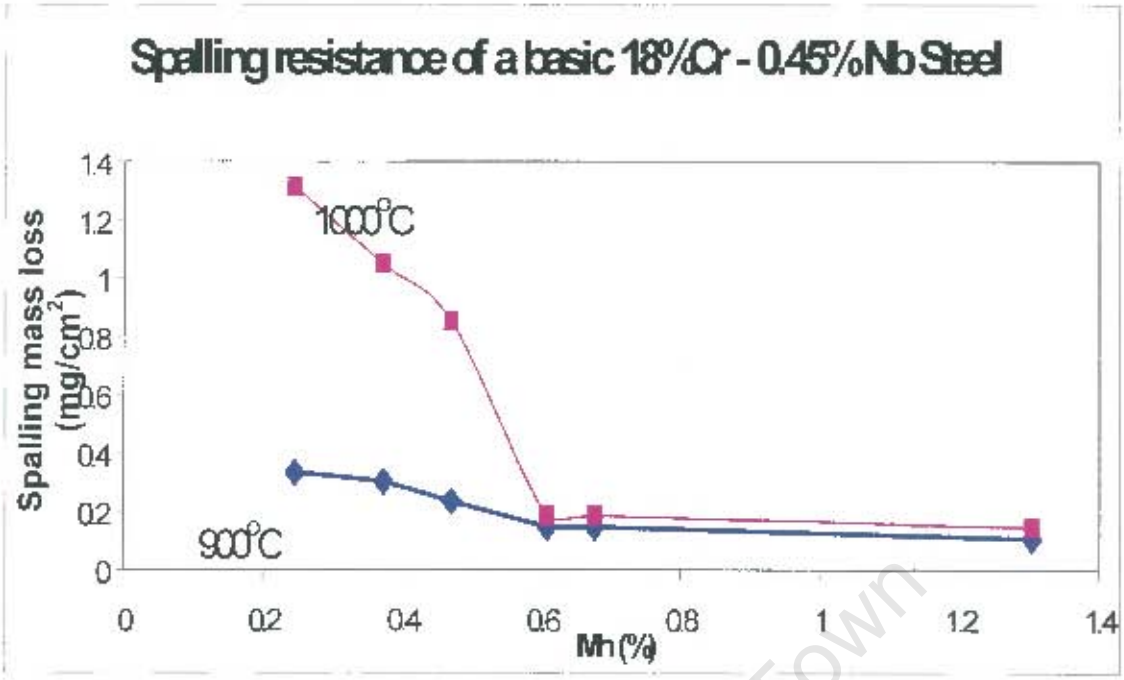

Figure 2.13: Spalling resistance of an 18%Cr – 0.45%Nb steel as a function of manganese (100hrs at temperature).

The rusting tendency in type 430 material (17 percent chromium), prior to (unwelded) and after TIG welding, in a salt spray-testing environment (5 per cent NaCl fog) can be significantly reduced by an over stabilisation of either titanium or niobium [45]. The minimum amount of excess titanium or niobium is 0.2 as determined by the following equations;

{Ti}% = Ti - 4C - 3.4N - 1.5S – 0.2 Minimum

{Nb}% = Nb -7.8C – 6.6N – 0.2 Minimum

Where:

Ti = Titanium in mass percentage

C = Carbon in mass percentage

N = Nitrogen in mass percentage

S = Sulphur in mass percentage

Nb = Niobium in mass percentage

The general pitting resistance (critical pitting potential and induction time for pitting) of a ferritic stainless steel (28Cr-4Ni alloy) generally increases as the niobium content increases in the steel [46]. A similar effect was found in a 20Cr-0.8Mo-0.5Cu alloy [47] and the optimum niobium to carbon plus nitrogen ratio was seen to be between 15 and

30, when copper is above 0.4%. The addition of niobium to a 17% chromium containing steel, in some instances, generally does not appear to increase its pitting resistance [48]. The reason for this is that the MnS inclusions act as pit initiation sites and the niobium does not combine freely with either manganese or sulphur. Titanium, however, appears to have an affinity for sulphur and forms insoluble TiS. The pits formed in steel alloyed with titanium are believed to initiate at the interface between the matrix material and the titanium carbo-nitride and titanium sulphides. This initiation is reportedly at a much higher potential than at MnS sites.

The ability of a ferritic stainless steel to exhibit resistance to intergranular corrosion after welding (sensitisation) is generally determined by its degree of stabilisation. The minimum alloying additions to obtain a stabilised alloy, either with titanium alone or dual stabilisation with titanium and niobium, for a steel containing 12 per cent chromium was found to be:

%Ti or %Ti + %Nb – 0.08 +8*(%C+%N)

This relationship was determined as the boundary between alloys that passed and those which exhibited inter-granular attack after welding (figure 2.14)[49].

Earlier work by Gates and Jago indicated that the minimum ratio of stabilisation elements to carbon and nitrogen content for a steel with 18%Cr and 2%Mo is 10 times the carbon and nitrogen content (figure 2.14) for complete stabilisation [50].

Sensitisation work by Onoyamo et al found the following relationship to prevent sensitisation [51]:

(Ti+Nb) ≥ 16X[C+N] for [C+N]≥ 0.017%
(Ti+Nb) ≥ 8X[C+N] for [C+N]< 0.017%

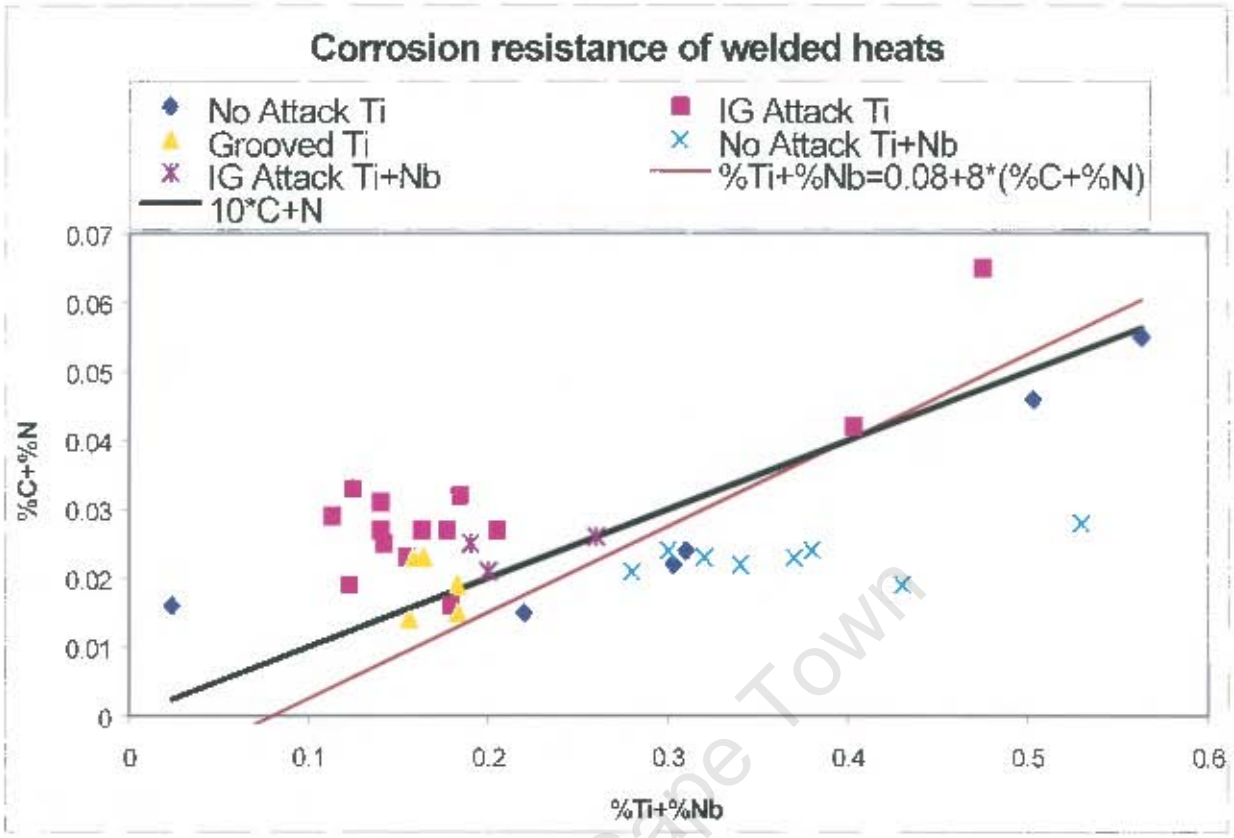

Figure 2.14: Stabilisation requirement for a 12% chromium containing steel to inhibit inter-granular attack.

2.4.5 Laves phase

The laves phase in a low C, N-19%Cr-2%Mo stainless steel appears to be a hexagonal precipitate in the form of $(Fe, Cr)_2$ (Mo, Ti, Nb)[25]. The precipitation behaviour of the laves phase was investigated in this steel by annealing samples, after hot rolling, at various temperatures for 1 hour followed by water quenching. The Laves precipitates appear to peak at about 700 °C (figure 2.15)[25]. The cooling rate affected the amount of precipitates that formed. The faster the cooling rate ($2.4*10^2$) the fewer precipitates formed and the higher the elongation. In addition the amount of cold reduction prior to final annealing also impacted on the amount of precipitates present. The higher the cold reduction the lower the amount of precipitates that formed.

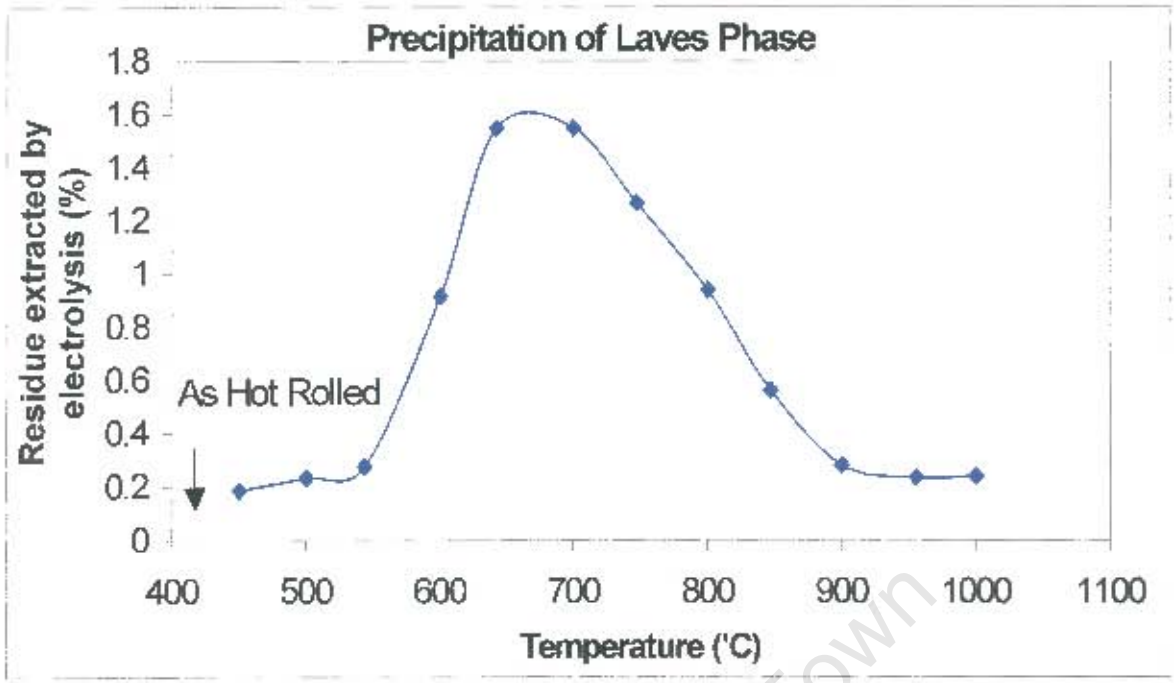

Figure 2.15: Precipitation characteristics of lave phase with isochronal annealing for 1 hr at each temperature [25].

2.4.6 Ridging

A number of investigators have identified that ridging or roping can occur in stabilised ferritic stainless steels [27, 28, and 52]. Ridging or roping is the formation of surface corrugations, due to crystallographic textural effects, which emerge, preferentially in the rolling direction during forming operations in ferritic stainless steels. All of the authors allude to optimum hot rolling and hot band annealing parameters. The purpose of these various optimum-processing parameters is to stimulate the most recrystallization in the material during hot band annealing. Thus by finishing cold on the hot mill with a relatively high reduction on the last pass imparts a high residual driving force for recrystallization to the material on subsequent annealing. The hot band annealing occurs at relatively high temperatures to take advantage of this stored energy and to overcome the materials sluggish response to recrystallization. The ideal hot band structure after annealing is one with a uniform equi-axed grain structure with an ASTM grain size number of approximately 6.

The effect of niobium on its own in reducing the ridging severity in a 18Cr-1.5Mo steel [53] was not as affective as titanium and in fact appeared to increase the severity

of ridging. The greater improvement due to titanium additions and not niobium is attributed to the fact that titanium precipitates out first on solidification and causes a finer as-cast grain structure. In addition the titanium alloyed material should theoretically recrystallise more readily during hot rolling than the niobium alloyed steel. Other investigators on the other hand have found that niobium additions in fact eliminate roping [54].

2.4.7 Niobium and titanium stabilised alloys in the automotive (exhaust) industry.

A number of ferritic stainless steel grades have been utilised in the manufacture of exhaust systems and for high temperature applications (Table 2.3)[55, 56, 57 and 58]. These steels have been selected for one or more of the following reasons; their relatively high oxidation resistance, corrosion resistance and high mechanical properties at elevated temperatures. The steels generally have the addition of aluminium, zirconium, yttrium, titanium, niobium, manganese and/or silicon to enhance the corrosion and oxidation resistance of the material.

Stainless steels will be used to a greater extent particularly in exhaust manifold systems. As engines become more economical and the air to fuel ratio approaches stiochiometric values [59], the temperatures in the exhaust gasses will be in excess of 1050°C.

2.4.8 Conclusions of literature search

Niobium when added to a ferritic stainless steel, appears to be beneficial to the oxidation, corrosion, weldability, formability, ridging and creep resistance of the material. The literature too indicates that the amount of niobium in solution predominantly determines the sag resistance of the material. The literature also indicates that material alloyed with niobium requires a certain degree of care when processing to obtain the optimum metallurgical properties.

Table 2.3

Chemistries of some typical alloys used in the automotive industry.

Alloy	Cr	Mo	Ti	Nb	Al	Cu	Zr	Y etc
409	11	-	0.16	-	-	-	-	-
Aluminised 409	11	-	0.16	-	-	-	-	-
FAL	13	-	-	-	4.0	-	-	-
466	11.5	-	0.15	0.25	-	-	-	-
Alfa II™ (406)	13	-	0.40	-	4.0	-	-	-
408 Cb or Nb	12	-	0.28	0.70	1.0	-	-	-
429M	14	-	0.20	0.40	-	0.4	-	1.2 Si
430M	17	-	-	0.25	-	0.5	-	-
Ugine FK	17	-	-	0.45	-	-	0.3	-
Inoxium 180 Al	17.5	-	0.5	-	2.0	-	-	-
439	17.5	-	0.42	-	-	-	-	-
436S or 434M	17.5	1.22	0.25	-	-	-	-	-
Fecralloy BF1	15.5	-	-	-	5.0	-	-	0.45
BF3	20	-	-	-	5.0	-	-	0.10
368	18	-	0.12	0.25	-	-	-	-
434LN2	19	1.9	-	0.35	-	-	-	-
436LT	17.7	1.23	0.27	-	-	-	-	-
441	18	-	0.29	0.71	-	-	-	-
444	18	2.0	0.12	0.35	-	-	-	-
468	18.25	-	0.12	0.25	-	-	-	-
Nishen steel	18.5	2.0	-	0.40	-	0.20	-	1.0 Mn
433	20	-	-	0.53	-	0.53	-	-
433Mo	20	1.0	-	0.5	-	0.50	-	-
Alfa IV(445)	20	-	-	-	5.0	-	-	0.03 Ce+La

Chapter 3 Experimental procedure

The main objective of the project was to characterise the sag resistance of Columbus type 441 material and determine methods of increasing the sag resistance. Based on this, the project can be broadly divided into two distinct areas (figure 3.1), which are;

1. The investigation of the sag resistance of production material randomly obtained from the plant and the determination by statistical means of any significant processing or compositional parameters that may impact on sag resistance of the material. The changing morphology of the precipitates through the production processes were analysed after each production process.
2. The investigation by experimental means to determine if any thermo-mechanical treatment could be identified that would significantly improve the sag resistance of type 441 material without impacting negatively on the material's mechanical properties. Due to the complex nature of determining the impact of various thermo-mechanical processing steps on a particular property of a material, the laboratory experiments were backward integrated. That is, experiments were started on the cold band material first to observe if the sag resistance could be improved significantly. This was done on cold rolled material at various temperatures. Ageing treatments were also attempted to facilitate the possible embryonic formation of precipitation zones. Following this attempts were made at increasing the sag resistance by various heat treatments on the hot band material while finishing the material at fixed cold band processing route parameters. Finally, the slab material was heat treated and the sag resistance determined on final product by applying a similar processing route to the hot band and cold band material. The rate of grain growth and precipitate percentage was determined for each of the experimental processing stages, namely hot band annealing and cold band annealing. Only the effect of temperature was investigated and not that of roll pass reduction on these material characteristics. The complete project flow is shown diagrammatically in figure 3.1.

The experimental techniques used during the investigation can be broadly categorised as:

- Metallographic analysis, grain size and amount of second phase.
- The sag test.
- Deep etching.
- Scanning electron microscopic analysis after bulk etching including energy dispersive spectroscopy.
- Statistical analysis.
- Heat treatment.
- Hot and cold rolling.

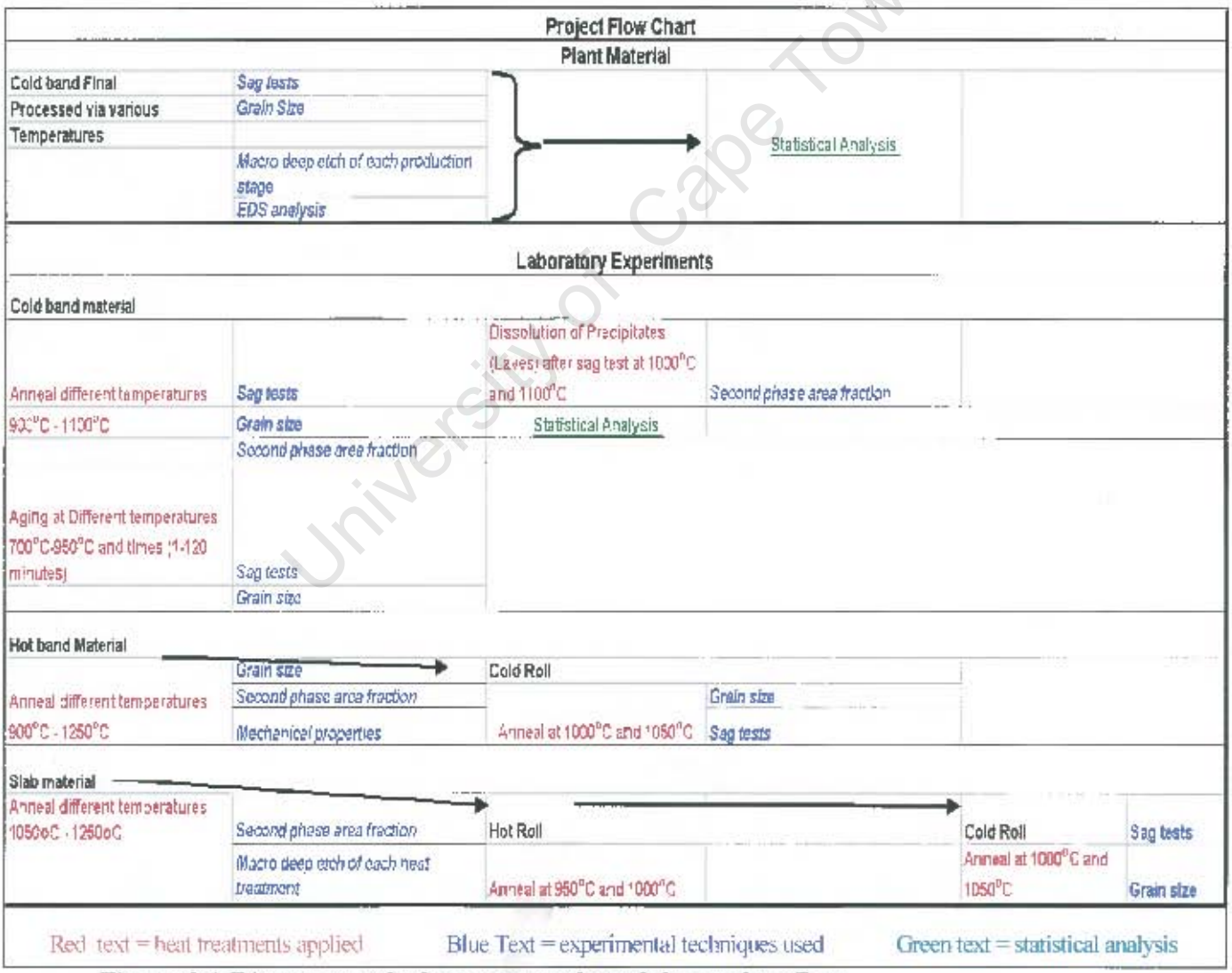

Figure 3.1 Diagrammatical representation of the project flow.

3.1 Metallographic procedure

The samples were prepared by standard metallographic techniques on an automatic polishing system (Struers Maps) to a 3μm finish. The samples were etched electrolytically in concentrated nitric acid [60] in order to optimise the phase contrast and grain boundaries for measurement using a Leco IA3001 image analyser. The samples were etched for a shorter period of time for second phase volume fraction analysis. This was followed by a longer etch time to determine the grain size. The Leco IA3001 image analyser enabled the user to optimise the contrast (via the threshold image command) for optimum coverage of the phase or grain boundary.

Although the utmost care was taken in ensuring that all measurements were done accurately, some variation could be attributable to sample preparation (scratches – only scratch "free" samples were used, however, there may still have been some residual scratch marks), etching (under-etching or the formation of micropits – these were also avoided and samples prepared again if found to be present) and finally measurement (over filling or under filling could give a large variation – this was avoided by checking the fill prior to measurement). The number of fields measured per sample were a minimum of three and four for the grain size and second phase fraction analysis respectively. The reason for the minimum number of fields required for grain size is given statistically below. In most cases the author tried to obtain a typical field and also fields that appeared to be significantly different from the norm. This was particularly necessary when investigating the second phase fraction analysis as:

- The second area fraction was very low and
- An indication of the possible spread in second phase fraction would be obtained, which could either be due to natural variation or due to the combined effect of sample preparation, etching and measurement.

3.1.1 Statistical analysis of grain size measurement

The grain size was measured on a transverse metallographic polished surface of a sample taken from the longitudinal sag specimen prior to testing at $850^{O}C$.

The linear intercept method was used for grain size measurement. The precision of the grain size measurements for a particular sample can be determined by calculating percent relative accuracy. The percent relative accuracy is calculated (according to the ASTM E112-96 [61] standard) by the following means;

- calculate the number of mean values N_A (number of grains per mm^2) or ℓ (mean lineal intercept length) from the individual field values according to:

  $X = \Sigma X_i/n$

  Where X_i is the individual reading (N_A or ℓ) and X is the mean and n the number of measurements.

- Calculate the standard deviation (s) of the individual measurements as

  $S = \sqrt{(\Sigma(X_I-X)^2/(n-1))}$

- Calculate the 95 % confidence interval (95% CI) as:

  $95\%\ CI = t^*s/\sqrt{n}$

Table 3.1 lists the 95 % confidence internal multipliers t as a function of sample size n

- The percent relative accuracy (%RA) is calculated as:

  $\%RA = 95\%CI/X^*100$

Table 3.1

95% Confidence internal multipliers, t

No. of fields, n	t	No. of fields, n	t
3	4.303	7	2.447
4	3.182	8	2,365
5	2.776	9	2.306
6	2.571	10	2.262

A %RA of less than 10 or lower is generally considered to be acceptable precision. The precision was obtained with the initial verification method (Table 3.2). The data obtained was for 12 samples spaced evenly across the width of a strip cut from a production coil of material. The width of material was 1310mm, the initial sample was taken 105mm from the edge and thereafter at every 100mm (12 samples in total). The data had a normal distribution (figure 3.2) and as such the sample size required for an ASTM grains size with a spread of +/- 0.3, to be accurately determined to a confidence level of 95% could be calculated by applying the following formula [62]:

$n = ((1.96*s)/(R/2))^2$ ---------- (Equation 3.1)

Where n = the number of the actual fields required to obtain an accuracy to 95%

s = the standard deviation of the measurements in this case it was determined as 0.0035mm.

R/2 = Range deemed acceptable. The ASTM grain size range was taken as +/- 0.3. Converted to mm for an ASTM grain size of 6.1, $\ell/2$ = 0.004mm

The result is a value of 2.9 which indicates that 3 fields of view will be required to obtain the desired accuracy at a 95% confidence level.

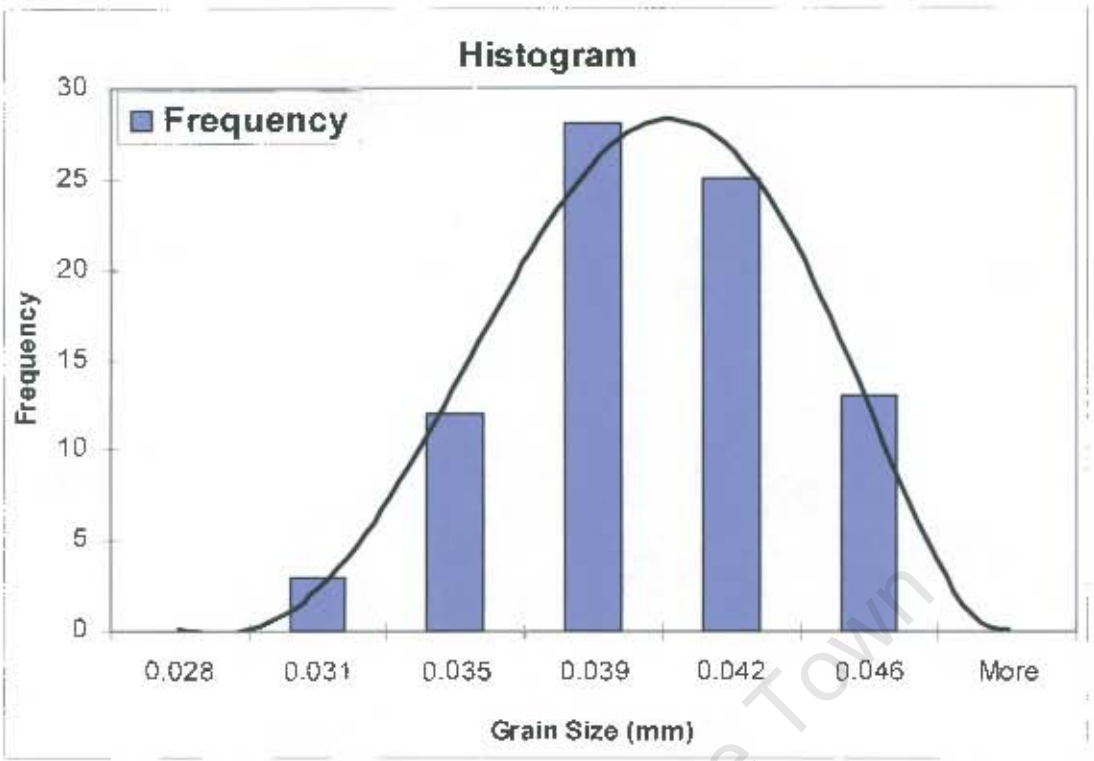

Figure 3.2: Histogram distribution of the mean lineal intercept length of 12 samples taken across the width of a strip of steel.

Table 3.2
Statistical analysis of grain size measurements using the mean lineal intercept length

ID No	Individual Field measurements of the intercept length (mm)										Avg.	S	95%CI	%RA	ASTM No
1	0.041	0.039	0.039								0.0396	0.0016	0.0040	10.05	6.0
2	0.040	0.034	0.041	0.036	0.041	0.042	0.034	0.037	0.037		0.0380	0.0032	0.0025	6.54	6.1
3	0.044	0.040	0.046	0.032	0.039	0.044	0.037	0.033	0.042	0.041	0.0399	0.0047	0.0034	8.50	6.0
4	0.034	0.040	0.039	0.031	0.036	0.036	0.038	0.038	0.038	0.037	0.0366	0.0025	0.0018	4.96	6.3
5	0.043	0.043	0.039	0.039	0.041						0.0409	0.0021	0.0027	6.49	5.9
6	0.041	0.040	0.041								0.0409	0.0008	0.0020	4.94	5.9
7	0.035	0.032	0.038	0.034	0.036	0.040	0.036	0.038			0.0363	0.0026	0.0022	5.92	6.3
8	0.036	0.041	0.035	0.037	0.043	0.031	0.041	0.034	0.040	0.039	0.0378	0.0037	0.0026	6.96	6.2
9	0.043	0.040	0.043								0.0419	0.0017	0.0041	9.82	5.9
10	0.044	0.046	0.039	0.041	0.039						0.0417	0.0032	0.0040	9.62	5.9
11	0.043	0.031	0.041	0.040	0.040	0.038	0.034	0.037	0.035	0.040	0.0379	0.0036	0.0026	6.80	6.2
12	0.041	0.035	0.041	0.036	0.037						0.0382	0.0031	0.0038	9.94	6.1
									Average		0.0386				6.1

The image analyser uses the following standard ASTM formula to determine the grain size number:

$G = 10+6.64\log_{10}(n/l)$

Where:
n = the number of horizontal intercepts (477) and
l = length of the test line at 100X

3.1.2 Statistical analysis of second phase fraction

Initially the second phase area fraction was not measured on the production material as it was observed to be extremely low. It was, however, necessary to attempt and quantify the second phase area fraction once laboratory experimentation was initiated. Area phase fraction analysis was performed to determine the dissolution rate of precipitates in the hot band material at 1100^{O}C. The statistical analysis carried out on this material was similar to that done for the grain size above and it was found that the data for this initial experiment had a normal distribution (figure 3.3).

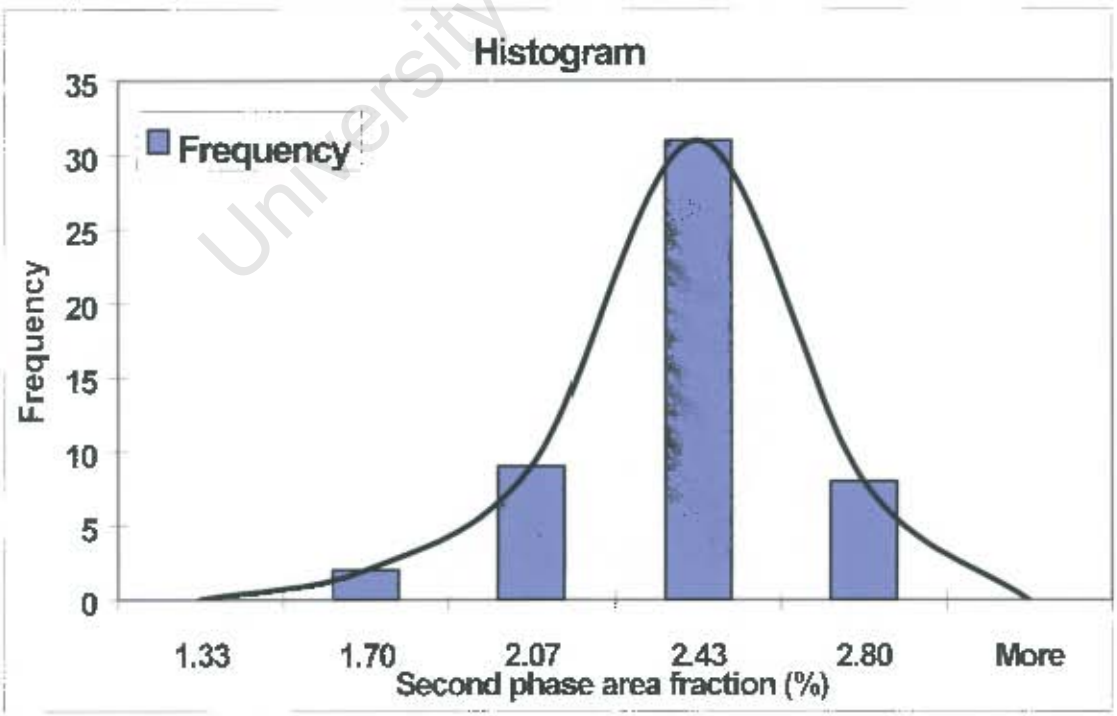

Figure 3.3: Histogram distribution of the second phase area fraction present in hot band material after annealing at 1100^{O}C.

The normal distribution had an average of 2.24% area fraction and a standard deviation of 0.234% area fraction. The value used as an indication that a significant change in area fraction had occurred was taken as +/-% of the average value. The change in second phase area fraction would thus be 0.224%, the range would thus be +/- 0.224%. The calculated sample size required to obtain a 95 percent and 90 percent (use 1.65 in place of 1.96 in equation 3.1) is 4.2 and 2.98 respectively, that is 4 and 3 fields of measure. The small percentage analysed is extremely difficult to accurately measure, it was thus felt that in most cases a sample size of 3 fields (90 per cent confidence level of being within 0.224% of the correct reading) could be used. The phase analysis thus is used to give a general trend of second phase area fraction and should not be seen as absolute values at the particular heat treatments.

3.2 Sag Test Alternative Creep Test

The creep test is used as a standard test in the automotive industry [63]. The test is reported to give a rapid indication of the sag (creep) resistance of a number of samples tested simultaneously. The results appear to correlate with the general creep properties of the steel (compare figure 2.4 to figure 3.4).

Figure 3.4: Sag resistance of various steels tested at 950°C for 100hrs (1.5mm gauge)[63]

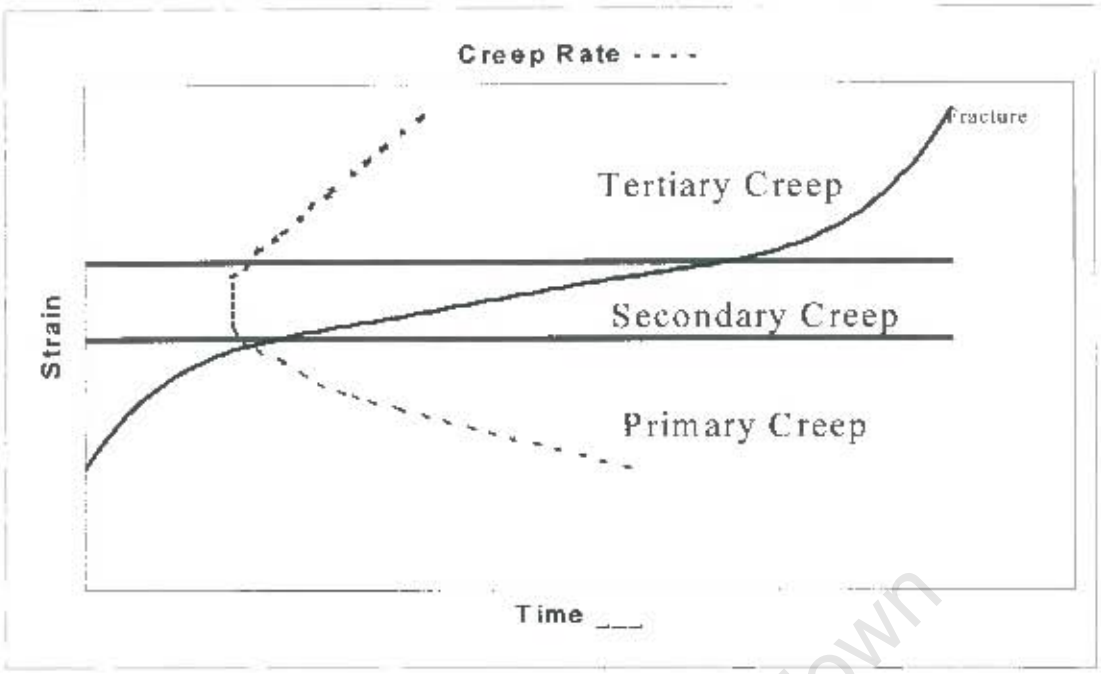

Figure 3.5: Classical Creep Curve under constant load.

Creep tests are normally done under a constant applied tensile load at a set temperature and the increase in length is measured periodically [64,36]. The engineering creep curve under constant load normally has three stages (figure 3.5), namely:

- Primary Creep

  This is a stage of decreasing creep rate (figure 3.5). This material normally exhibits an increasing resistance to creep with time due to the amount of deformation that the material experiences at this stage. The stage is characteristic of low temperature and stress scenarios and is sensitive to temperature and stress [36].

- Secondary or Steady State Creep

  The creep rate in this stage is constant and is called the minimum creep rate [64]. There is a balance between strain hardening (increasing dislocation lengths) and recovery (decreasing dislocation lengths i.e. screw slip annihilation and edge dislocation climb) of the material [36]. This stage is sensitive to temperature and stress [36].

- Tertiary Creep

  There is a reduction in cross-sectional area at this stage. It is also normally associated with high temperature and stresses. Metallurgical changes such as

precipitate coarsening, recrystallization or diffusional changes in the phases present occur at this stage [36].

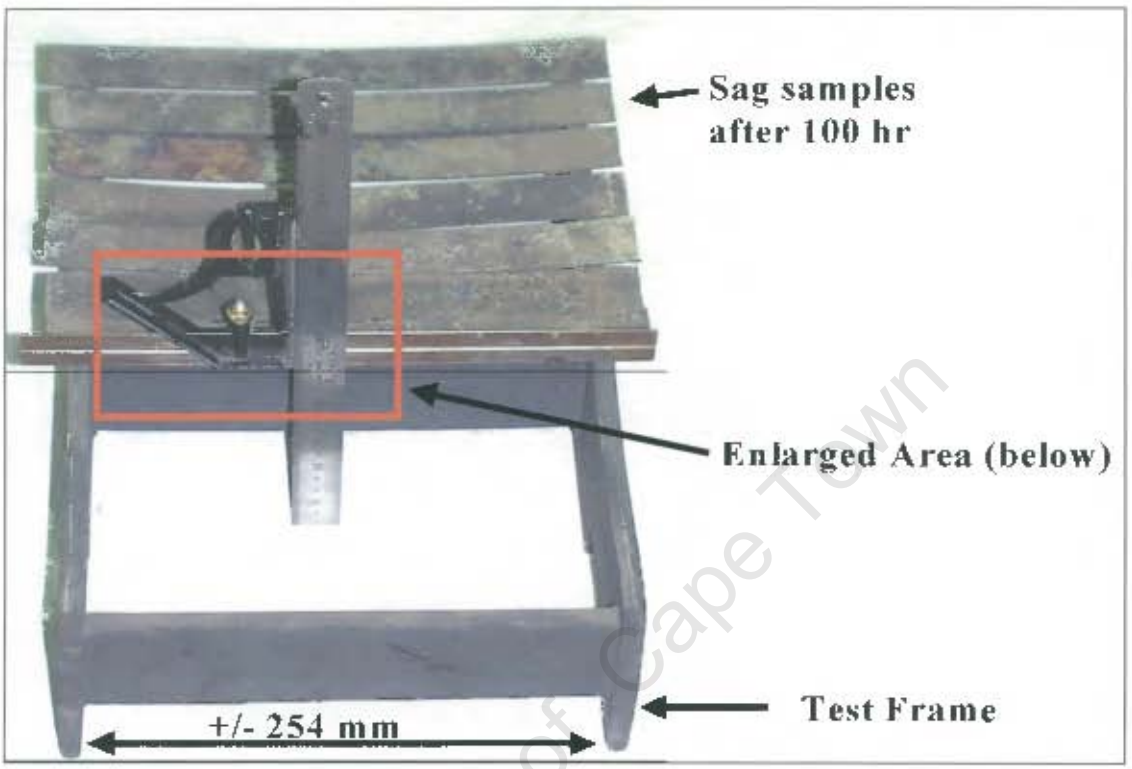

Figure 3.6: Sag test frame

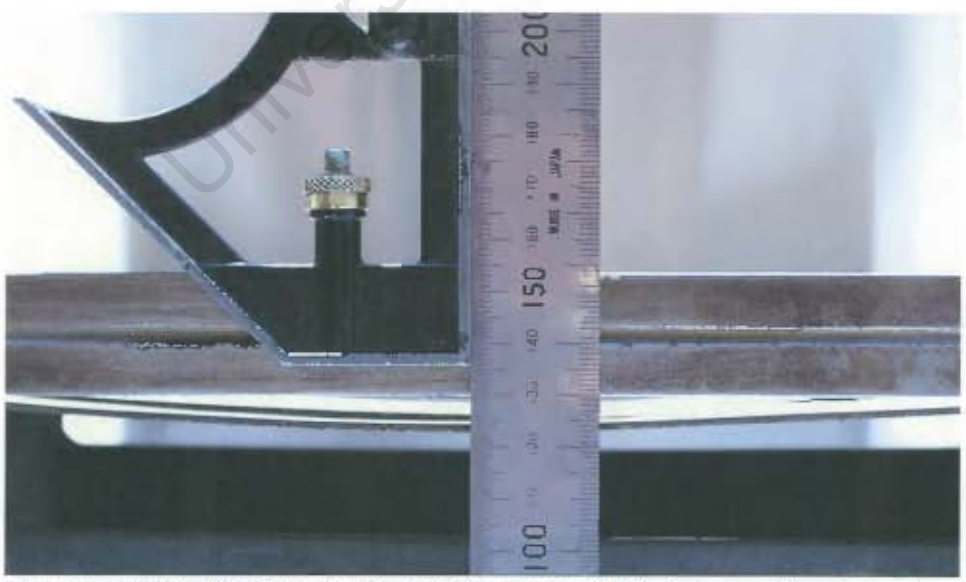

Figure 3.6b: Enlargement of the sag test frame showing the in situ measurement of the sag.

The samples are placed on a rectangular frame (figure 3.6) where the sample supports have an outer radius of 5mm and are 254mm apart. The design is similar to that used by J.A. Douthett [65]. The deflection was measured in situ on the frame prior to placing the samples in the furnace at 850°C for 100 hr. The permanent deflection of the samples is measured, in situ, at the point of lowest sag between the supports from a horizontal line joining the two supports after the 100 hr test period.

3.2.1 Effect of gauge on the sag test

The idealised stress strain curve (figure 3.7) used for the determination of inelastic (plastic) bending of beams appears to simulate in many respects the steady state of creep (stage 2 strain rate is constant for a constant applied stress).

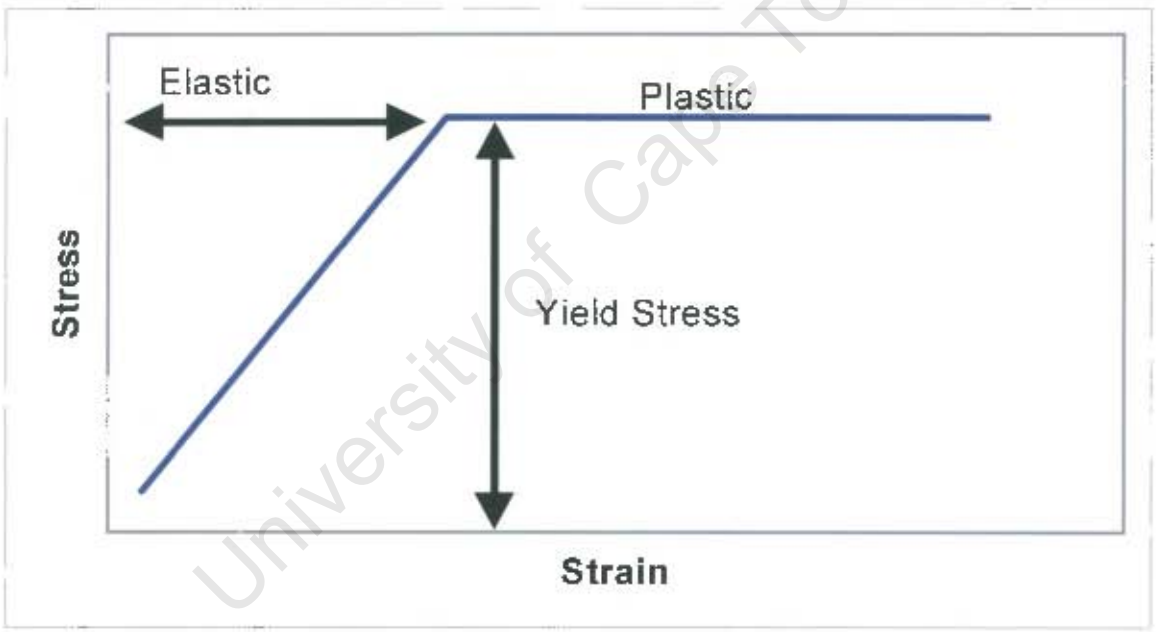

Figure 3.7: Idealised stress strain curve for elastic and plastic deformation.

The maximum stress moment or moment of resistance for a rectangular beam that is stressed in the fully inelastic (plastic) region has been determined as [66, 67].

$M_{ult} = ¼ Sbh^2$

Where:

S = the yield point of the material

b = breadth and

h = depth or thickness.

This formula indicates that the strength of beam-sections is directly proportional to the square of the depth or thickness of the material.

Theoretically, therefore, it can be postulated that thinner gauge material would show a higher degree of sag (creep) at elevated temperatures as the inherent strength would be weaker. The degree to which the same material would exhibit a change in strength is related to the square of the thickness (given that the other dimensions are fixed). Multiplying by the square of the gauge should normalise the deflection. The normalised sagging should theoretically, therefore, be the same for all the gauges.

3.2.2 Effect of grain size on the sag test

Nabarro and Herring have found that diffusion creep is the determining mechanism at high temperatures and relatively low stresses as would be the case for the sag test. The Nabarro-Herring creep equation is [36, 68],

$$\varepsilon_\sigma = (14\sigma b^3 D_v)/(kTd^2)$$

Where;

d = Grain diameter

σ = Applied stress

k = Boltzmann's constant

ε_σ = Minimum creep rate

D_v = Lattice diffusion coefficient

b = Burgers vector of the dislocation

T = Temperature, absolute scale

The degree of sagging is seen to be inversely proportional to the square of the grain diameter. A finer grain sized material (larger ASTM grain size number) will exhibit a higher degree of sagging to that of a sample with a larger grain diameter. At temperatures approximately 100^{O}C or more below the melting point grain boundary diffusion creep predominates (Coble - type). The reason for this is that the activation energy for self-diffusion along the grain boundary is considerably less than self-diffusion through the bulk of grains [68]. The rate of creep in this case is inversely proportional to the cube of the grain diameter. The control of the grain size is thus an

important factor in controlling the creep resistance of a material in the temperature regimes being investigated.

This is contrary to the findings of Irvine, Murray and Pickering [19] who have found that grain size in both austenitic (see section 2.2.1.2) stainless and ferritic steels has no effect on the creep rate.

The gauge and the grain size nevertheless appear to be the two most predominant factors that affect the degree of sagging from the formula above.

3.2.3 Effect of chemistry on the sag test

Theoretically, from the Nabarro - Herring equation above, the chemistry can affect sagging in as much as it would change the lattice diffusion coefficient or the Burgers vector of dislocations. Since the Fe-Cr balance will give the effective lattice size other elements would have to be present in significant amounts to change the lattice parameter and the lattice diffusion coefficient.

3.2.4 Verification of sag test

The sag test had to be verified to determine the spread in sag resistance within the length of the laboratory furnace (a thermal gradient of approximately 10 °C was measured in the furnace). The sag resistance across the width (1275 mm wide, samples marked 1 to 12) of a coil processed in the plant was tested to determine the variability that may exist. The grain size for this particular coil of material varied between an ASTM number of 5.9 and 6.3 (Table 3.3). The grain size measurement is an average of three results per field. The grain size appears to be uniform throughout the width of the sample with an average ASTM grain size of 6.1 +/- 0.3. The sag resistance varies between 2 and 3.5mm(Table 3.3) and no correlation can be drawn to the position of the specimen in the furnace and the sag observed (figure 3.8).

Table 3.3

Sag across the width and through the furnace of MPO 3132870 (Gauge 1.25mm)

No*	Position in furnace	ASTM Grain Size	Sag (mm)
1	Front 1	6.0	2.0
2	Front 2	6.1	2.0
3	Back 9	6.0	2.0
4	Back 10	6.3	2.5
5	Middle 7	5.9	3.0
6	Middle 8	5.9	3.5
7	Middle 5	6.3	2.0
8	Middle 6	6.2	2.5
9	Front 3	5.9	3.0
10	Front 4	5.9	3.0
11	Back 11	6.2	3.0
12	Back 12	6.1	2.0
Average		6.1	2.5
	Std Deviation	0.26	0.54

- Position of sample across the width of the strip from edge (1) to edge (12).

In order to test the sensitivity of the sag test for determining creep rate behaviour, the rate of sag was determined for a 0.97mm gauge material (MPO 3196653) with an average ASTM grain size of 6.5 for up to 170 hrs at 850 °C. The sag tests indicate that a typical creep rate curve is obtained from production material when testing the material at 850 °C for 100hrs (figure 3.9).

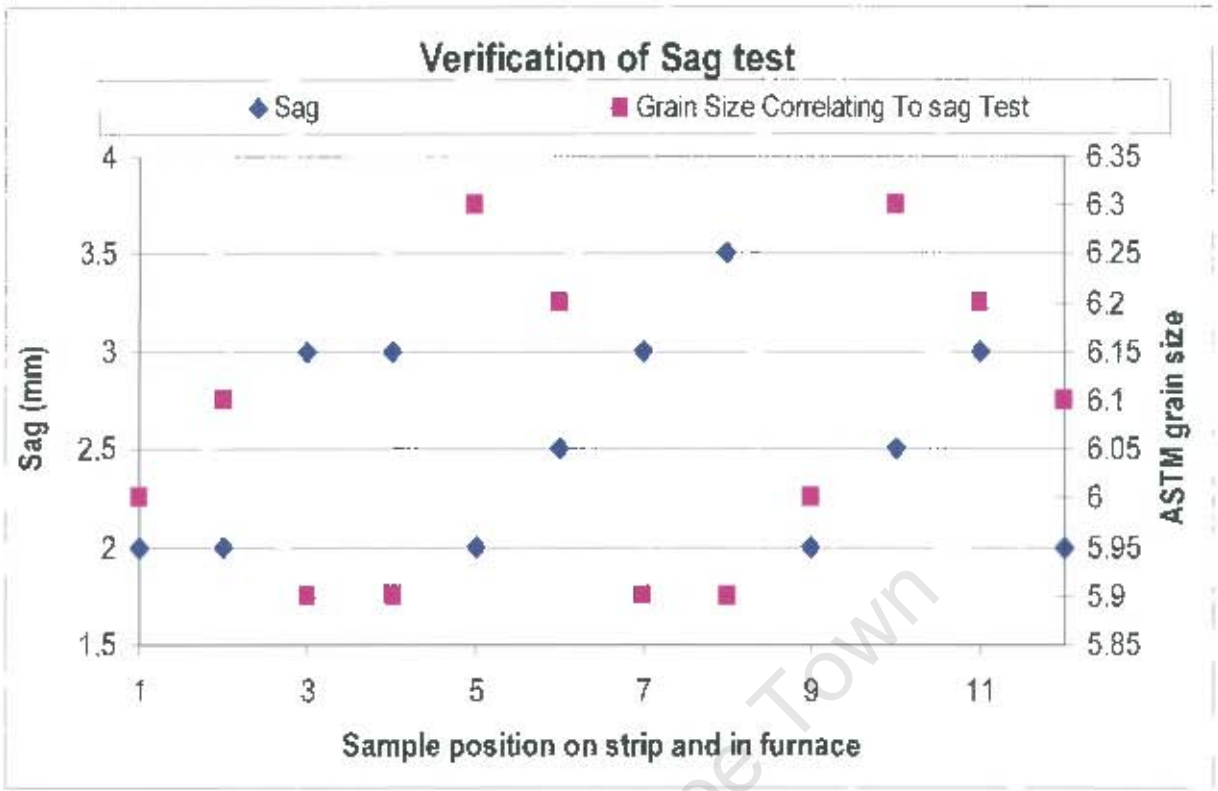

Figure 3.8: Verification of the sag test indicating no significant variation in sagging across the width of a sample and within the length of the furnace.

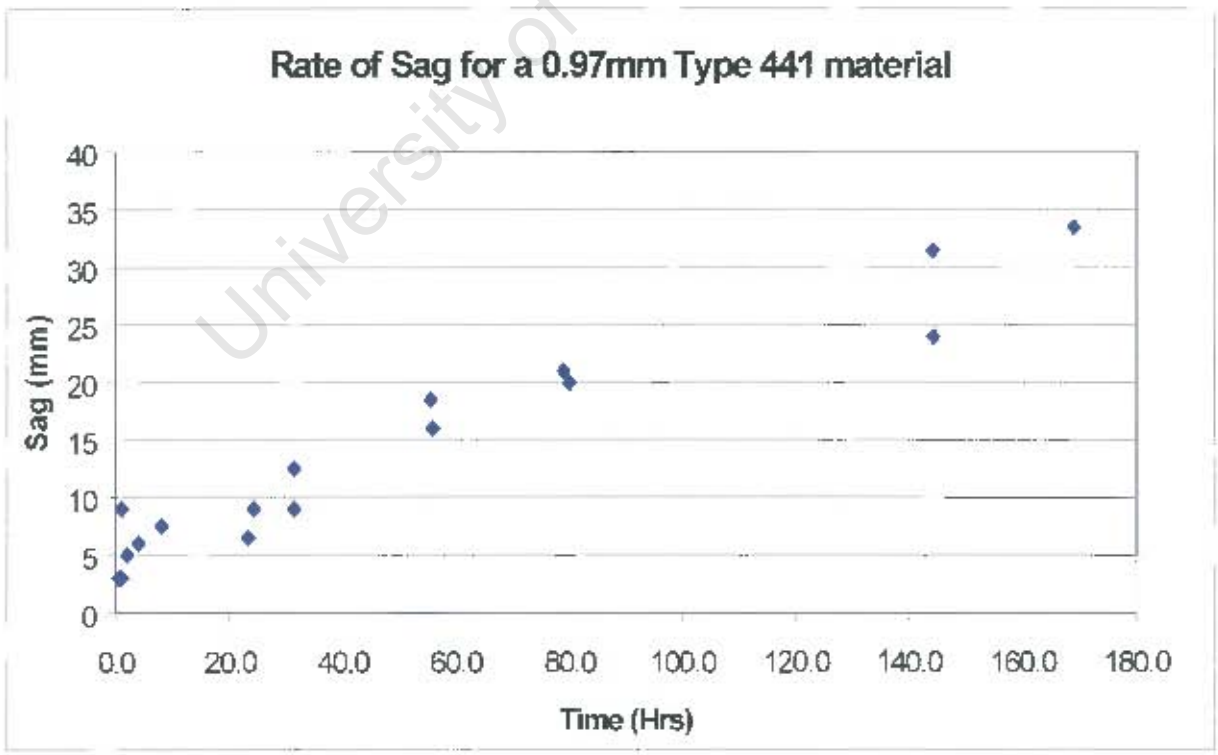

Figure 3.9: Creep rate observed for a 0.97mm 441 material.

Statistical analysis to determine the number of samples required

The confidence limits required to make an accurate assessment of any change in the degree of sagging would be +/- 1mm. The 12 samples tested above are the largest group of sags originating from one sample base. They give an indication of the spread or standard deviation that may exist for sag values. The standard deviation was determined as 0.54mm. The population of sag values is assumed to have a normal distribution based on the small sample size (figure 3.10). The sample size required for a 95 percent confidence within +/- 1mm of the measured sag value was calculated as 1.13 (applying equation 3.1 on page 34).

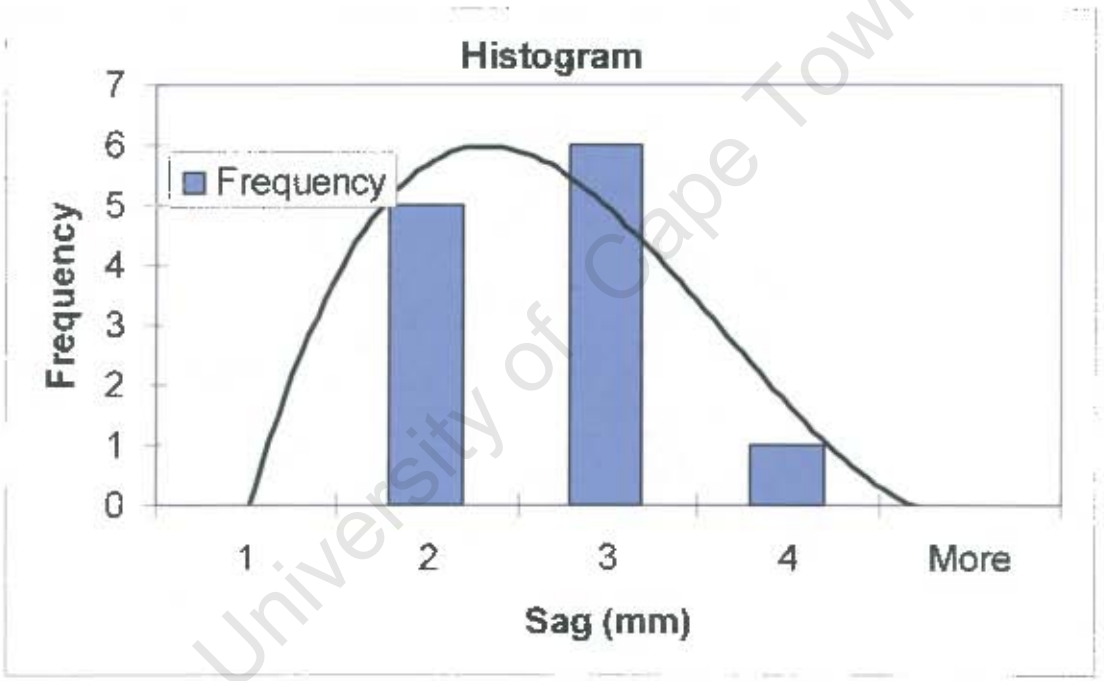

Figure 3.10: Histogram plot of the sag values originating from the verification samples.

3.3 Deep etching, SEM and EDS analysis

The samples were deep etched at various stages to investigate the morphology of the most common precipitates. The bulk etchant was a concentrated nitric acid solution (65%) used electrolytically at 0.8 Amps. The sample was left in the solution (normally 3 hrs) until sufficient material was removed. The etched samples were

evaluated in a scanning electron microscope (Cambridge Instruments Stereoscan 240). The chemical compositions of the precipitates were determined semi-quantitatively via energy dispersive spectroscopy (Cambridge Instruments AN10000 x-ray analyser attached to the SEM).

3.4 Statistical methods

The initial results were obtained from actual plant material. The data obtained from the plant material was analysed via linear and non-linear regression modelling to observe if any relationship existed between the various processing and chemical constituents in the material. The statistical mathematical package used was Statgraphics-plus (version 6). Initially the data was subjected to correlation analysis. The correlation analysis generates a table containing the correlation coefficients between the various components and the probability that this relationship can occur by chance. The analysis eliminates duplication of components for use in regression analysis. An example is that grain size can be converted to the number of grains and the mean grain size in micrometers. There is a strong relationship between all of these as would be expected, thus in theory only one of these should be used when applying regression analysis. The results of this analysis (correlation and regression) indicated that further experimental work was necessary.

3.5 Heat treatment, hot rolling and cold rolling

The samples were heat treated in a glow bar furnace. The furnace temperature was monitored via a calibrated independent thermocouple and multimeter using the Temperature Electromotive Force (EMF) tables for standardised thermocouples [69]. The total time the samples are in the furnace is given and not the time at temperature. The time at temperature can, however, be calculated as the heating rates have been determined to be approximately 170sec/(mm thickness) and 85sec/(mm thickness) for cold rolled and hot band ferritic stainless steels respectively [70]. All samples were water quenched after heat treatment. The experimental heat treatment matrix (Table 3.4) mainly incorporated those temperatures and times that were considered feasible for a continuous production line.

Cold Rolling

The material that was cold rolled received a total cold reduction of +/- 77 per cent. The reduction per pass was not consistent and varied between 6 to 15 per cent. The mill used was a laboratory scale two high mill with a roll circumference of 644mm. The roll speed was +/- 26m/minute (0.666 rev/sec).

Hot Rolling

Slab samples (40mm thick by 200mm long and 100mm wide) were hot rolled after preheating in the glow bar furnace and received a total hot reduction of approximately 85 percent. The reduction per pass was kept at +/- 25 percent. The aim final hot band gauge was 6mm. The roll circumference was 784mm with a roll speed of about 20m/minute (0.425rev/sec)

Table 3.4 Experimental Matrix

Cold band material														
Dissolution of precipitates														
Temperature	Time in furnace (sec)													
1000	60	120	240	360	480	960	1920							
1100	60	120	240	360	480	960		3600						
Anneal at different temperatures, phase fraction and grain growth														
Temperature	Time in furnace (sec)													
900								300	350	410	530	750		
925								300	350	410	530	750	1080	
950								300	350	410	530	750	1080	
975								300	350	410	530		1080	
1000					180	240	270	300	350	410	530			
1025	60	120		150	180	240	270	300	350	410	530			
1050	60	120	135	150	180	240	270	300	350	410				
1075	60	120	135		180		270	300	350	410				
1100	60	120			180	240	270	300	350	410				
Ageing at different temperatures sag test														
Temperature	Time in furnace (sec)													
700	60		240		960		3600							
750		120		480		1920		7200						
800	60		240		960		3600							
850		120		480		1920		7200						
900	60		240		960		3600							
950		120		480		1920		7200						

Table 3.4 Continued

Hot band material								
Grain growth and phase fraction								
Temperature	Time in furnace (sec)							
1000	60	120	240	480	960	1920	3600	5400
1100	60	120	240	480	960	1920	3600	5400

Anneal at different temperatures prior to final anneal after cold rolling at 1000 (264 sec) and 1050 (140 sec), sag test	
Temperature	Time (sec)
900	7200
950	7200
1000	7200
1050	7200
1100	7200
1150	7200
1200	7200
1250	7200

Slab material	
Phase fraction, sag samples hot band anneal at 950 (15 minutes) and cold rolled material annealed at 1050 (140 sec), sag test	
Temperature	Time (Sec)
1050	7200
1100	7200
1150	7200
1200	7200
1250	7200

Chapter 4 Analysis of production material

4.1 Statistical analysis of production material

The data analysis is of 178 individual sag values originating from 96 randomly obtained production samples (appendix 1). The mechanical properties and chemical composition of the material is shown in table 4.1 and 4.2.

Table 4.1

Typical mechanical properties of type 441 materials investigated.

Mechanical Property	Average	Std. Deviation
UTS (MPa)	495.4	20.0
Proof Stress (MPa)	322.9	16.6
Elongation (%)	29.5	1.6
Hardness (Vickers)	152.9	6.9
ASTM grain size No	6.6	1.1

Table 4.2

Typical chemical composition of type 441 used in the research.

Element	Avg. Per Cent By Mass	Standard Deviation
C	0.0176	0.003
S	0.003	0.002
P	0.0251	0.003
Mn	0.5255	0.062
Si	0.5226	0.045
Cu	0.0972	0.02
Ti	0.1808	0.022
Mo	0.0346	0.017
Cr	17.927	0.101
Ni	0.2506	0.073
Nb	0.4931	0.067
Al	0.0058	0.001
N	0.0209	0.003
V	0.1153	0.016

The statistical analysis included the following parameters:

- Major alloying elements.
- Thermo-mechanical processing parameters, notably the slab reheat temperature, annealing temperatures and the cold reductions.
- The grain size, which in essence is the accumulative effect of the thermo-mechanical history
- Calculations of the predicted percent niobium in solution.

The following statistical methodology was followed once all the relevant data had been obtained:

- Correlation analysis
- Determination of a linear regression model from the elements with the strongest relationship
- Non-linear regression analysis of the strongest relationship with sag.
- Determination of a linear regression model from the elements with the strongest relationship to the normalized sag value.

4.1.1 Determination of niobium in solution

The amount of niobium in solution is determined from the solubility products of TiC and NbC. It has been shown that the solubility products in a 16 percent chromium ferritic stainless steel [52] containing both niobium and titanium can be expressed approximately as;

$$[Nb+Ti]\,[C] = y\,K_{NbC} + (1-y)\,K_{TiC} \quad \text{----------Equation 4.1}$$

It was further shown that the solubility products at different temperatures could be calculated using the following formula.

$$\log K_{NbC} = \log [Nb]\,[C] = -\,10860/T + 4.71$$

$$\log K_{TiC} = \log [Ti]\,[C] = -\,12130/T + 6.14 \text{ and}$$

$$\log [Nb+Ti]\,[C] = -11520/T + 5.40$$

Where

[Nb+Ti], [Nb], [Ti] and [C] are the equilibrium concentration in mass % of each element

y is the mole fraction of niobium in the precipitate $(Nb_yTi_{(1-y)})C$

K_{NbC} and K_{TiC} are the solubility products of NbC and TiC respectively and

T is the absolute temperature (Kelvin).

The mole fraction y for a particular composition can thus be determined from equation 4.1 above as;

$$y = ([Nb+Ti][C] - K_{TiC})/(K_{NbC} - K_{TiC})$$

The amount of niobium in solution for a ferritic stainless steel containing both niobium and titanium as alloy additions can therefore be obtained directly as

$$[Nb][C] = y K_{NbC}$$ ----------Equation 4.2

The weight percent of niobium in solid solution requires that the weight percent of precipitates is known. The following calculation [19] determines the amount of niobium in solution related to the weight percent of precipitate. An alloy of known composition contains niobium and carbon, which precipitates as NbC_n; the weight percent of niobium in NbC_n is given as

$$(W_x A_{Nb}) / (A_{Nb} + n A_C) = p W_x$$

Where:

W_x = the weight percent carbide un-dissolved

n = 1 for NbC and 0.75 for Nb_4C_3 (stiochiometric value)

A_{Nb} = the Atomic weight of niobium = 92.91

A_C = the Atomic weight of carbon = 12.013

$p = (A_{Nb}) / (A_{Nb} + n A_C)$

The weight percent niobium in solid solution is thus given as;

$$W_{Nb} - pW_x$$ ----------Equation 4.3

The weight percent Carbon in solution is given as;

$W_C - (1\text{-}p)W_x$ ----------Equation 4.4

Where:

W_{Nb} is the total weight percent niobium in the alloy and
W_C is the total weight percent carbon in the alloy.

Thus from equation 4.2, 4.3 and 4.4 the following relationship is found between the niobium solubility product, the weight percent niobium and carbon in solution and the weight percent carbide un-dissolved;

$$[Nb]\,[C] = y\,K_{NbC} = (W_{Nb} - pW_x)(W_C - (1\text{-}p)W_x)$$

Therefore

$$W_{Nb}\,W_C - y\,K_{NbC} - W_x\,(W_{Nb}\,(1-p) + p\,W_C) + p\,(1\text{-}p)\,W_x^{\,2} = 0$$

Solving the quadratic equation for the weight of un-dissolved carbide yields

$$W_x = ((W_{Nb}\,(1-p) + p\,W_C) +/- \sqrt{((W_{Nb}\,(1-p) + p\,W_C)^2 - 4\,(W_{Nb}\,W_C - y\,K_{NbC})(p\,(1\text{-}p))})/\,2\,p(1\text{-}p)$$

The weight of un-dissolved carbide (W_x) is used in equations 4.3 and 4.4 above to determine the percent weight of niobium and carbon in solution.

The theoretical effect of various additions of niobium to the steel if the carbon content is kept constant (mass percent = 0.017) can be investigated using this equation. It can be seen that the curves have a power relationship and that the asymptotic (to the x-axis) residual niobium value increases as the addition of niobium increases (figure 4.1). The amount of niobium going into solution as the temperature increases depends on the quantity of niobium that has been added to the alloy. This calculation was used to determine the amount of niobium in solution after reheating and also after down

coiling. The assumption was made that the material would preferentially form the cubic NbC carbides [71, 72].

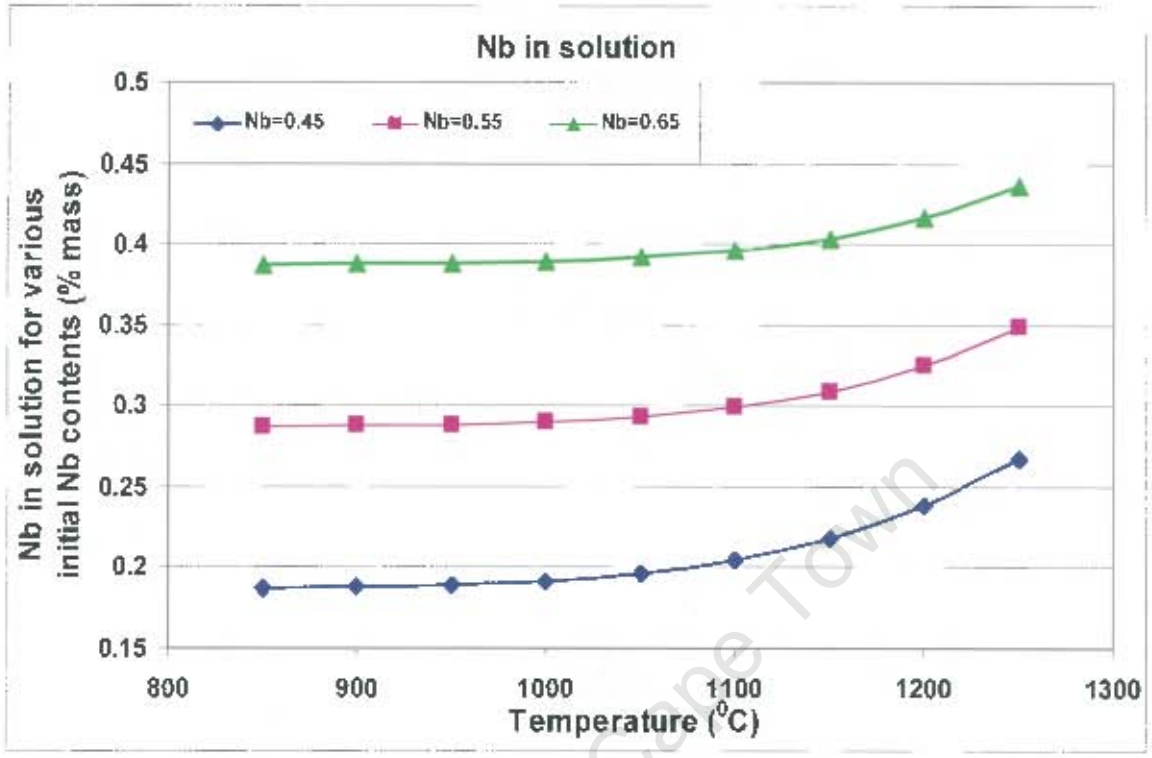

Figure 4.1: The calculated solid solubility of niobium in a ferritic stainless steel based on Fujimura.

4.1.2 Correlation analysis

The correlation between all of the various data drawn for analysis was determined by means of the standard formula for the correlation coefficient [73,74]. The strongest relationship existed between the sag value and the final gauge (table 4.3) of the material tested. In essence this is a logical consequence of the relationship between the strength of a beam and the thickness as shown in the previous section 3.2.1.

The non-linear regression analysis package from Statgraphics was applied to the sag value and the final cold rolled gauge to obtain the relationship between the two parameters. The relationship obtained was:

$Sag = 12.7987689 * gauge^{-2.0266270}$ Correlation Coefficient = 0.604608

Table 4.3

Initial correlation analysis of all 31 parameters obtained for investigation.

Parameter	Sag	Grain size (mm)	Final Gauge
Sag	1.00	-0.24	-0.62
Calculated grain size	-0.24	1.00	-0.19
Final Gauge	-0.62	-0.19	1.00
Hot Gauge	-0.53	-0.13	0.85
Reheat Retention Time	0.04	0.06	0.02
Discharge Temperature	0.23	-0.46	0.08
Number of Passes on Hot Mill	0.21	0.23	-0.49
Max. Last Pass Temp	0.22	-0.46	0.08
Ave. Last Pass Temp	0.23	-0.45	0.13
Down Coil Temp	0.16	-0.48	0.19
Hot Band Line Speed	0.20	0.16	-0.50
Hot Band Time at Temp	0.46	-0.07	-0.53
Hot Band Strip Temp	0.13	0.25	-0.35
Cold Band Final Line speed	0.36	0.14	-0.67
Cold Band Final Time at Temp	-0.04	-0.07	0.12
Cold Band strip Temp	-0.23	0.66	-0.09
C	-0.05	0.04	0.09
S	0.04	-0.34	0.19
Mn	0.21	0.18	-0.20
Si	0.01	-0.19	-0.03
Ti	0.27	-0.12	-0.11
Mo	-0.03	-0.10	0.08
Cr	-0.17	-0.04	0.05
Nb	0.54	-0.24	-0.20
Al	0.00	0.35	-0.06
B	0.24	-0.10	-0.05
N	0.07	0.31	-0.23
O	0.10	-0.41	0.18
Calculated Reheat Nb	0.47	-0.25	-0.17
Calculated Down coil Niobium	0.47	0.31	-0.13
% Cold Reduction	0.35	0.12	-0.48

The formula was simplified to:

$$Sag = 13*Gauge^{-2}$$

The normalized values for sag would thus be:

$$(Sag*Gauge^{2}) / Constant = 1$$

The above analyses vindicates the use of the plastic region in the analysis of the gauge on the sag test in section 3.2.1 and correlates with the theoretical analysis that the maximum stress moment is directly related to the square of the thickness. When the sag values are normalized the next strongest relationship is the calculated grain size (table 4.4) and is visually shown in figure 4.2.

Table 4.4

Correlation analysis matrix after normalizing the sag values.

Parameter	(Sag*Gauge2)/Constant	Grain size (mm)	Nb
(Sag*Gauge^2)/Constant	1.00	-0.59	0.56
Grain size (mm)	-0.59	1.00	-0.24
Hot Gauge	-0.06	-0.13	-0.23
Reheat Retention Time	0.10	0.06	0.00
Discharge Temperature	0.32	-0.46	0.48
Number of Passes on Hot Mill	-0.06	0.23	0.16
Max. Last Pass Temp	0.34	-0.46	0.41
Ave. Last Pass Temp	0.37	-0.45	0.43
Down Coil Temp	0.41	-0.48	0.36
Hot Band Line Speed	0.00	0.16	-0.05
Hot Band Time at Temp	0.24	-0.07	0.39
Hot Band Strip Temp	-0.09	0.25	0.11
Cold Band Final Line speed	0.00	0.14	-0.16
Cold Band Final Time at Temp	-0.02	-0.07	0.20
Cold Band strip Temp	-0.38	0.66	-0.18
C	0.02	0.04	-0.12
Mn	0.09	0.18	0.10
Si	-0.04	-0.19	-0.09
Ti	0.13	-0.12	0.47
Mo	0.07	-0.10	-0.02
Cr	-0.06	-0.04	-0.12
Nb	0.56	-0.24	1.00
Calculated Reheat Nb	0.51	-0.25	0.92
Calculated Down coil Niobium	0.52	-0.31	0.94
% Cold Reduction	0.03	0.12	-0.02

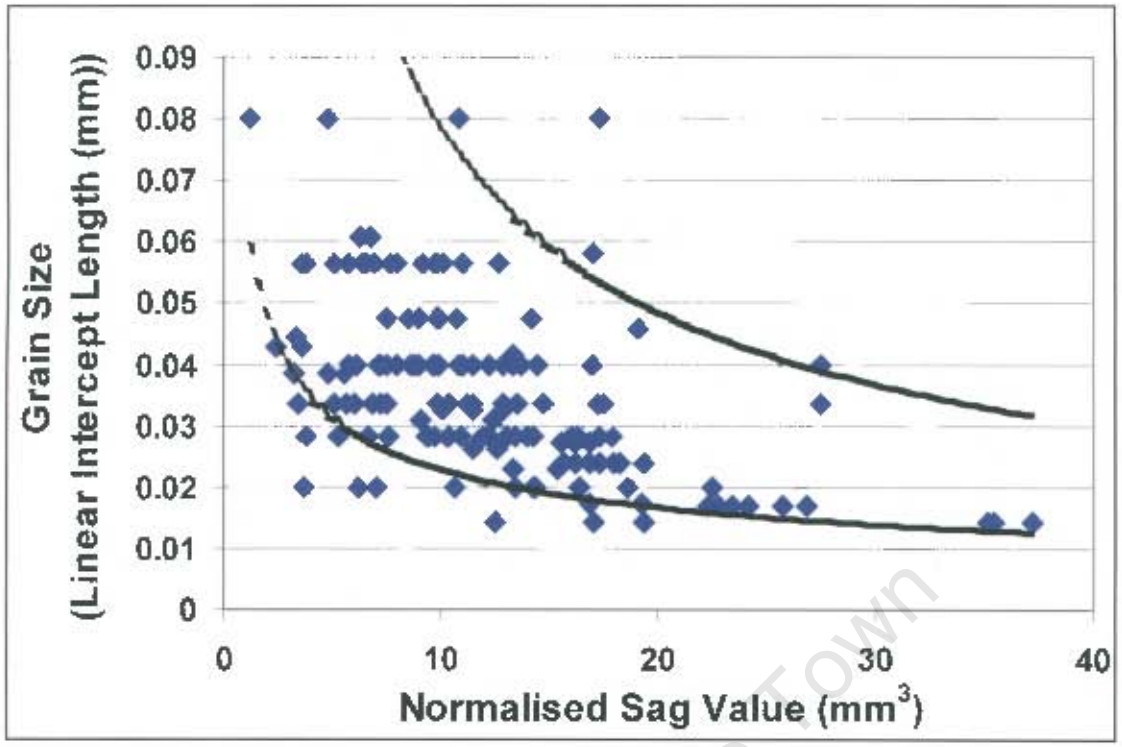

Figure 4.2: Graph of grain size versus the normalised sag value

The Nabarro-Herring diffusional creep equation described in section 3.2.2 indicates that the degree of sagging would be inversely proportional to the square of the grain size. If this is applied to the above matrix it is seen that the correlation coefficient increases significantly between the grain size and the normalized sag value (table 4.5). In addition it is seen that the niobium has a relatively strong relationship with the sag value. The three most significant parameters that affect the creep strength in type 441 material have thus been identified as the gauge, grain size and the niobium content.

In light of the fact that both the gauge and grain size have squared relationship with the sag value, the regression analysis included the square and inverse square of all of the parameters. The most simplistic model obtained (table 4.6), had an adjusted correlation coefficient (R.SQ. (ADJ.) = adjusted for the number of independent variables in the model) of 0.7777. This means that the model accommodates approximately 78 percent of the variance observed in the data. The standard error of estimate (SE) is the calculated square route of the residual mean square and gives an indication of the unexplained variability of the dependent variable. The mean absolute error (MAE) is the average error to be expected in a prediction and in this case it is 2.94. The model thus predicts a sag value plus or minus 3mm. The Durban-Watson

statistic is included for reference and is a measure of the serial correlation of the residuals (normally used for time based statistics).

Table 4.5

Change in correlation coefficients due to the inverse squared value of grain size.

Parameter	(Sag*Gauge^2)/Constant	1/Calculated grain size^2	Nb
(Sag*Gauge^2)/Constant	1.00	0.72	0.56
1/Calculated grain size^2	0.72	1.00	0.41
Hot Gauge	-0.06	0.07	-0.23
Reheat Retention Time	0.10	0.03	0.00
Discharge Temperature	0.32	0.51	0.48
Number of Passes on Hot Mill	-0.06	-0.13	0.16
Max. Last Pass Temp	0.34	0.50	0.41
Ave. Last Pass Temp	0.37	0.49	0.43
Down Coil Temp	0.41	0.44	0.36
Hot Band Line Speed	0.00	-0.13	-0.05
Hot Band Time at Temp	0.24	0.16	0.39
Hot Band Strip Temp	-0.09	-0.23	0.11
Cold Band Final Line speed	0.00	-0.24	-0.16
Cold Band Final Time at Temp	-0.02	0.06	0.20
Cold Band strip Temp	0.38	-0.53	-0.18
C	-0.02	0.01	-0.12
Mn	0.09	-0.06	0.10
Si	-0.04	0.18	-0.09
Ti	0.13	0.17	0.47
Mo	0.07	-0.02	-0.02
Cr	-0.06	-0.03	-0.12
Nb	0.56	0.41	1.00
Calculated Reheat Nb	0.51	0.34	0.92
Calculated Down coil Niobium	0.52	0.41	0.94
% Cold Reduction	0.03	-0.16	-0.02

Table 4.6

Most simplistic model.

Independent variable	coefficient	std. error	t-value	sig.level
CONSTANT	-8.451	1.0367	-8.152	0.0000
1/grainsize^2 (mm)	0.0023	0.0003	7.2059	0.0000
13/Final Gauge^2 (mm)	1.037	0.0476	21.776	0.0000
4*Nb^2 (Mass %)	5.0366	1.05	4.7969	0.0000
R. SQ. (ADJ.) = 0.7777				
SE = 4.256472	MAE= 2.940791		DurbWat= 1.498	
177 observations fitted, forecast(s) computed for 0 missing val. of dep. var.				

Std. Error = standard error of the coefficients **t-value** = coefficient/std.error

Sig.level = probability that if no contribution was made by that variable a larger absolute t-value would occur.

The model does not appear to give the full picture of the interaction between niobium, grain size and the sag observed. It would be expected that as the niobium content increased the sag would decrease, due to either more residual niobium in solution (solid solution strengthening) or more niobium available to form the laves phase to inhibit sagging. This is not observed and it is felt that niobium has a more significant effect on the grain structure either by pinning of the grain boundaries (due to precipitates) or by the retardation of recrystallization and grain growth due to solute drag [75]. A model that attempted to relate the sag value to a greater number of processing parameters was formulated and is discussed in Appendix 2.

4.2 Precipitate morphology and composition at the various production stages.

The morphology of the precipitates at every stage from the tundish to the final cold rolled product was investigated. The morphology of the precipitates was determined by electrolytically deep etching as this gave a three dimensional view of the precipitates. The samples were examined in an electron microscope and Energy Dispersive Spectroscopy (EDS) analysis was performed on the precipitates.

4.2.1 Tundish sample

The tundish sample[1] is a molten sample (+/- 1500 ^{O}C) taken from the tundish that is rapidly solidified (air cool followed by a water quench). The tundish sample was taken in order to determine if any second phase existed in the liquid at this temperature.

Figure 4.3: SEM micrograph exhibiting the general morphology of the precipitates found in the tundish sample (1500X)

The tundish sample exhibited fine precipitates (less than 15 microns in size, figure 4.3) with a composition consisting primarily of niobium. It is uncertain if iron and chromium are present as they are expected to occur in the spectrum due to the large interaction volume of the beam with the specimen (spectrum 4.1). The general shape of the precipitates are plate-like and cruciform (figure 4.3). The absence of titanium carbonitrides concurs with literature [76,23] that these would be in solution at this temperature. The presence of a niobium rich or pure niobium phase at these temperatures does not appear to have been reported. The presence may in itself not be

[1] Columbus Stainless Heat 312218

strange as niobium melts at a temperature of 2468 ^{O}C and could possibly have segregated within the melt to form the precipitates.

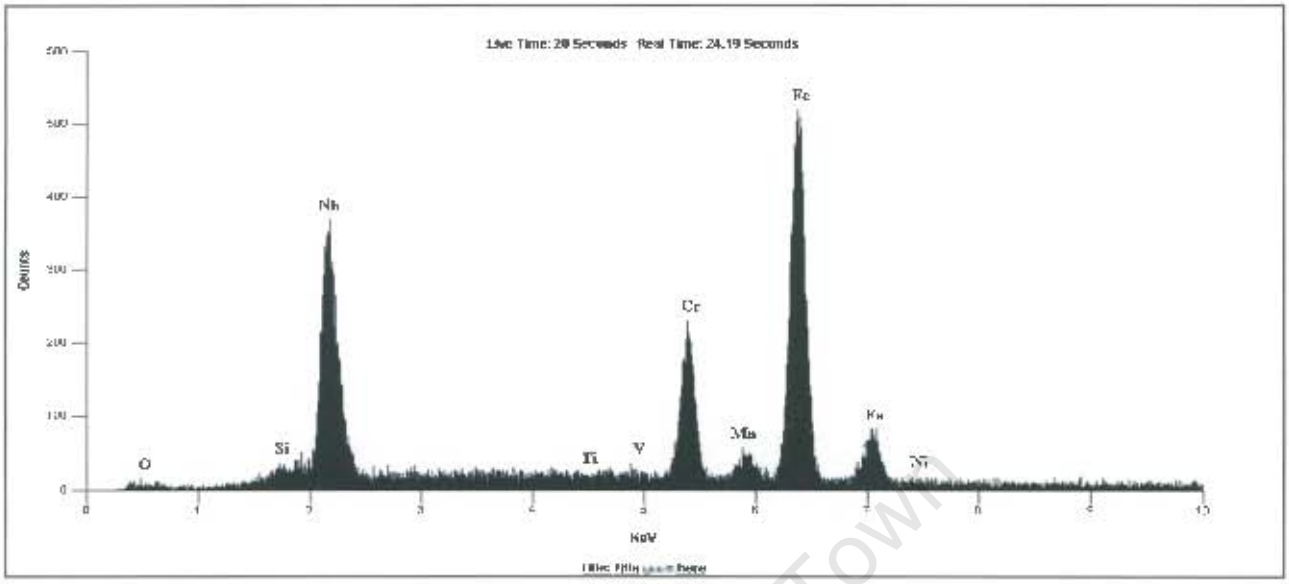

Spectrum 4.1 EDS analysis of the precipitates present in the tundish sample.

4.2.2 As -cast sample

The as-cast structure obtained from a slab sample[2] exhibited larger precipitates than were observed in the tundish material (figure 4.4). The niobium has attached itself to the titanium carbonitrides that have formed during solidification. The niobium has precipitated out as nodules or platelets mainly on the sharp corners of the titanium precipitates (figure 4.4A and 4.4B). The precipitates are therefore a composite consisting primarily of a titanium core (presumably carbonitride (spectrum 4.2A)) with protrusions of niobium (presumably carbonitrides (spectrum 4.2B)). The titanium precipitates appear mostly as clusters.

[2] Columbus Stainless slab material from MPO 3295803

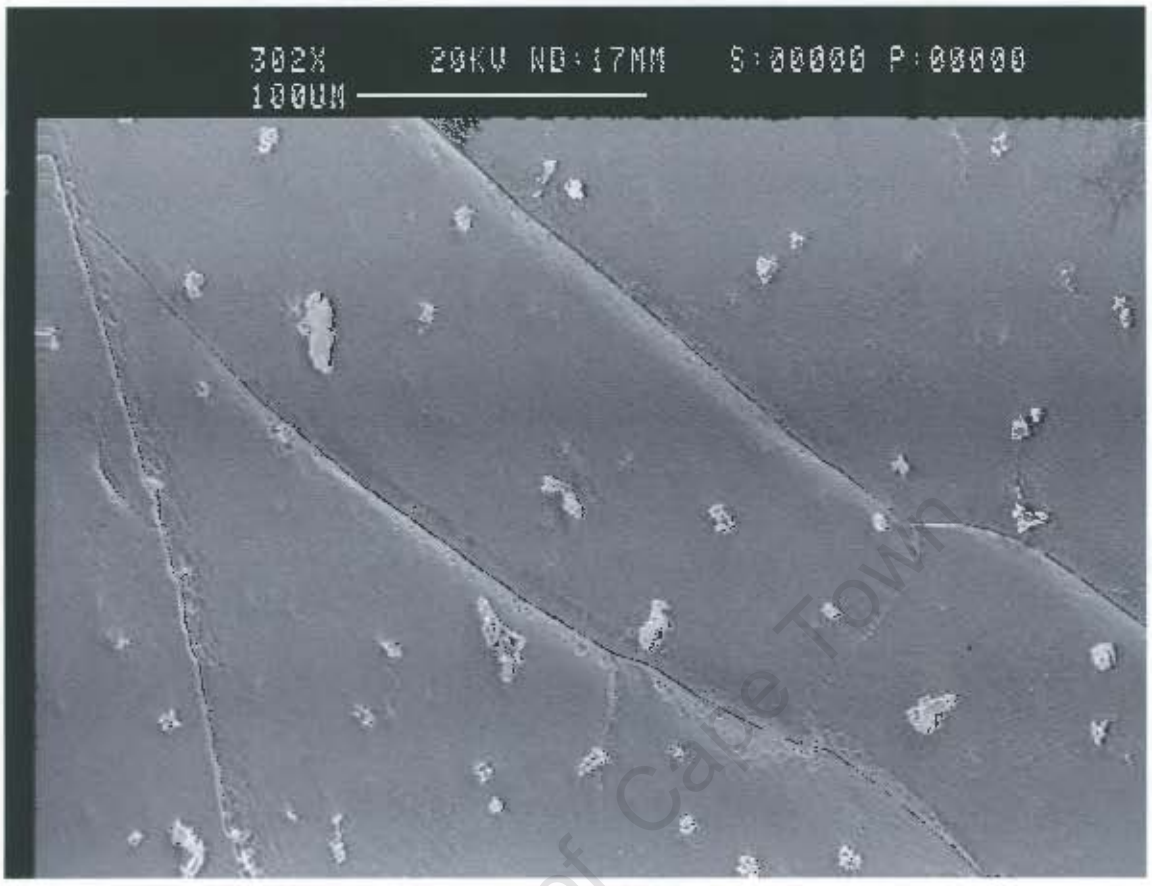

Figure 4.4: SEM image of the general distribution and morphologies of precipitates in the as-cast material after deep etching.

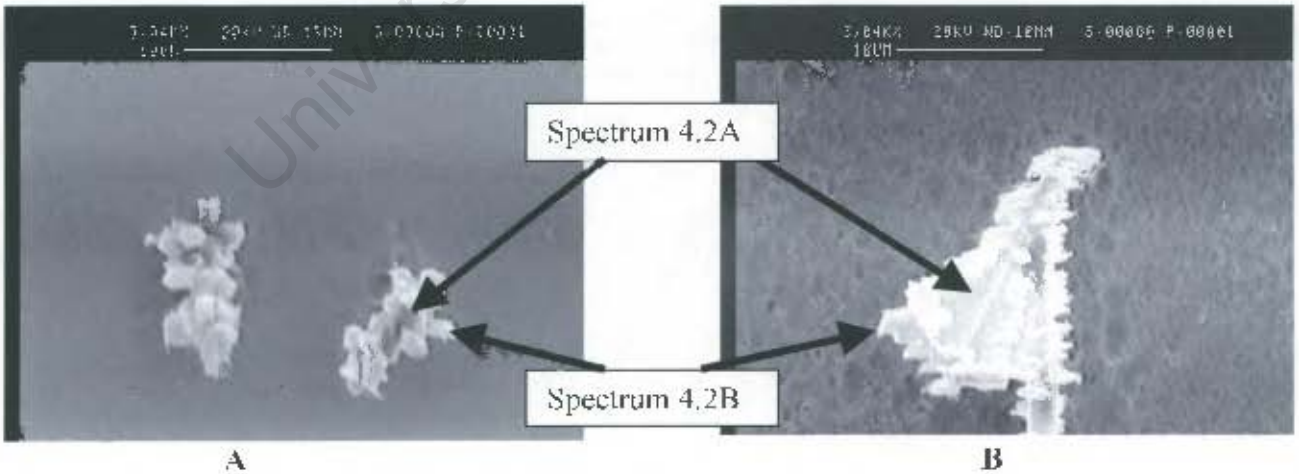

Figure 4.4: A and B: SEM images of the representing the typical precipitates in the as-cast material after deep etching.

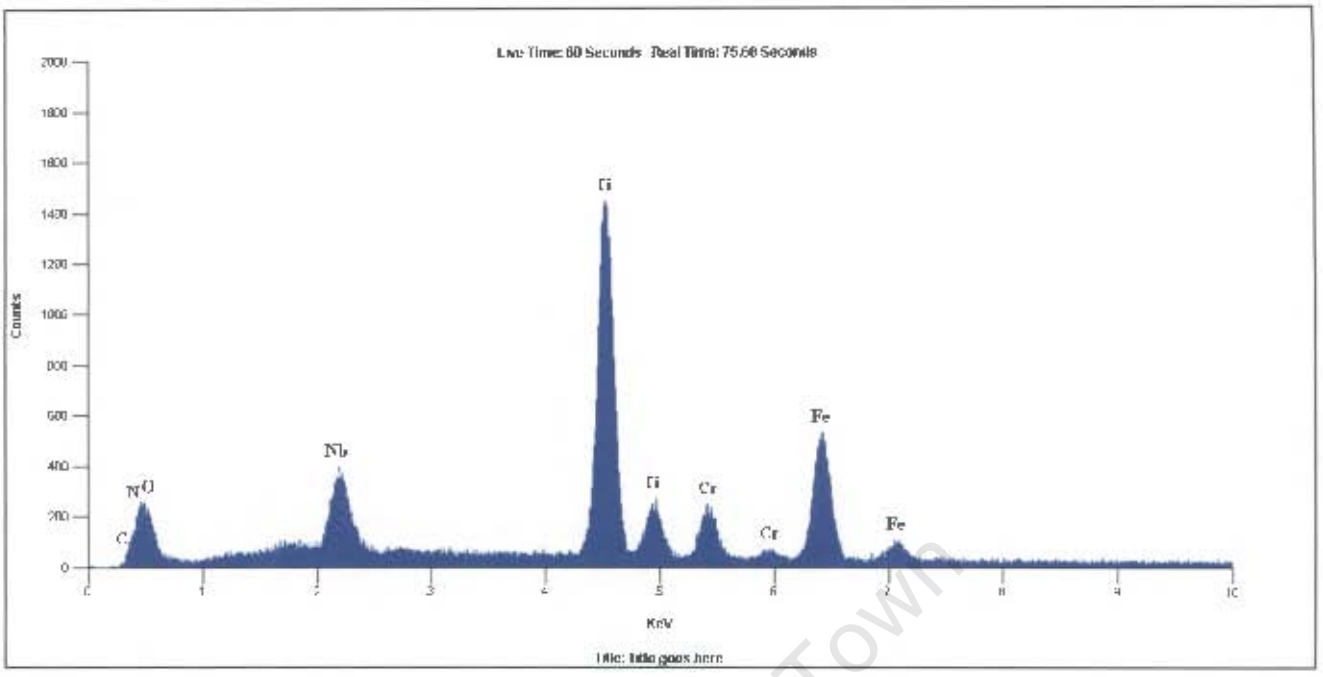

Spectrum 4.2A: Spectral analysis of the titanium inner core of many of the precipitates in the as-cast material.

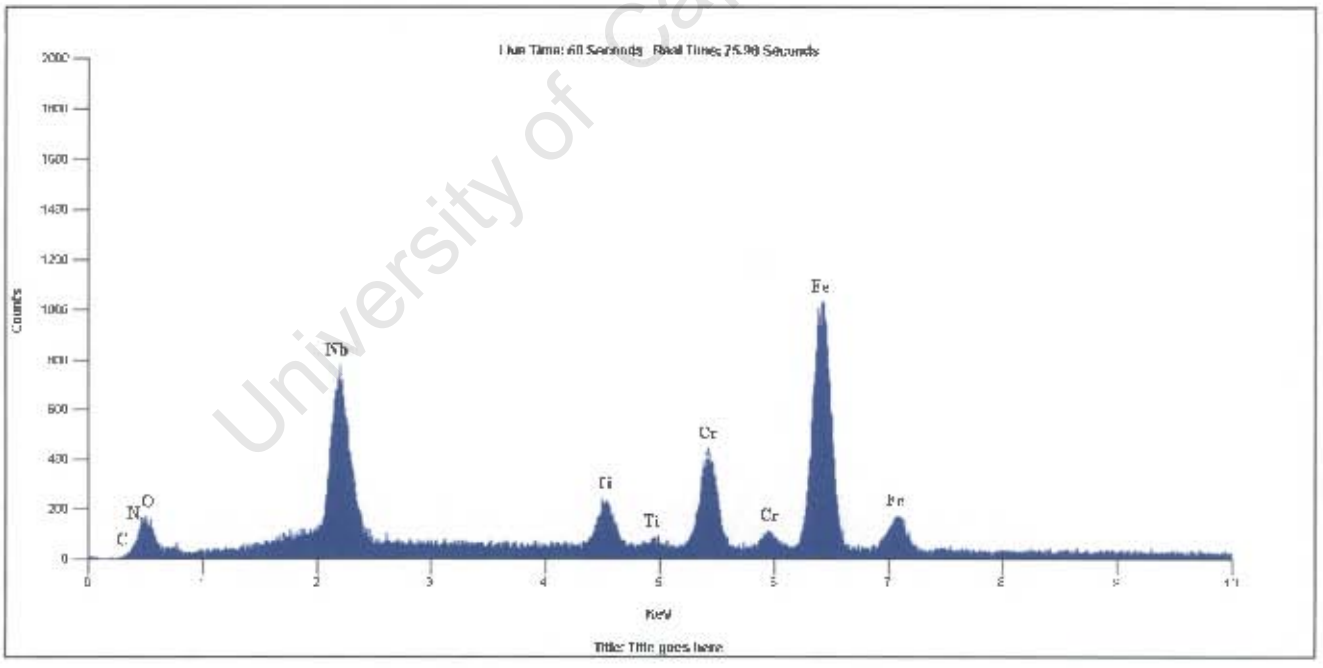

Spectrum 4.2B: Spectral analysis of the niobium protrusions observed on many of the precipitates in the as-cast material.

4.2.3Transfer bar sample

The transfer bar (approximately 28mm thickness) represents the transition stage between the roughing mill and the hot finishing mill (Steckel mill). The material has been reduced from 200mm in approximately seven passes and has cooled from about 1090°C (reheat furnace drop-out temperature) to approximately 950°C prior to quenching. The transfer bar exhibited precipitates consisting primarily of titanium (carbonitride) containing cuboids surrounded by nodules of precipitates consisting primarily of niobium (figure 4.5, 4.5A 4.5B). EDS analysis of the precipitates (core and protrusions) is similar to that found in the as-cast structure; however, the chromium and iron peaks are lower (spectrum 4.3A and 4.3B) and this could be a function of the larger size of the precipitates as the beam is probably analyzing more of the precipitate than the matrix material. It is at this stage that the cuboid titanium precipitate is present in rather large numbers and persists through all of the process stages. The reheating at approximately 1090°C modifies the morphology of the precipitates and it could be postulated that titanium carbo nitrides grow/form preferentially, these in turn form preferential energy sites for niobium precipitation.

4.2.4 Hot band sample

A sample was taken from a hot rolled coil[3] prior to annealing. This material has been rolled down from approximately 28mm to 3-6mm in 5-7 passes with a final pass temperature of approximately 850 °C. The strip is then rapidly cooled (to avoid the laves phase transformation temperature range) to approximately 650°C by means of laminar cooling with water and is then coiled. The coil is left to cool for 3-5 days to approximately 50 °C before further processing. Two differently shaped precipitates could be identified in the hot rolled material. These consisted of the same cuboids found in the transfer bar (figure 4.6A) and a plate like precipitate (figure 4.6B). The plate like precipitates were not as abundant but had a similar composition as the protrusions surrounding the titanium precipitates and consisted primarily of niobium. The possibility exists that this precipitate is a laves phase, although these reportedly only start forming at approximately 700 °C.

[3] Columbus Hot rolled coil number 3122184

Figure 4.5: Deep etch of transfer bar material

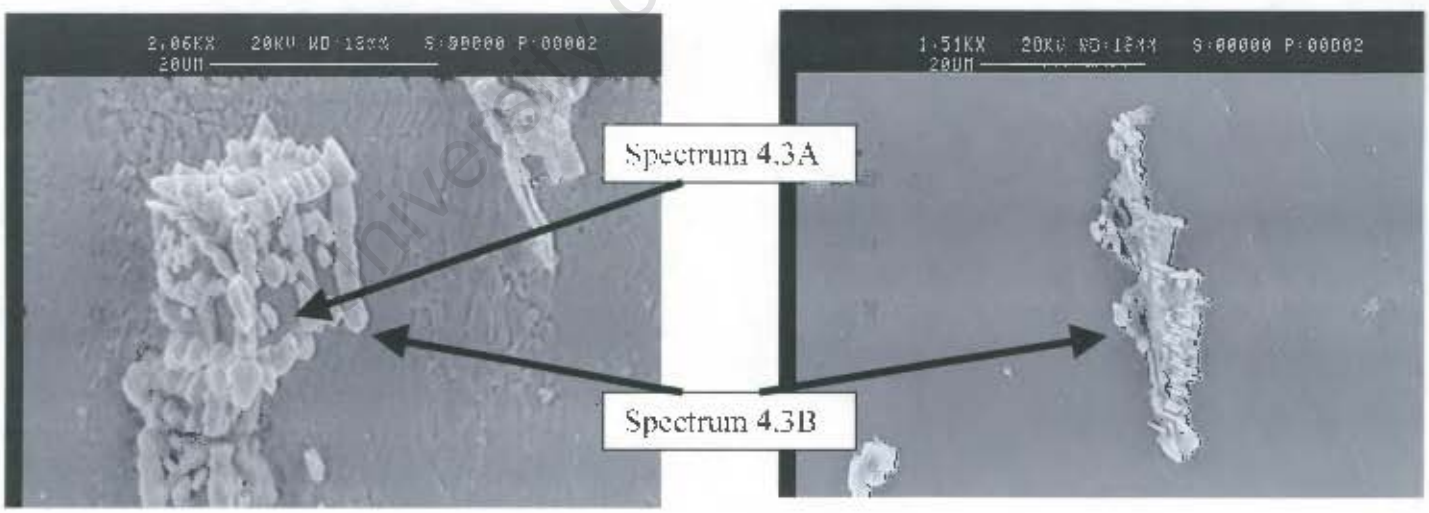

A **B**

Figures 4.5 A and B: Deep etch of two types of different morphologies of pits identified on the transfer bar material.

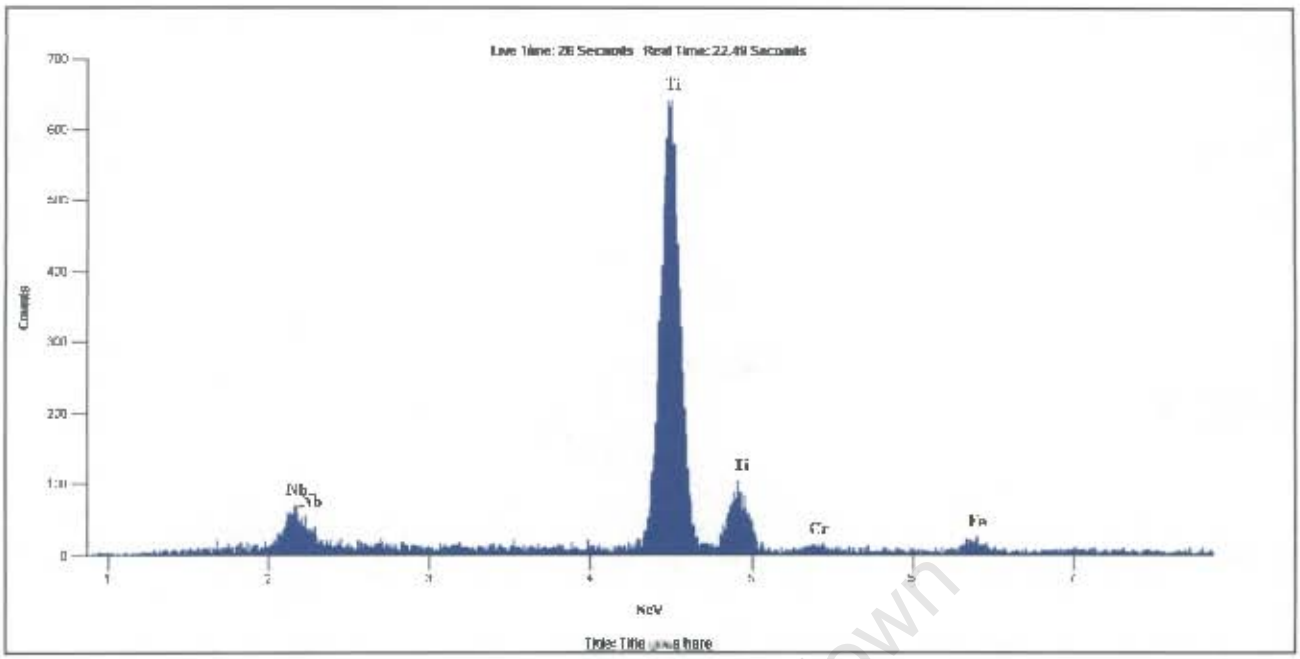

Spectrum 4.3A: Spectrum analysis of the core of the precipitates in the transfer bar sample exhibiting mainly titanium

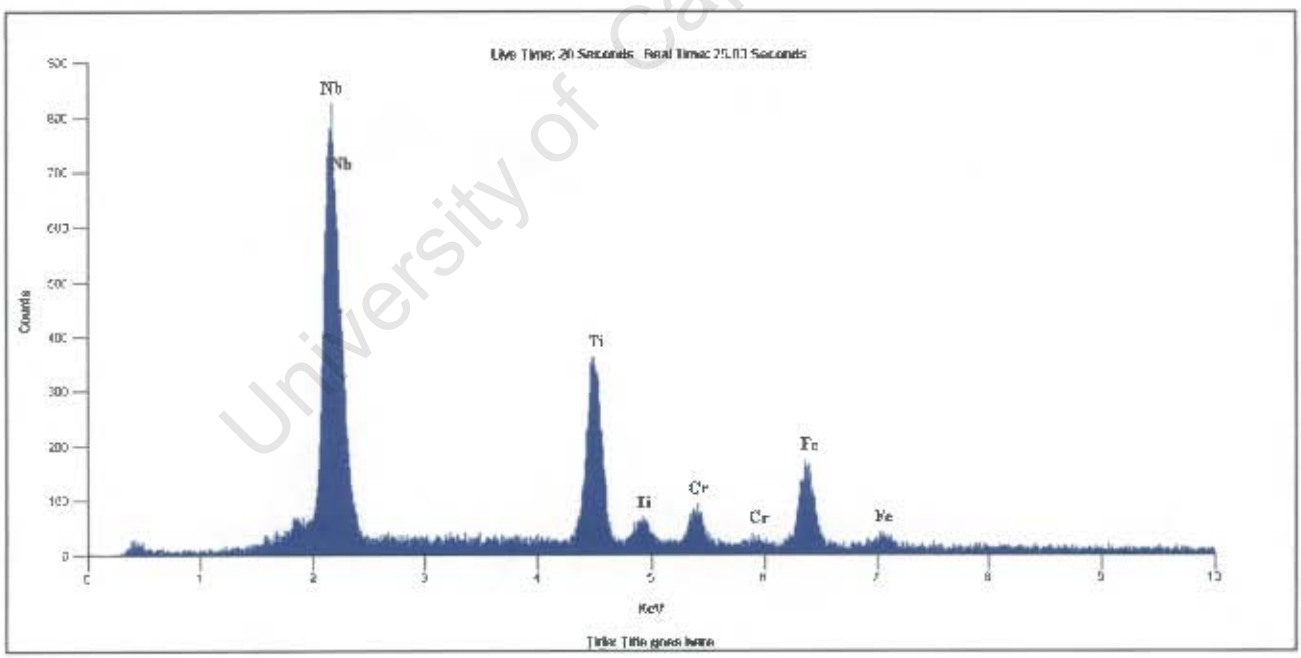

Spectrum 4.3B: Spectrum analysis of the protrusions seen on the precipitates in the transfer bar showing that they contain mainly niobium

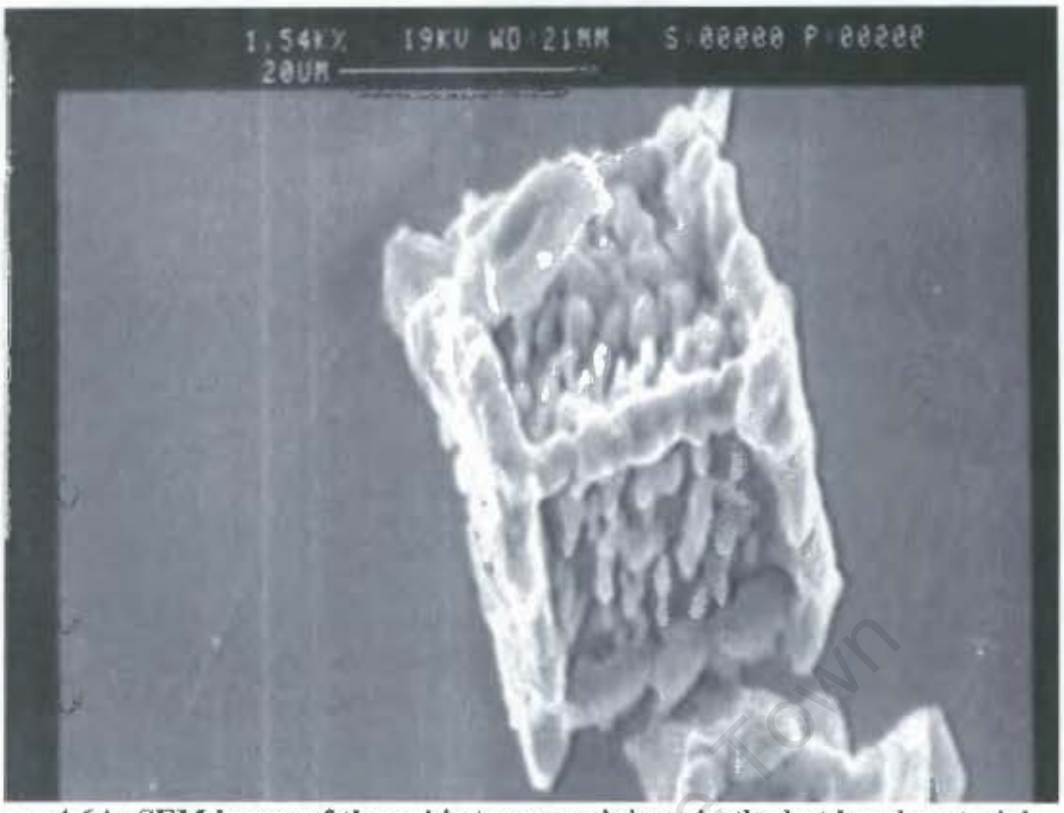

Figure 4.6A: SEM image of the cubic type precipitate in the hot band material.

Figure 4.6B: Image of the plate like precipitates – possibly laves phase in the hot band material.

4.2.5 Hot rolled and annealed sample

The hot rolled and annealed (950°C) sample[4] exhibited precipitates (figure 4.7) similar in shape and chemistry as that obtained after hot rolling. The number of fine niobium rich precipitates, however, appeared to be significantly more.

4.2.6 Cold Rolled Material

The cold rolled (approximately 70 per cent cold reduction) and annealed (approximately 1050 °C) material[5] after deep etching once again revealed (figure 4.8) precipitates predominantly rich in niobium and titanium (see spectrum 4.5 A and B). The cuboid clusters present after hot rolling have been broken down into stringer precipitate arrays. The fine randomly distributed precipitates were analyzed as mainly consisting of niobium (spectrum 4.5A). The semi-quantitative analysis also picked-up iron and chromium although this is assumed to come from the surrounding matrix material.

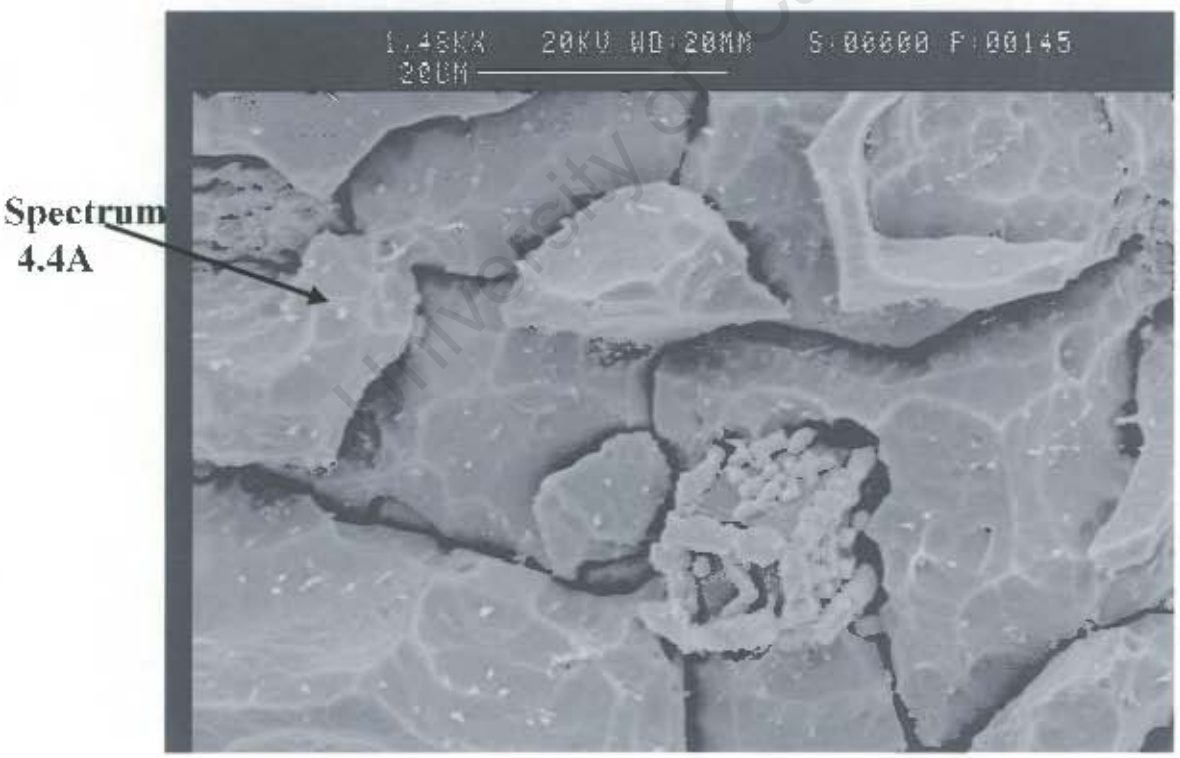

Figure 4.7: SEM image of the hot band annealed deep etched structure.

[4] Columbus Hot Rolled and annealed Material MPO 3290782
[5] Columbus Final Material MPO 3287411

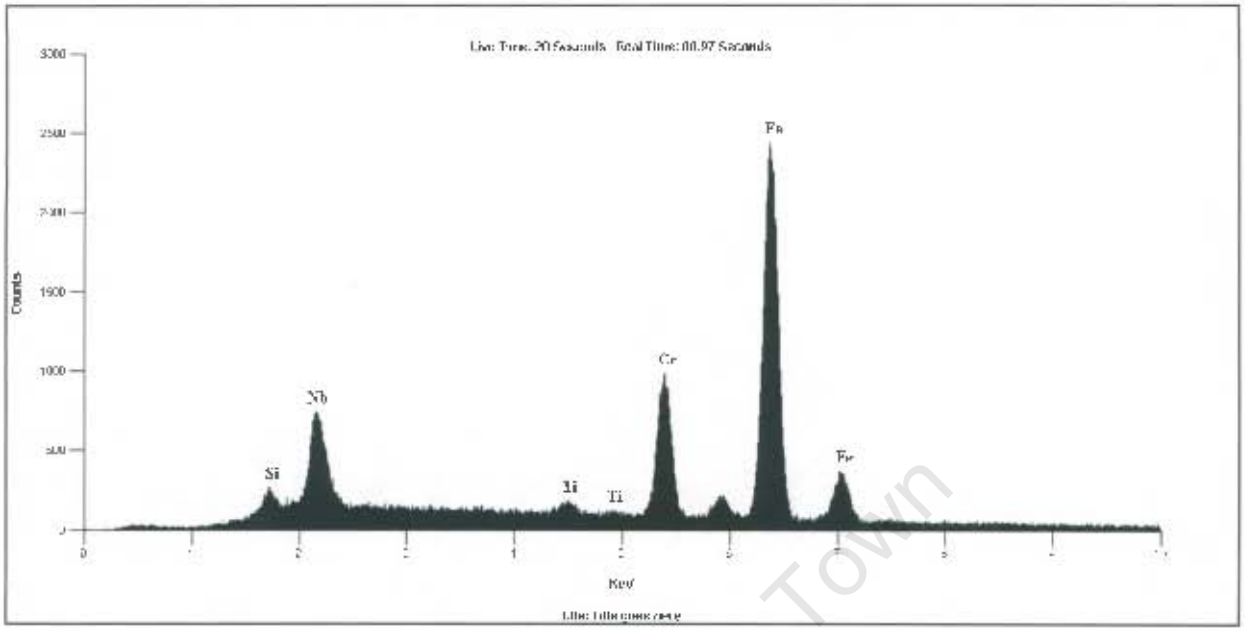

Spectrum 4.4A: EDS analysis of the fine precipitates in the hot band annealed material after deep etching.

Spectrum 4.5A

Spectrum 4.5B

Figure 4.8 SEM image of precipitates present in final cold rolled and annealed material after deep etching.

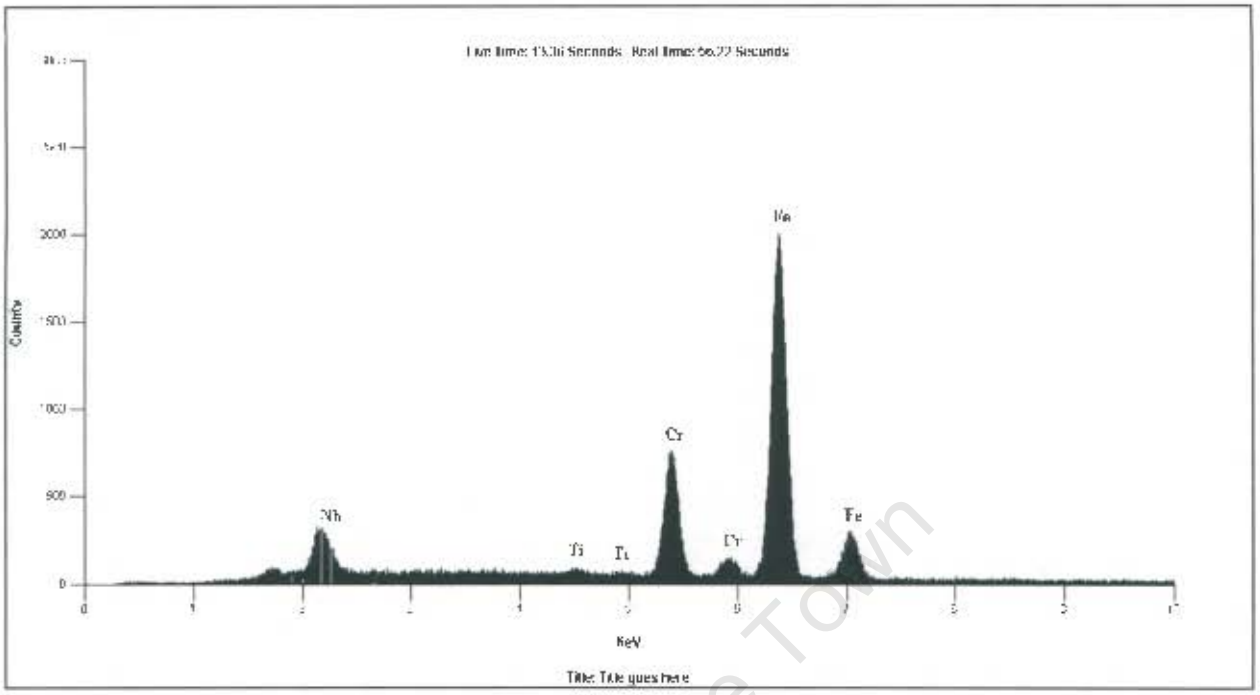

Spectrum 4.5A: EDS analysis of the small precipitates as marked in the figure 4.8 above.

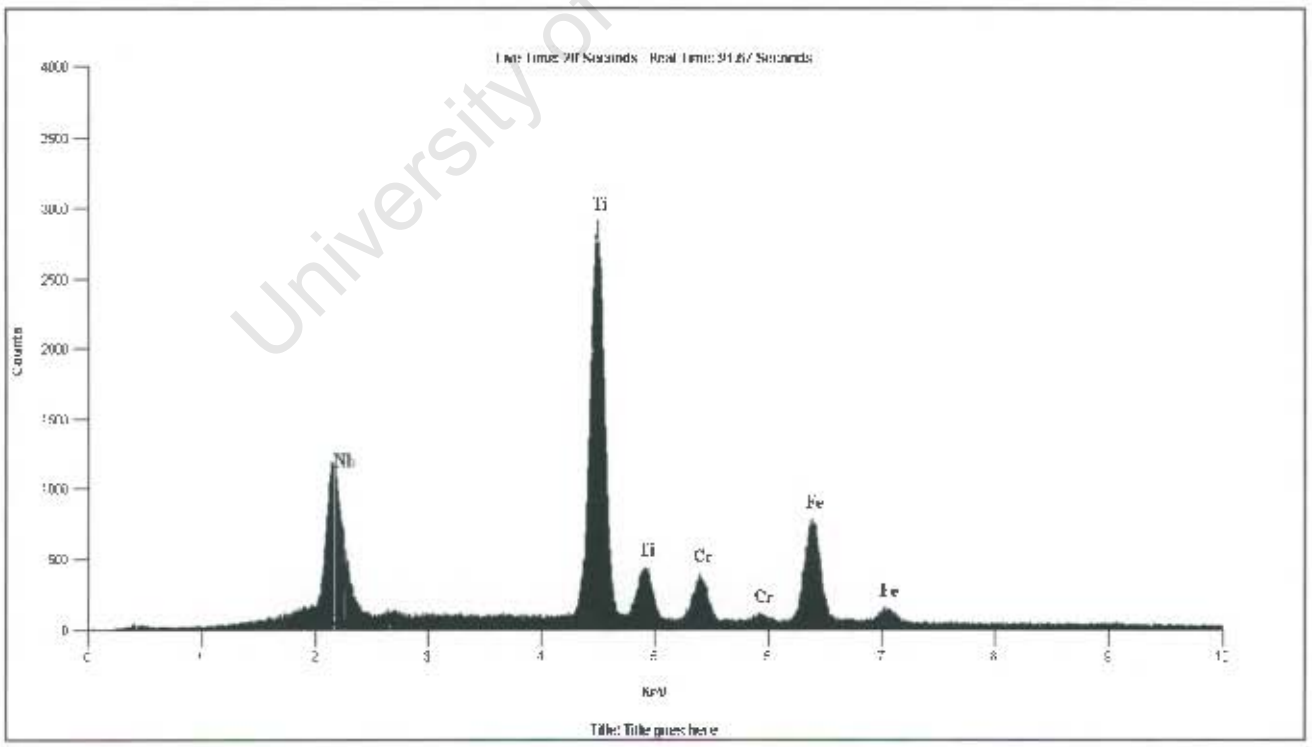

Spectrum 4.5B: EDS analysis of precipitate at position 4.5B in the SEM figure 4.8 above.

Chapter 5 Experimental results

5.1 Experimental heat treatment of cold band material

A particular production heat of as-cold rolled sheet was subjected to various heat treatments in the laboratory to investigate the affect that annealing time and temperatures has on the following metallurgical properties:

- Area percent of precipitates
- Grain growth characteristics
- Sag resistance

In addition the dissolution of the laves phase was investigated after sag testing. The possibility of increasing the sag resistance was explored by altering the final annealing practice, as well as by introducing an ageing treatment.

The cold rolled material had received a cold reduction of 75 per cent and had a gauge of 1.59mm. The micrographs of this material annealed at various times and temperatures are given in appendix 3.

5.1.1 Effect of annealing temperature on the second phase area fraction.

The cold rolled material[1] generally did not appear to exhibit a significant change in the volume fraction of precipitates for the time and temperatures investigated (figure 5.1A and 5.1B). The second phase area fraction appears to show a possible increase in the second phase for material tested at 975°C and below after approximately 1000 seconds. In addition a visual qualitative analysis of the micrographs indicated that the material exhibited a significant amount of very fine small precipitates at temperatures below 1000°C than above this temperature (appendix 3).

[1] Columbus cold rolled material number 3193754

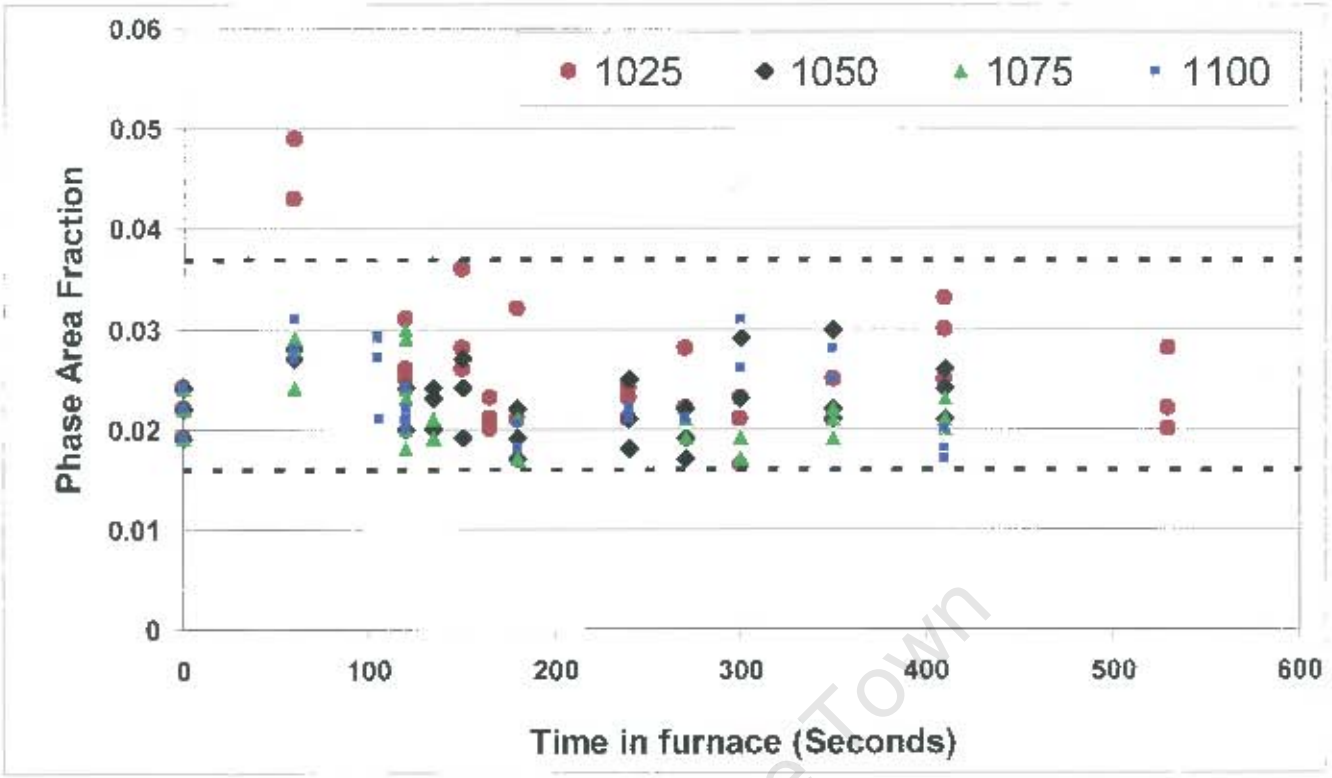

Figure 5.1A: Phase percent at various times and temperatures.

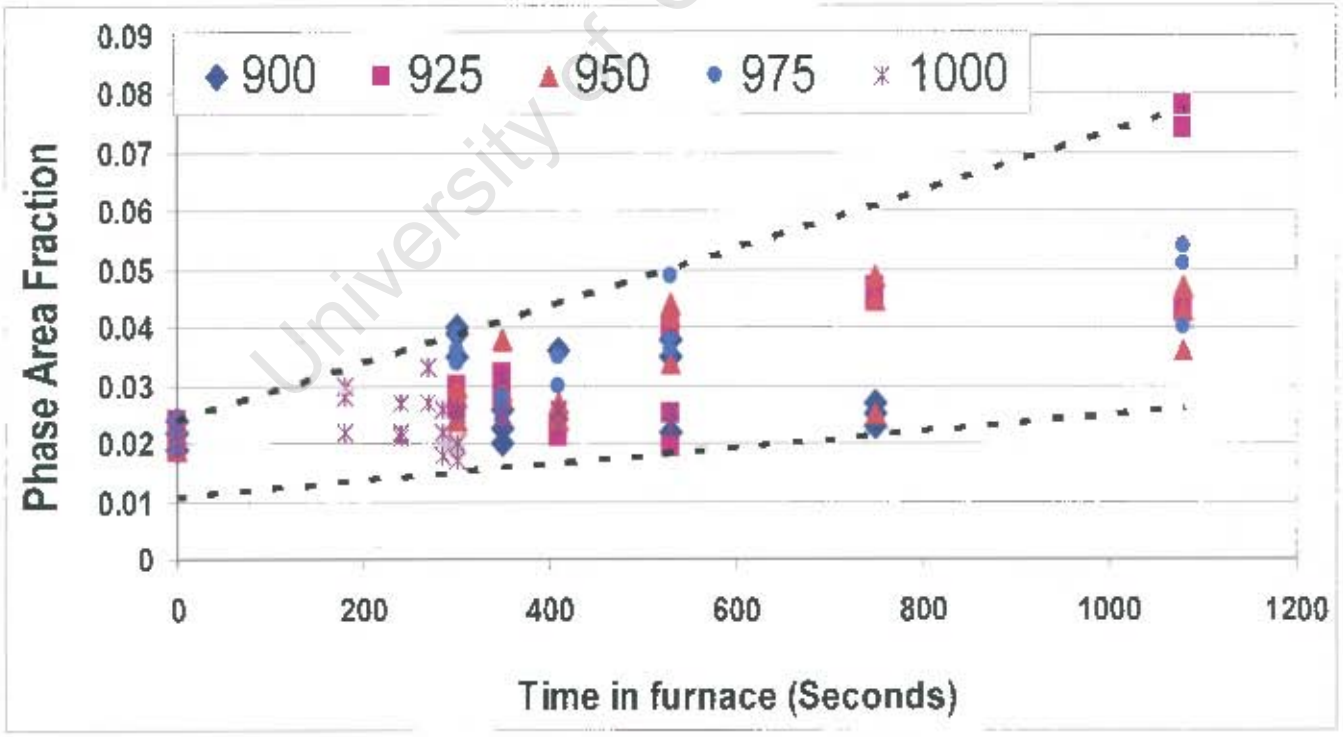

Figure 5.1B: Phase percent at various times and temperatures.

5.1.2 Grain growth in cold rolled material

The grain growth (including recovery and recrystallization) of the cold rolled material was investigated and it was found that by using an exponential relationship the time required to obtain a certain grain size at a fixed temperature could be mathematically simulated. The mathematical relationship (using the data in appendix 4) is given as:

$$t = Ke^{nDg}$$

Where:

t = is the annealing time in seconds for the time in the furnace.
D_g = the average grain diameter in millimeters and
K and n are constants, which depend in this case on the annealing temperature.

The values for K and n (table 5.1) can be determined by plotting the natural log of the annealing time against the average grain diameter. The data in the temperature range 950 to 1100 ^{O}C was used as no significant grain growth occurred at 900 and 925 ^{O}C. The expression enables an accurate prediction of grain size for the production cold rolled material at different temperatures (figure 5.2). The above approach included the recovery and recrystallization that the material would observe during normal annealing of cold rolled production material. This is unlike the approach commonly used in literature, where grain growth is considered on its own.

Table 5.1

Values for K and n in the exponential grain size Equation.

Temperature (^{O}C)	n	K	R = Cor. Coef.
1100	23.77	43.28	0.858
1075	27.58	42.37	0.912
1050	33.00	40.77	0.688
1025	50.83	26.02	0.819
1000	43.54	63.14	0.768
975	141.80	13.26	0.849
950	212.75	5.39	0.990

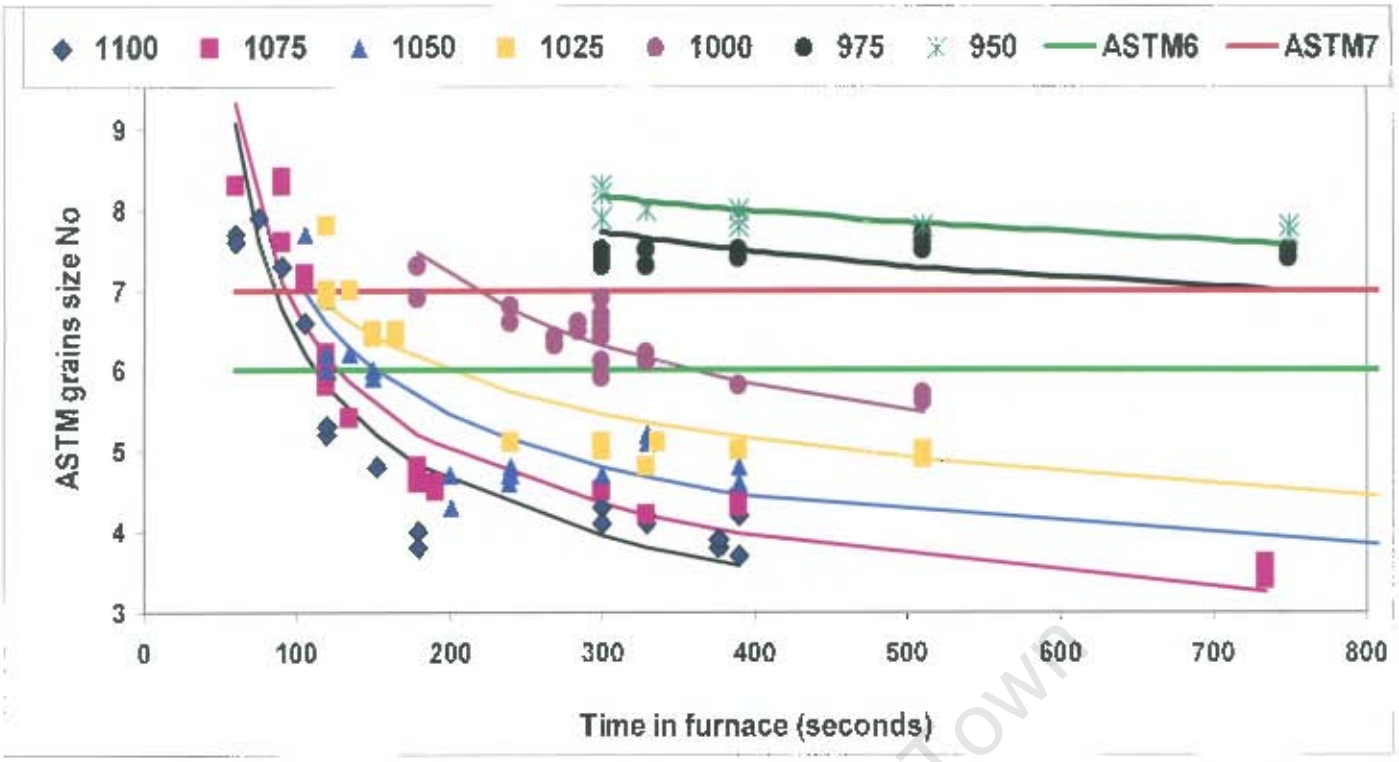

Figure 5.2: Grain growth in cold rolled material.

The general formula normally [7.1] found to correlate with experimentally obtained data to describe the increasing grain size after initial primary recrystallization is a simple parabolic equation (empirical kinetic relationship):

$D_g = Kt^n$

Where:

t = is the annealing time in seconds for the time in the furnace.
D_g = the average grain diameter in millimeters and
K and n are constants, which depend in this case on the annealing temperature and metal's composition.

This equation was not used in this case as all of the data obtained included the effect of recovery and recrystallization and the above equation is reportedly only valid for pure grain growth. The equation was, however, applied to the present data to observe what the correlation would be. The time exponent (n) is normally found to lie between 0.05-0.5[7.1]. In addition it was found to increase in value as the temperature increased. A similar trend was found for the present data (table 5.2). The data used in this

analysis excluded any values in time below 270 seconds, as this is approximately the time required for the present steel to reach temperature [7.2]. It is assumed that for these longer times the affect of recovery and recrystallization can be minimised to some extent.

Table 5.2

Values for K and n in the parabolic grain size Equation.

Temperature (^{O}C)	n	K	R = Cor. Coef.
1100	0.4319	0.00631	0.427
1075	0.3628	0.00861	0.888
1050	0.1915	0.01956	0.686
1025	0.1458	0.02411	0.913
1000	0.5303	0.00170	0.596
975	0.1650	0.00901	0.808
950	0.1415	0.00873	0.988

The derivation from basic principles of grain growth after primary recrystallization has been done by various authors [7.1]. The formula postulated by Burke is;

$$D_g^2 - D_g^2(0) = 2c_1 t e^{-Q_g/RT}$$

Where:

D_g – the average grain size diameter

t = the annealing time

c_1 – a constant that includes the grain-boundary specific interfacial energy

Q_g = the activation energy for grain boundary migration

R = the Universal (international) gas constant = 8.314 X 10^4J/(kg)(mole)(deg)

T = the absolute temperature

The data that has been obtained by experimental means to determine the grain size of the material includes all aspects relating to the recovery, recrystallization and grain growth as it would pertain to heating a specimen in a laboratory furnace. The analysis of the data by using the above equation to determine the activation energy for grain boundary migration is therefor incorrect. The above equation can, however, be used to

determine a single activation energy [7.3], which can be used to indicate if any fundamental change in the activation energy has occurred. The activation energy required to obtain an average ASTM grain size of 6 was determined by plotting the natural log of time against the inverse of the absolute temperature (figure 5.3). The plot should theoretically give a straight line from which the activation energy can be determined. In this case a point of inflection is noted at approximately 1007^{O}C. This appears to indicate in general terms that there is a significant difference in the recovery, recrystallization and grain growth characteristics of this material above and below approximately 1000^{O}C. This change in activation energy, in addition, is significant as it is an order of magnitude larger below 1000^{O}C than it is above 1000^{O}C 1114kJ/mole and 113kJ/mole respectively (gradient of curve multiplied by the Universal gas constant).

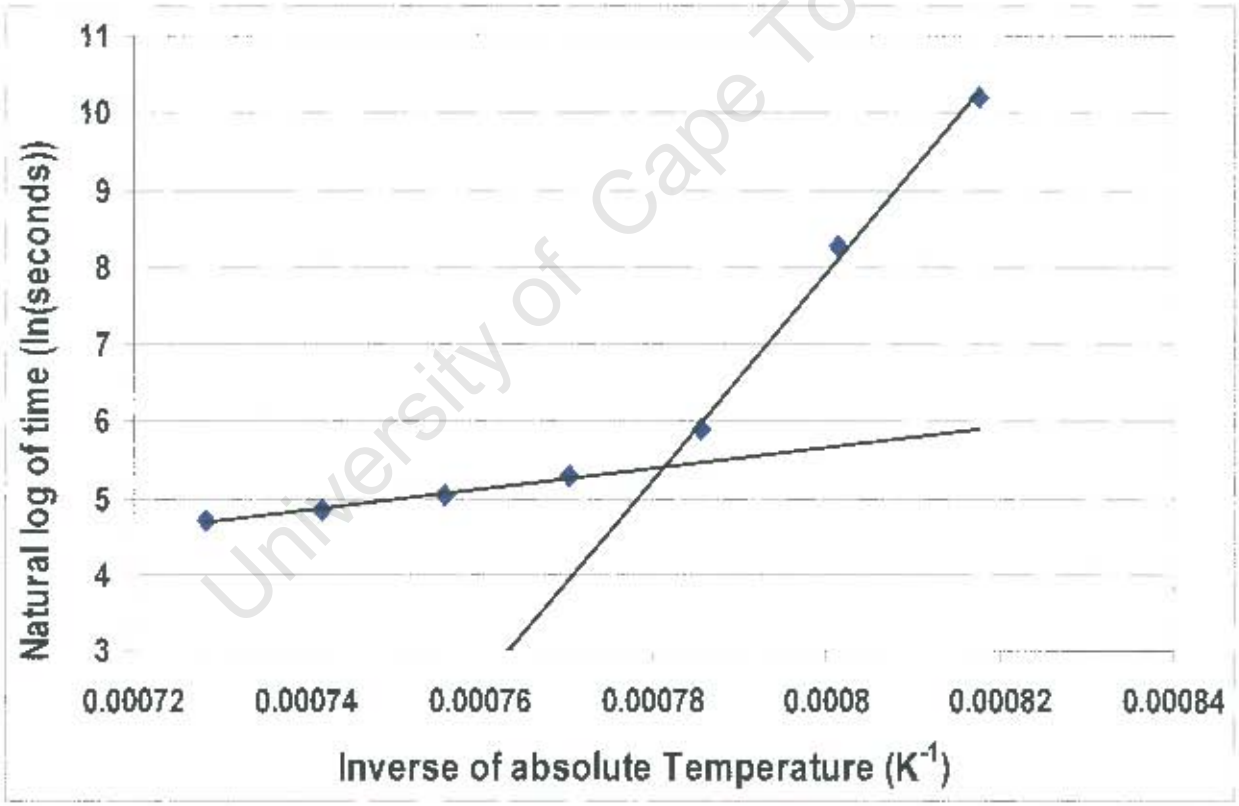

Figure 5.3: Plot of the Ln (time) versus the inverse of the absolute temperature for a fixed grain size to determine the activation energy.

5.1.3 Sag resistance of material after various experimental heat treatments on cold rolled material.

Two lines of investigation were followed. The initial was to obtain an optimum annealing cycle with a single anneal to obtain the maximum resistance to sag. The second was to identify if the sag resistance could be enhanced by a secondary temper or ageing treatment to promote the precipitation of a secondary phase prior to testing. In addition, the production material appeared to indicate a rather strong link between the final anneal and the sag resistance of the material. This part of the investigation would also determine if this link exists after experimental heat treatments.

Material[2] after cold rolling was heat-treated in the temperature range 925 °C to 1100°C to obtain an ASTM grain size of between 3 and 8. The data collected for sag testing after annealing is presented in figure 5.4. Although significant scatter is present, there is a general increase in sag resistance with an increase in grain size.

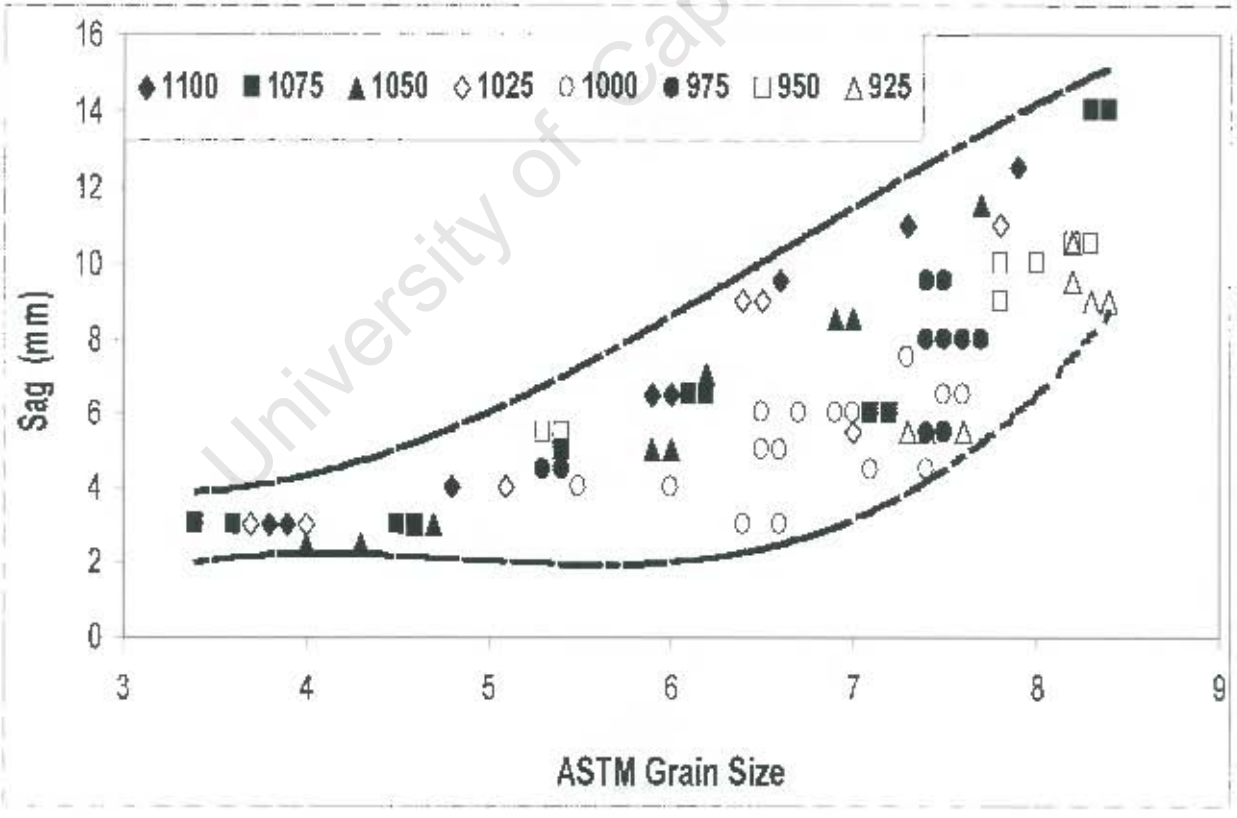

Figure 5.4: The experimental results of the effect of various heat treatments and grain size on the sag value.

[2] Columbus heat number 319375

5.1.4 Statistical analysis of experimentally annealed cold band material

The correlation coefficient was calculated, by means of the Statsgraphics package [7.4] for following parameters obtained for the cold rolled experimentally annealed material:

- Sag
- Time in furnace (seconds)
- Furnace set temperature (^{O}C)
- Niobium in solution using the set temperature and
- The calculated grain size, linear intercept length (mm).

Table 5.3

Correlation Coefficients for the experimentally annealed cold rolled material.

Parameter	Sag	1/Temp	1/Time in Furnace	1/Grain Size	Niobium in Solution at Annealing Temp.
Sag	1	0.121	0.4949	0.7827	-0.0146
1/Temp	0.121	1	-0.7005	0.4728	-0.9342
1/Time in furnace	0.4949	-0.7005	1	0.1793	0.7086
1/Grain size	0.7827	0.4728	0.1793	1	-0.3773
Niobium in solution at annealing Temp.	-0.0146	-0.9342	0.7086	-0.3773	1

The calculated grain size was seen to have the greatest correlation with the sag followed by the time in the furnace (table 5.3), given that the grain size and time in the furnace are related, this observation is not surprising. The reasonable fit (multiple linear regression analysis) for the data was obtained by using only these parameters (table 5.4, figure 5.5). The model obtained from experimental annealing of cold rolled material is thus:

$$\text{Sag} = 2.866471 + 0.002348/\text{grain size}^2\ (\text{mm}) + 30056.038725/\text{Time in Furnace}^2\ (\text{sec})$$

Table 5.4

The sag model obtained from experimentally annealed cold band material.

Indcpendent variable	coefficient	std. error	t-value	sig.level
CONSTANT	2.866471	0.234489	12.2243	0
1/grainsize^2 (mm)	0.002348	0.000148	9.0784	0
1/Time in Furnace^2 (sec.)	30056.038725	3310.703799	15.8461	0
R. SQ. (ADJ.) = 0.7722				
SE = 1.307142	MAE= 1.02984	DurbWat= 0.787		
115 observations fitted, forecast(s) computed for 0 missing val. of dep. var.				

Std. Error = standard error of the coefficients **t-value** = coefficient/std.error

Sig.level = probability that if no contribution was made by that variable a larger absolute t-value would occur.

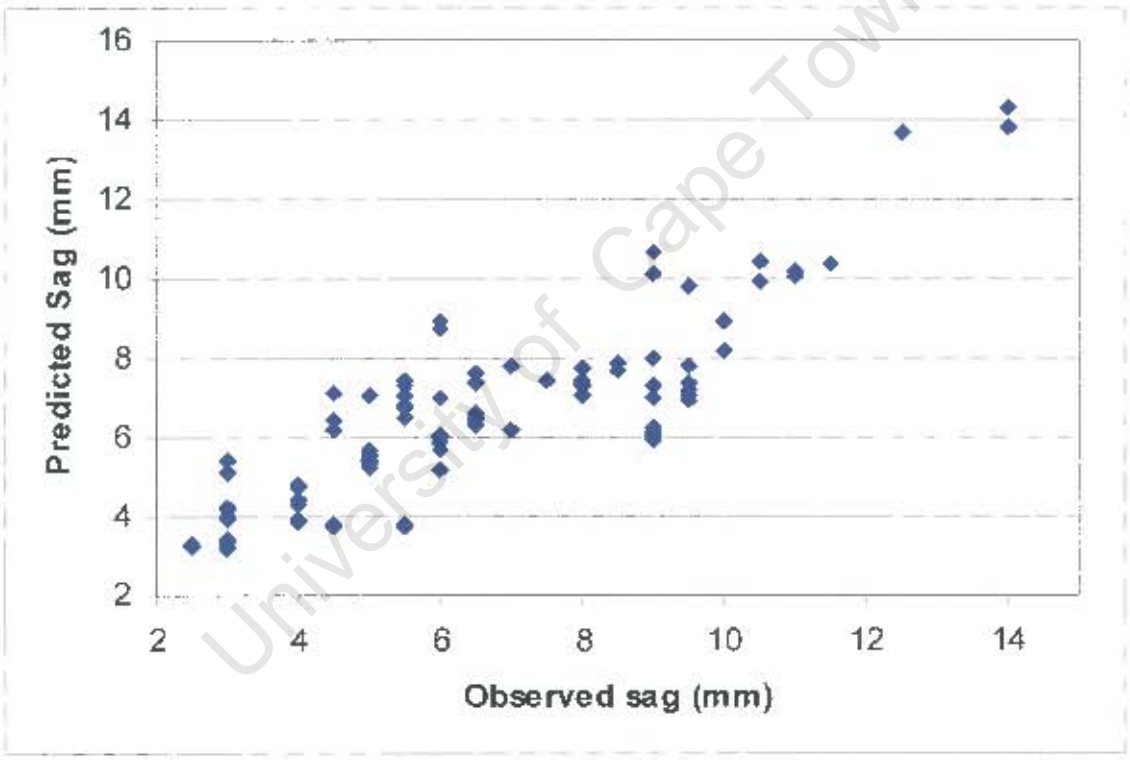

Figure 5.5: The predicted sag versus the observed sag for the model obtained by multiple linear regression.

5.1.5 Secondary ageing treatments applied to cold rolled annealed material.

The material that was aged (from 1 minute to 2hrs at temperature (140 seconds required for the material to reach temperature)) at various temperatures was initially

annealed at 1050^{0}C to obtain an average ASTM grain size of approximately 8. The logic followed for the smaller grain size (larger ASTM number) was that should the ageing prove successful, the result would be a significant increase in sag resistance at this fine grain structure. The sag values of the material in the annealed only condition were 8 and 13 for the two batches tested. The aged material appeared to indicate that there was a central zone (topographical plot, figure 5.6) at all temperatures in which the normalised sag resistance is increased slightly but, the majority of the sag values appeared to fall in the range of approximately 8-13mm indicating that the ageing treatments do not significantly improve the sag resistance.

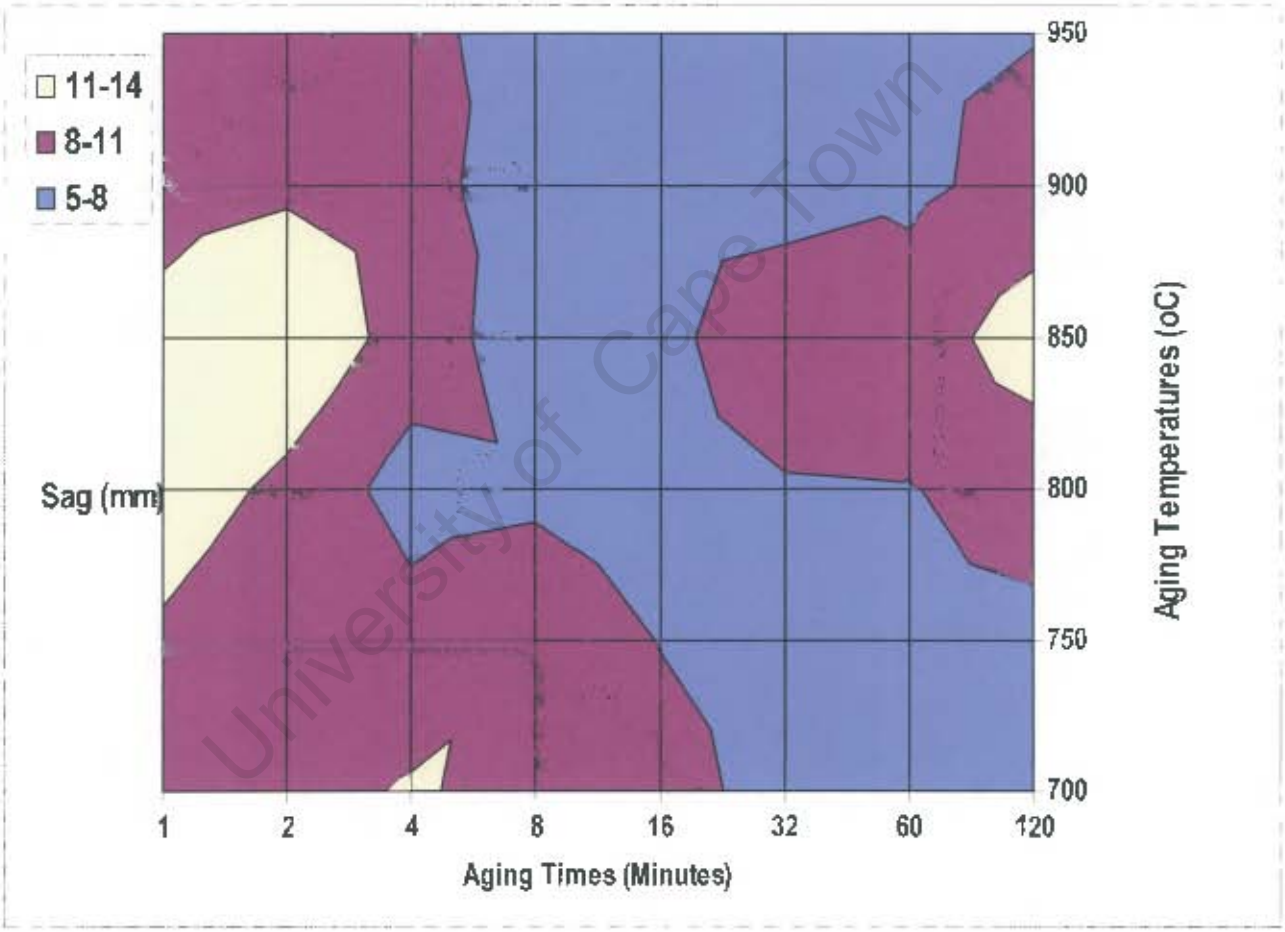

Figure 5.6: Topographical plot of the degree of sagging obtained at various ageing times and temperature.

A significant amount of precipitates formed in these steels after long periods of ageing at all the temperatures (particularly 750 and 800 ^{O}C), there is a much more obvious sprinkling of fine precipitates in figures 5.8 compared to figure 5.7.

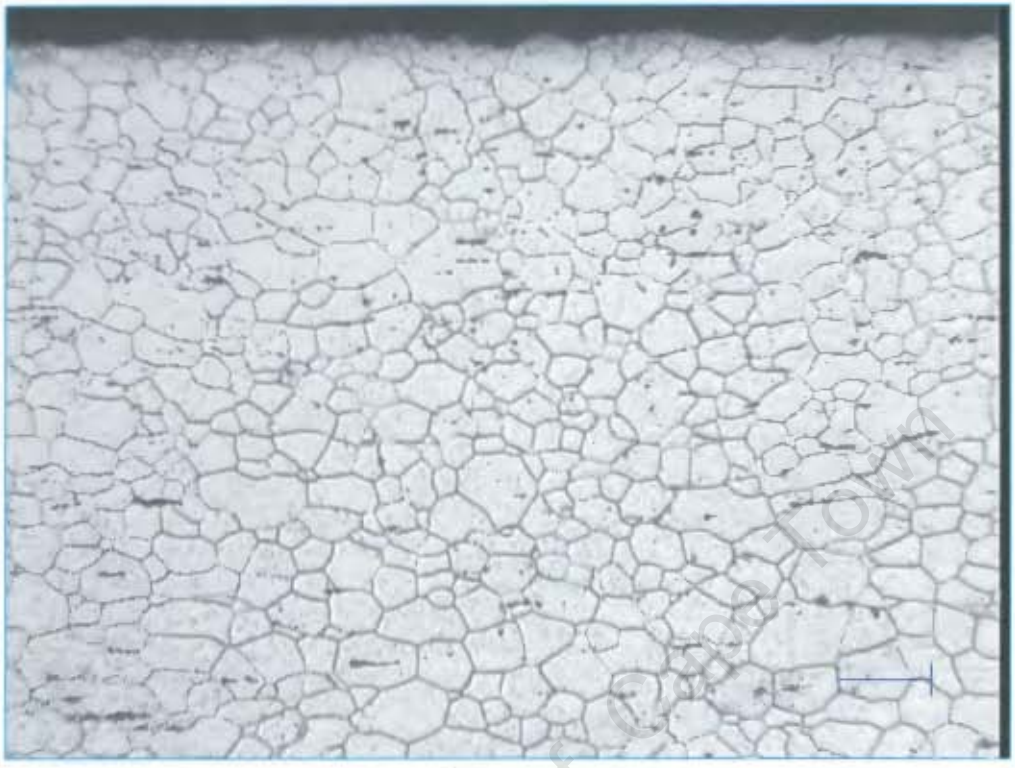

Figure 5.7: Sample aged at 800^{O}C for one minute at temperature.

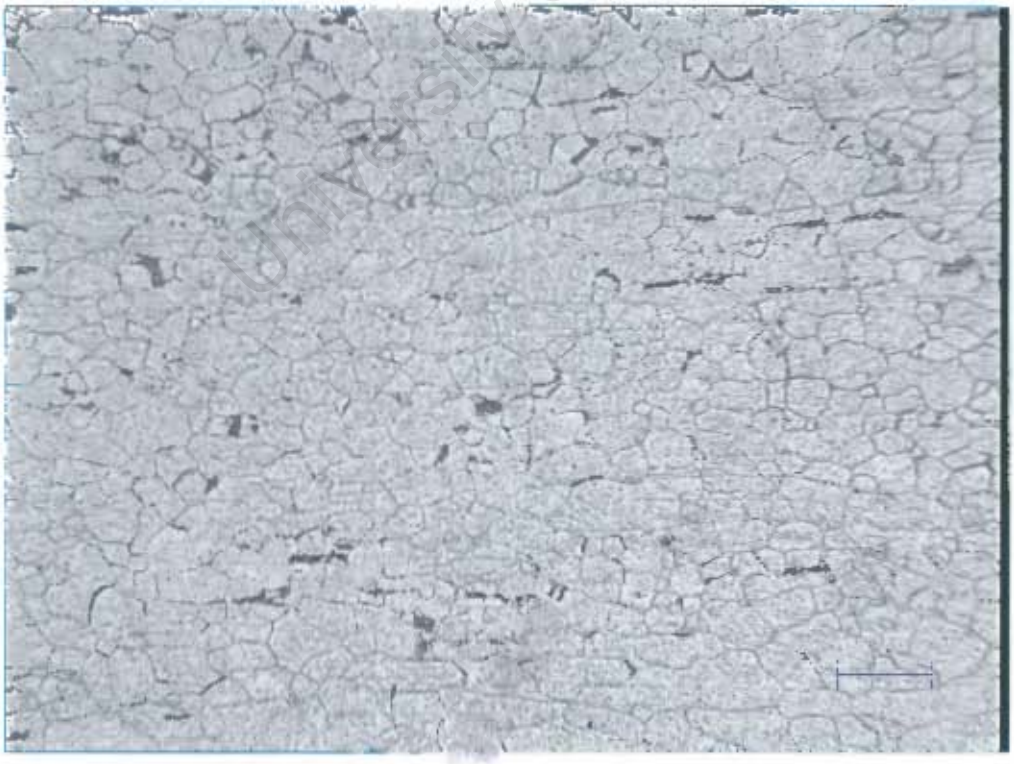

Figure 5.8 sample aged at 750^{O}C for 2 Hrs.

5.1.6 Dissolution of precipitates after sag test

The material after sag testing (850°C for 100Hrs) usually exhibits a significant increase, from a residual level of approximately 2 to 7 phase percent, in the amount of precipitates (figure 5.9 and 5.10). These precipitates could not be accurately analysed on the SEM due to their small size. The dissolution rate of these precipitates was investigated at two temperatures, 1000 °C and 1100 °C (figure 5.11). The precipitates appeared to dissolve rapidly within 1 to 2 minutes of the samples being placed in the furnace and stabilised to the residual limiting precipitate level of approximately 2 to 2.5 per cent area. This appears to indicate that if these precipitates possibly formed during hot band annealing they would rapidly dissolve during final cold band annealing at temperatures above 1000°C.

Figure 5.9: Micrograph of the material[3] of the material prior to sag testing. 1000X magnification micron marker = 50μm.

[3] Columbus cold rolled material number 3133933

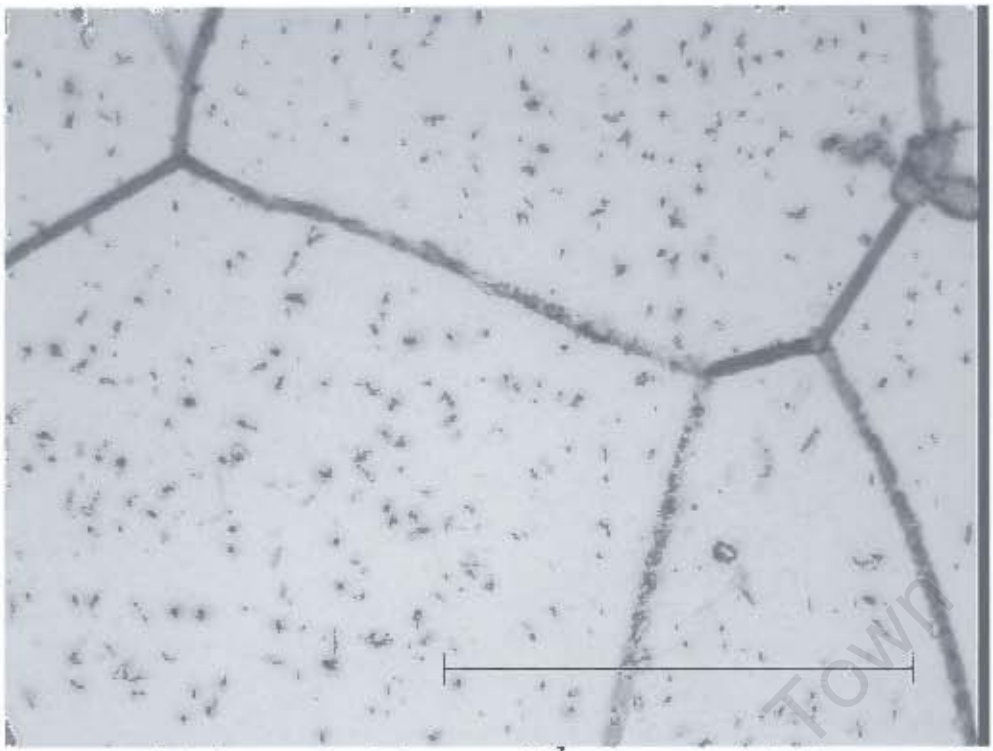

Figure 5.10: Micrograph of the material[3] of the material after sag testing. 1000X magnification micron marker = 50μm.

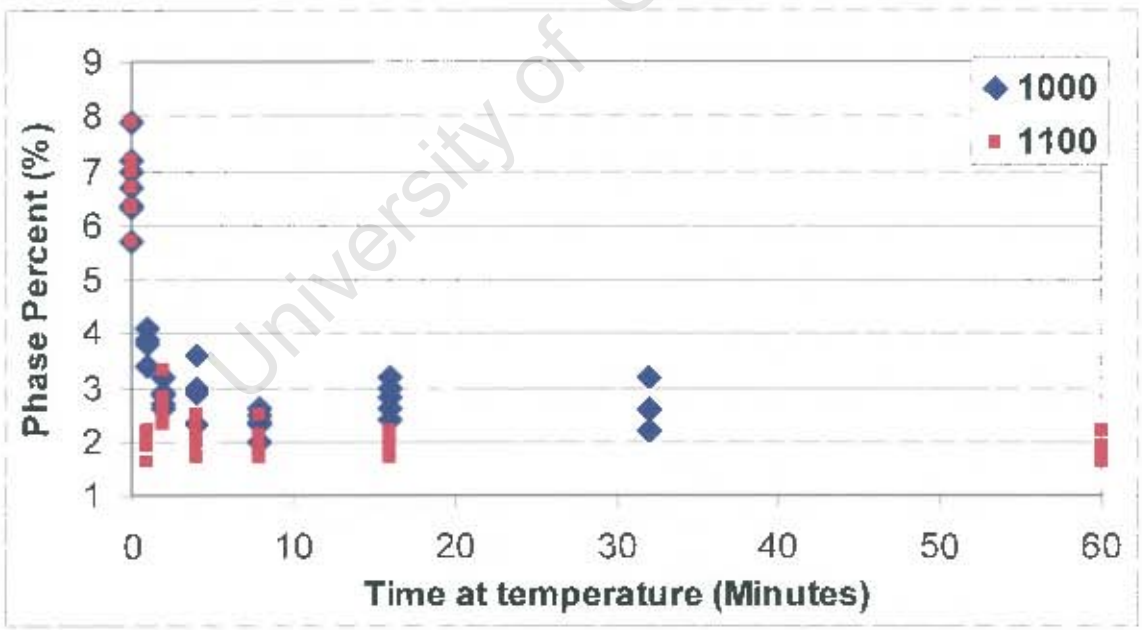

Figure 5.11: Dissolution rate of precipitates of a material after a sag test at 850°C for 100hrs.

[3] Columbus cold rolled material number 3133933

5.2 Experimental heat treatment of hot band material.

In this section, the material received in the as-hot rolled condition (post the Steckel mill - no annealing) is subjected to various heat treatments in the laboratory to investigate the effect that annealing time and temperature has on the following metallurgical properties:

- Area fraction of precipitates
- Grain growth characteristics
- Sag resistance

The hot rolled material is rolled from a slab with a thickness of approximately 200mm to a final gauge of 3 to 6mm (total reduction of approximately 97.8 per cent). The average last pass temperature on the Steckel mill is approximately 900^{O}C, which is above the laves phase transformation temperature. The coil is then quenched via lamina water cooling to a temperature of approximately 650^{O}C, which is reportedly below the Laves transformation temperature.

5.2.1 Effect of annealing temperature on the area fraction of second phase and grain size after hot rolling

A hot band sample[5] was obtained to determine the influence of time at 1000 °C and 1100 °C on the second phase area fraction. Given the scatter in the data presented in figure 5.12, there is no discernible variation in the second phase area fraction over this heat treatment range. There may of course be a change in the second phase area fraction that is not detected by the microscopy technique employed here. The grain size of the hot band material was also recorded (figure 5.13). The ASTM grain size number stabilises between 4 and 4.5 for the temperatures 1000°C and 1100°C. The material at 1100°C reaches the limiting grain size at a faster rate than at 1000°C, as would be expected.

[5] Columbus Hot Rolled Coil Number 3182872

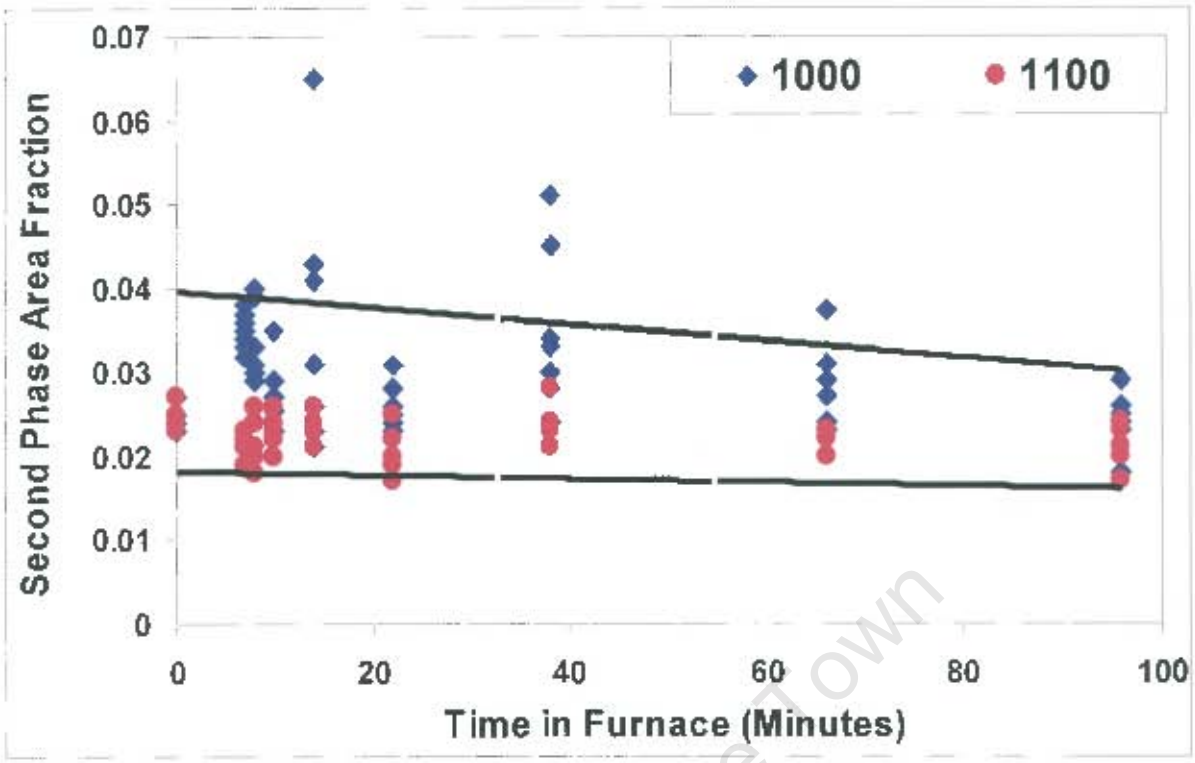

Figure 5.12: Second phase area fraction in the hot band material after annealing.

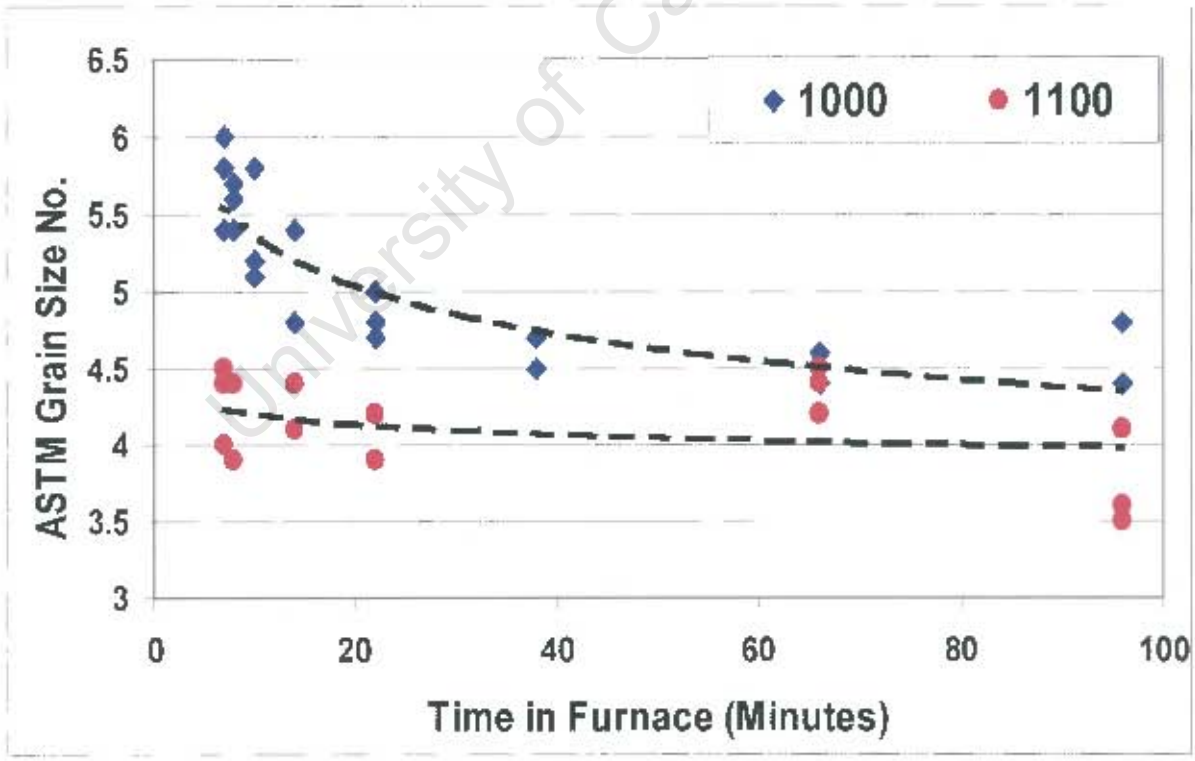

Figure 5.13: Grain size of material after hot rolling.

5.2.2 Sag resistance of material after various experimental heat treatments on hot rolled material

Hot band material[6] (6-mm gauge) was obtained post hot rolling and exposed to various hot band-annealing temperatures from 900°C to 1250°C for two hours. This was done to investigate the possible affect that various hot band annealing temperatures prior to cold rolling would have on the sag resistance of the material. The excessively long time in the furnace was to simulate a batch annealing process, as this probably would be the only logical way of annealing these steels at these high temperatures. The poor tensile strength of the steels at these high temperatures (above 1100 °C) prohibits the processing of this steel on the continuous anneal and pickle lines. After the experimental heat treatments, the hot band materials were cold rolled to a final gauge of approximately 1.5mm. The cold rolled steels were then subjected to an anneal at 1000 °C and 1050 °C for 264 and 140 seconds respectively with the aim of obtaining an average ASTM grain size number of approximately 6. However, this grain size was only obtained in the final material after the hot band had been annealed for two hours in the temperature range 1000 °C to 1100°C (table 5.5) and when the cold band annealing was carried out at 1050 °C. The etched grain shape changed from equiaxed to a microstructure that contained wavy grain boundaries when the hot band material was annealed at temperatures above 1100 °C. The microstructure in most cases also consisted of a dual (bimodal) microstructure with bands of fine and coarse grains (appendix 5). This could be related to the fact that excessive grain growth (secondary recrystalisation) occurred in the hot band material annealed at 1050°C and above (appendix 5).

The material showed a consistent improvement in sag resistance to approximately 3-4mm (table 5.5), when the hot band is annealed at 1000 °C and above, as is shown in figure 5.14.

[6] Columbus material MPO 3284253

Table 5.5

Sag for different hot band anneals

Hot Band Anneal Temperature (°C)	Cold band anneals at 1000 °C				Cold band anneals at 1050 °C			
	ASTM Grain size NO. SD, D*		Gauge (mm)	Sag (mm)	ASTM Grain size NO. E, D, SD*		Gauge (mm)	Sag (mm)
900					7.8, 7.7, 7.9	E	1.45	15
950					7.5, 7.7, 7.6	E	1.32	17.5
1000					5.4, 5.5, 5.6	E	1.52	4.5
1050					5.7, 5.6, 5.7	E	1.5	4
1100	7.4, 7.1, 7.6	SD	1.42	7.5	5.8, 5.9, 5.9	E	1.42	4.5
1150	7.7, 7.7, 7.6	D	1.46	4	7.2, 7.3, 7.3	D	1.46	4.5
1200	7.1, 7.5, 7.3	D	1.44	5	7.4, 7.6, 7.4	D	1.44	3
1250	6.9, 7.0, 7.1	SD	1.48	4	7.1, 7.1, 7.1	SD	1.5	3

*SD = Slightly dual structure, D = Dual structure, E = Equiaxed – non-dual structure.

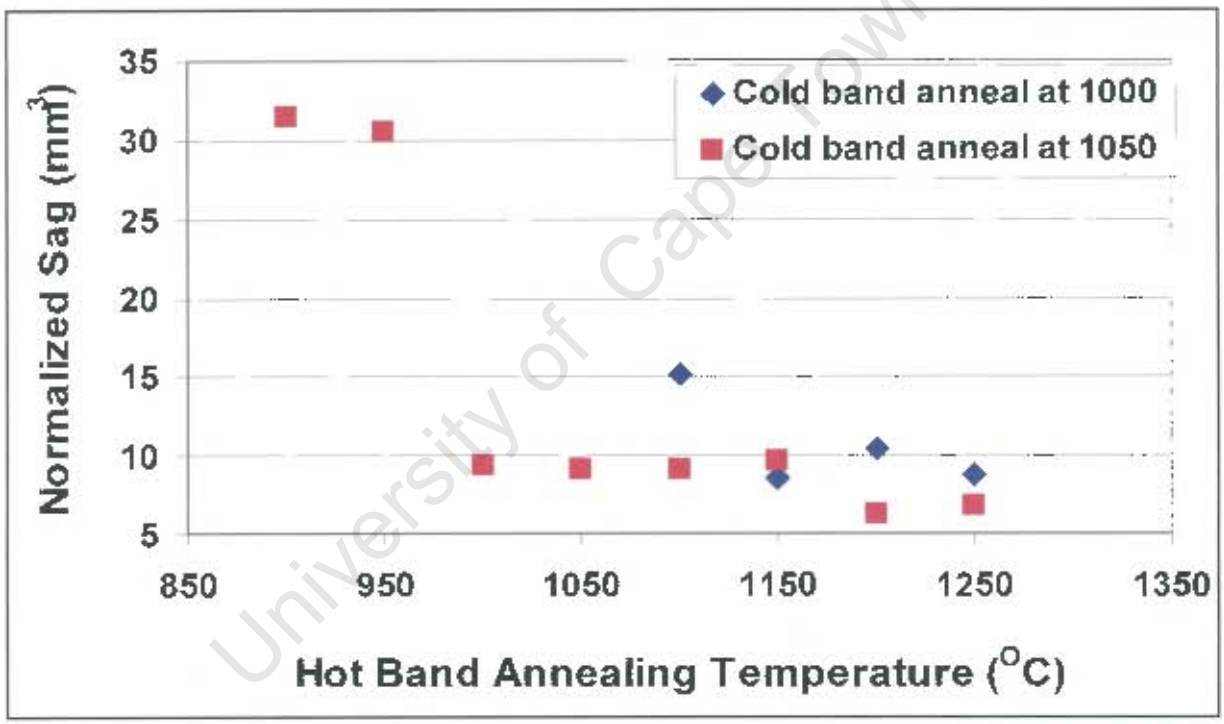

Figure 5.14: Graph indicating the effect of hot band annealing temperature on the normalised sag resistance of the final cold rolled annealed material.

5.2.3 Effect of various hot band annealing temperatures on the final mechanical properties.

It may be postulated that as the hot band annealing temperature increases the amount of niobium in solution should increase. This should increase the proof stress of the final cold rolled and annealed material due to solid solution strengthening. The proof

stress did indeed show a slight increase with increasing hot band annealing temperature (figure 5.15). There is also a slight downward trend in elongation that may impact on the formability of the material.

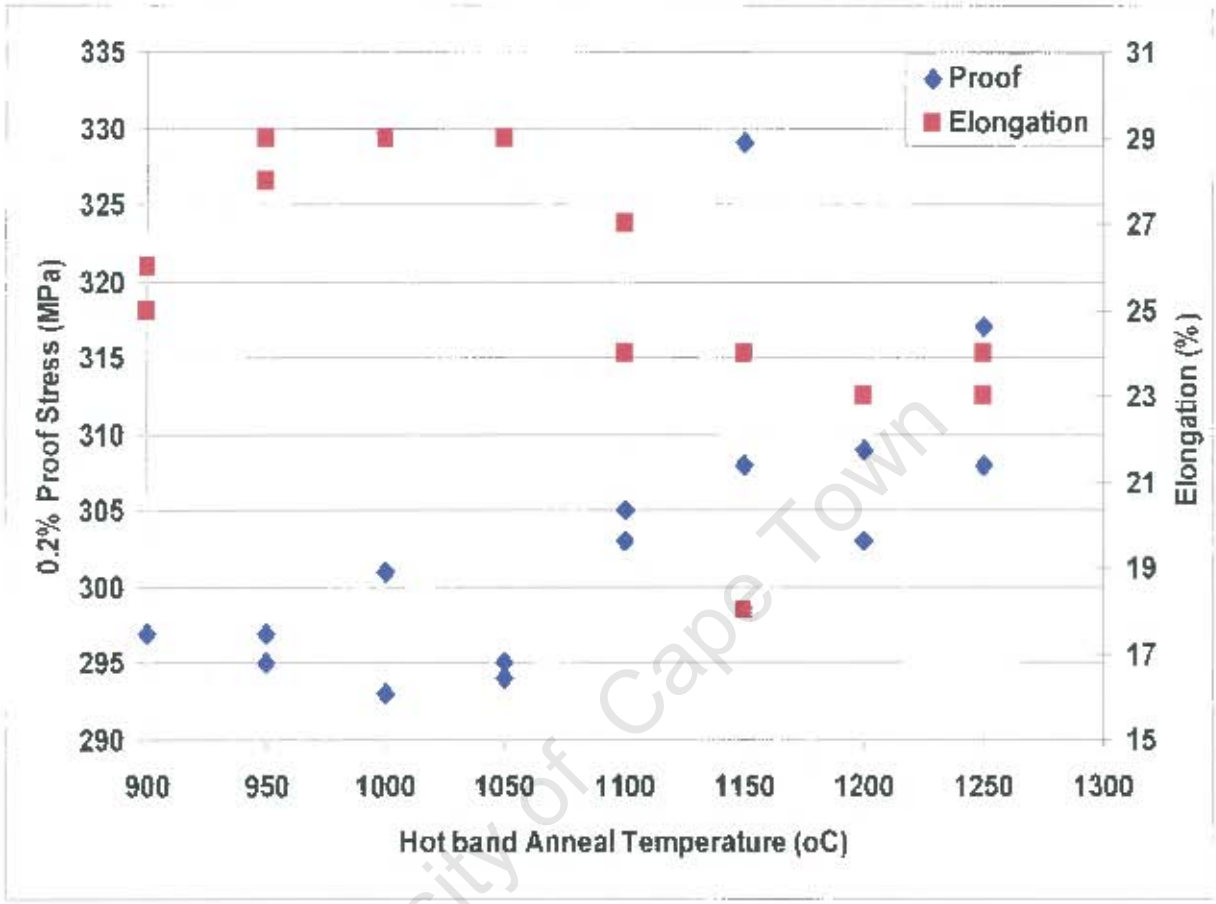

Figure 5.15: Effect of hot band annealing temperature on the proof stress and elongation of type 441 material.

5.3 Experimental heat treatment of as-cast material

In this section the material received in the as-cast condition (prior to the reheat furnace and the Steckel mill) is subjected to various heat treatments in the laboratory to investigate the effect that annealing (reheat) temperature has on the following metallurgical properties:

- Area fraction of precipitates
- Morphological examination of precipitates after each heat treatment – the morphology of the as-cast structure has already been investigated in chapter 4.
- Sag resistance

5.3.1 Analysis of the precipitate area fraction after various reheat treatments

A slab sample[7] was obtained after continuous casting and subjected to the following reheat temperatures: 1050 °C, 1100 °C, 1150 °C, 1200 °C and 1250 °C for 2 hours. No significant trend was obtained from the data (figure 5.16).

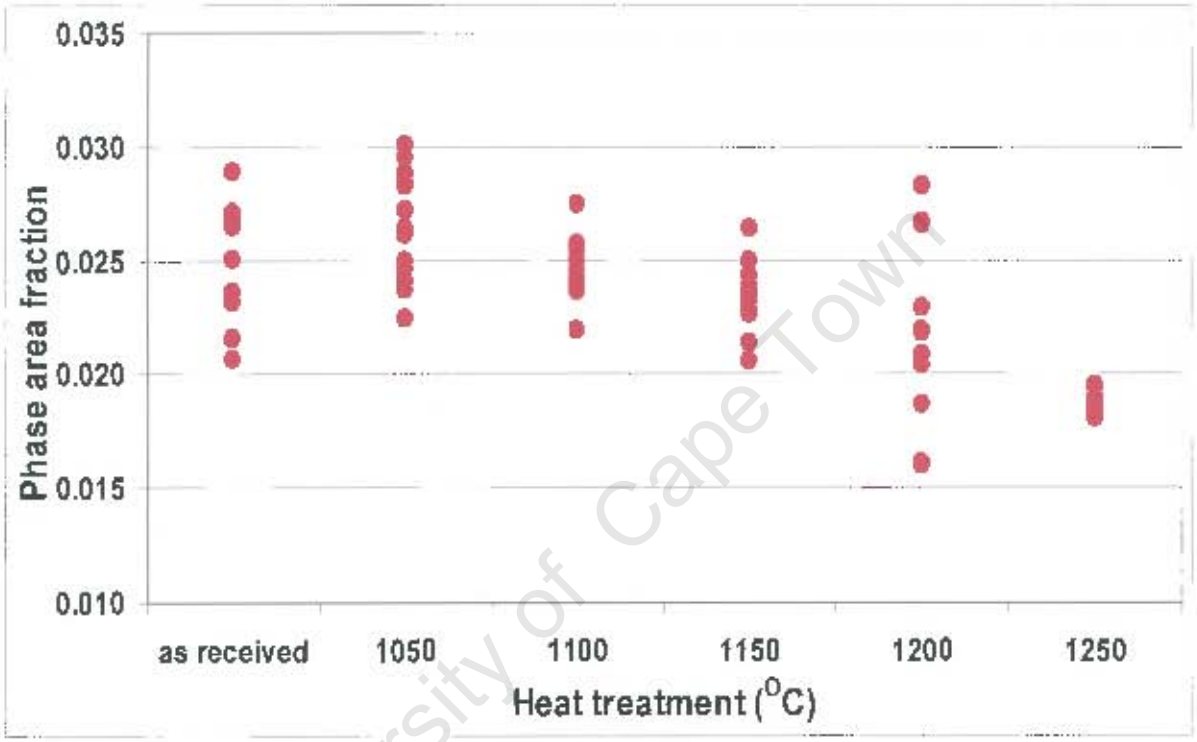

Figure 5.16: Area percentage of precipitates after various heat treatments of as cast material. The micron markers in the micrographs represent 50 microns.

5.3.2 Morphological examination of precipitates

The morphology of the precipitates appears to change with the various heat treatments as revealed by deep etching of samples. There generally appeared to be two morphologies of precipitates throughout the heat treatments. The first is a dendritic type that appears to be composed of a central cruciform consisting primarily of titanium and surrounded by platelets consisting primarily of niobium (figure 5.17). The second type is a standard cubic titanium carbonitride, which has varying degrees of niobium precipitation (figure 5.18).

[7] Columbus Stainless slab material from MPO 3295803

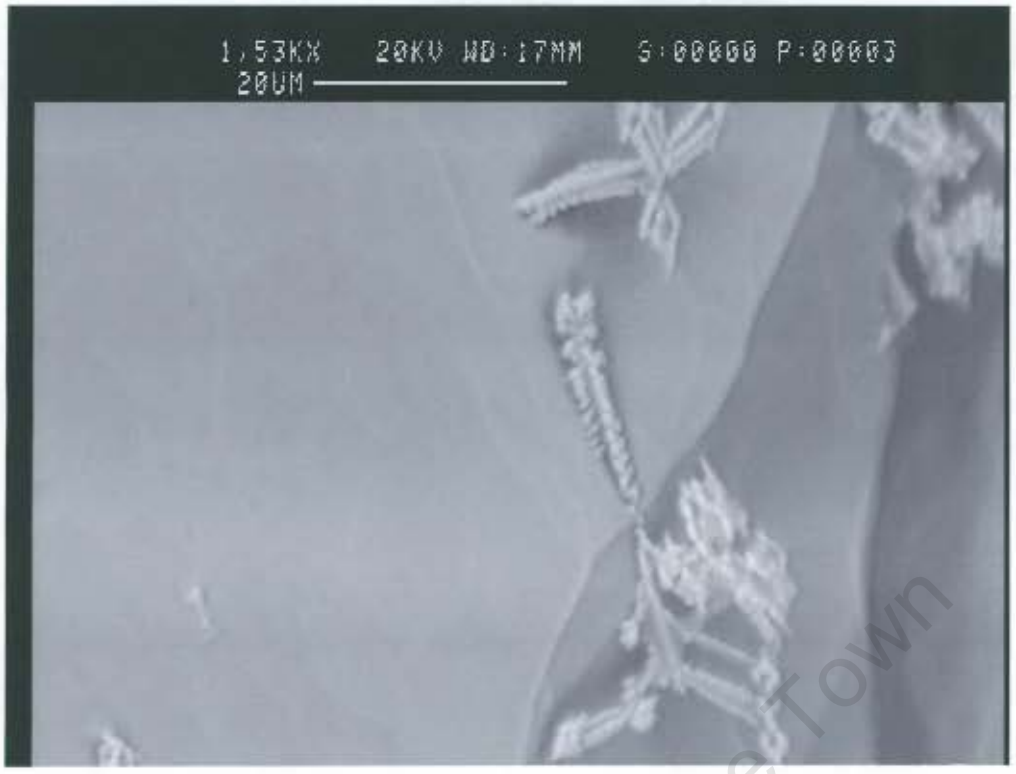

Figure 5.17: Dendritic type precipitate with a central core cruciform and arms of primarily titanium and attached platelets of mainly niobium. As-cast sample annealed at 1050°C for 2 hours.

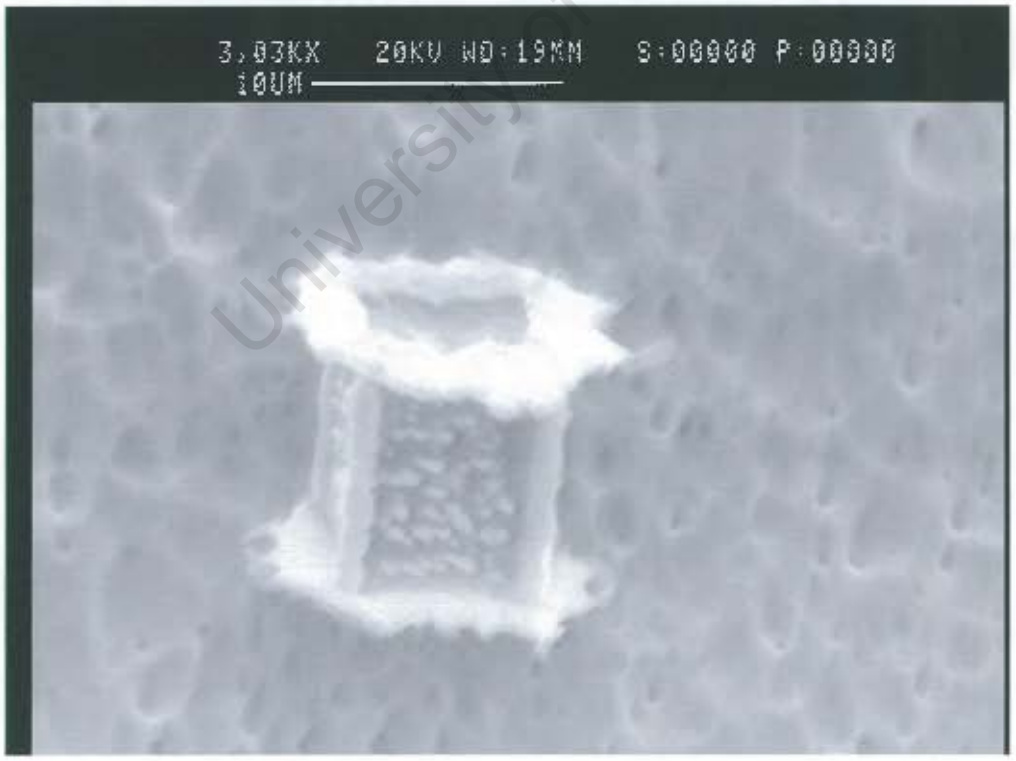

Figure 5.18: Precipitate consisting of a central cubic core composed mainly of titanium surrounded by the growth of niobium precipitates. As-cast sample annealed at 1100°C for 2 hours.

The amount of niobium precipitation appeared to decrease in quantity as the heat treatment temperature increased (composite figures 5.19 and 5.20). This would, if true, theoretically increase the amount of niobium in solution and consequently increase the creep (sag) resistance of the material.

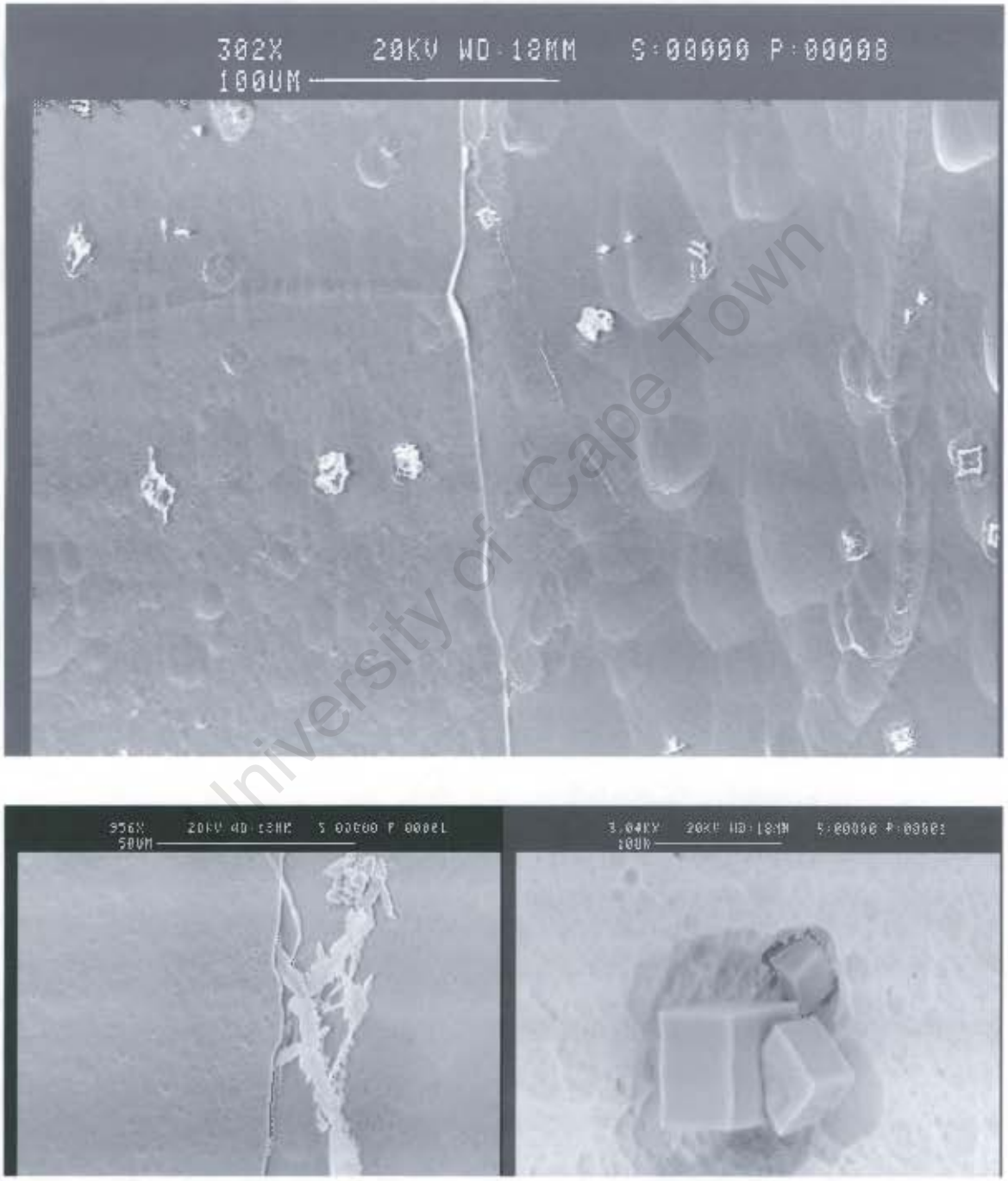

Figure 5.19: Composite SEM Images of the as-cast material after annealing at 1200^{O}C for 2 Hrs.

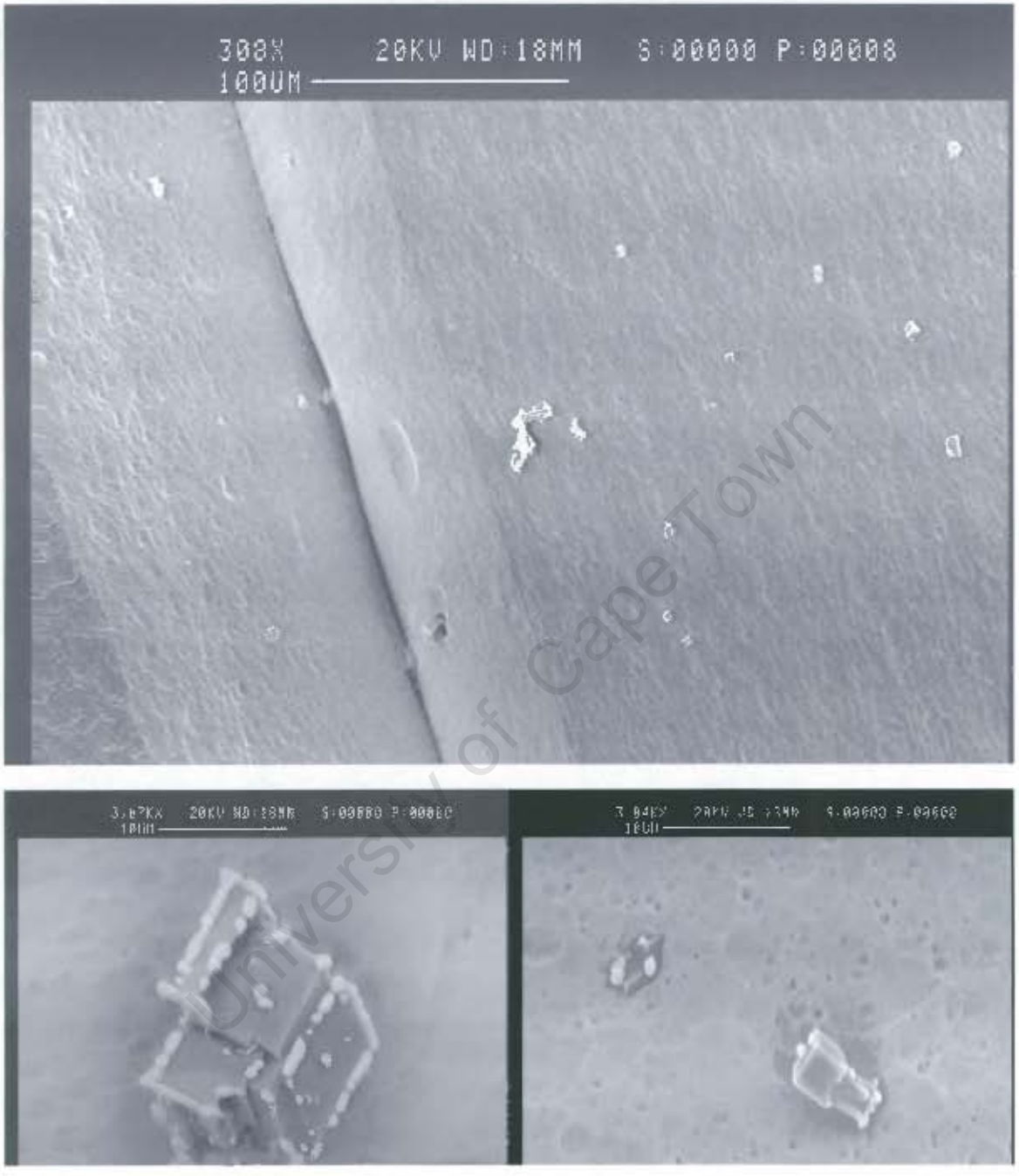

Figure 5.20: Composite SEM Images of the as-cast material after annealing at 1250^{O}C for 2 Hrs.

5.3.3 Sag resistance of as-cast annealed material after final cold rolling and annealing.

After subjecting the as-cast slab material[8] to the reheat treatments described in section 5.3.1, the material was then hot rolled to a gauge of approximately 6.5mm (6.46-6.6mm). The hot band material was annealed at 950°C for 10 minutes and water quenched. The ten minute anneal was used to simulate the plant as the hot band material is reportedly at temperature for approximately 0.5 to 1 minute. The hot rolled annealed material was then cold rolled to a gauge of approximately 1.5mm and annealed at 1050°C for 140 and 245 seconds (total time in furnace to obtain an ASTM grain size number of approximately 6 and 5 respectively (table 5.6)). There appeared to be a general downward trend in the degree of sagging (normalised) as the as-cast annealing temperature was increased (figure 5.21).

Table 5.6

Sag for different on As Cast Material after final Cold rolling

As-cast Anneal Temperature (°C)	Cold band anneals at 1050 °C for 140 Sec.			Cold band anneals at 1050 °C for 245 Sec.		
	ASTM Grain size NO.	Gauge (mm)	Sag (mm)	ASTM Grain size NO.	Gauge (mm)	Sag (mm)
1050	7.6, 7.4, 7.6	1.42	5.5	6.1, 6.1, 6.0	1.45	3
1100	6.5, 6.7, 6.8	1.37	6.5	5.3, 5.3, 5.2	1.4	4.5
1150	6.8, 7.1, 7.0	1.44	3.5	6.4, 6.8, 6.8	1.46	2.5
1200	7.1, 6.9, 7.0	1.32	3.5	5.8, 6.0, 6.0	1.32	4
1250	6.8, 6.8, 6.9	1.41	3.5	6.0, 6.1, 6.1	1.41	2

5.3.4 Effect of various as-cast reheat temperatures on the final mechanical properties.

The results in figure 5.22 were rather interesting in the fact that there appeared to be a window of opportunity to anneal the material at a low temperature of 1050°C to obtain a rather significant increase in sag resistance. The tensile results (although these are only individual points they give a general trend) were, however disappointing from an elongation perspective at 1050 °C (figure 5.22). The most promising result as far as the elongation is concerned is to reheat the as-cast material at a temperature of 1150 °C.

[8] MPO 3295803

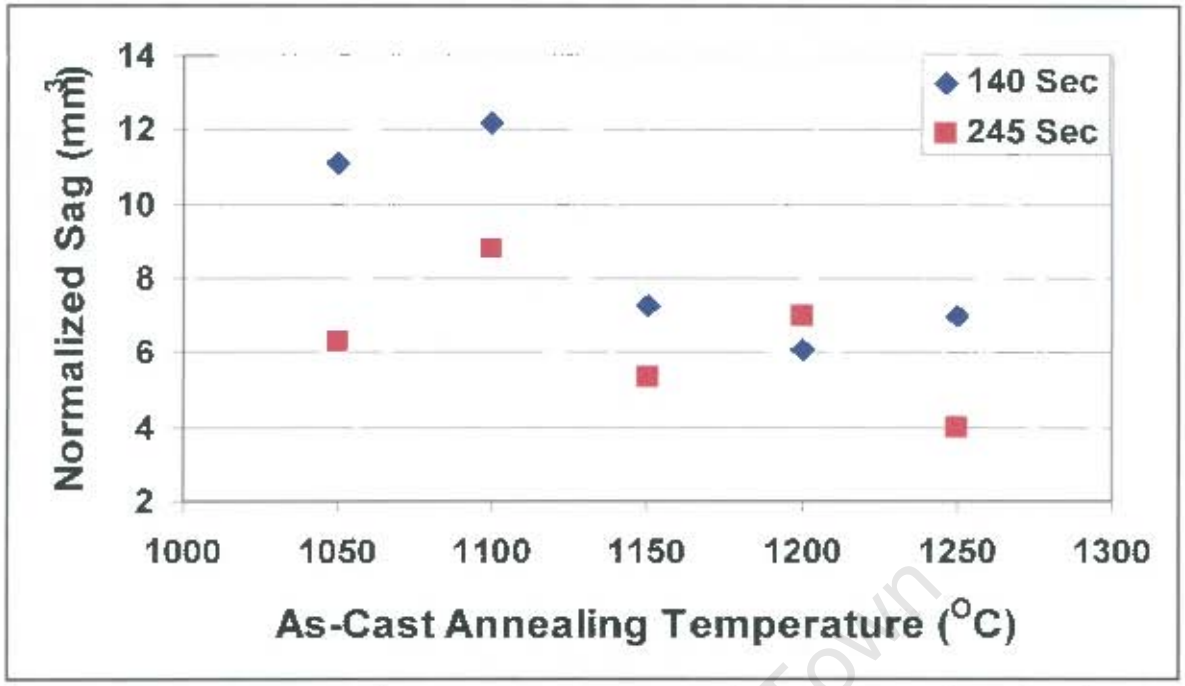

Figure 5.21: Graph indicating the downward trend in the degree of sagging in the final cold rolled material after the various heat treatments of the as-cast material.

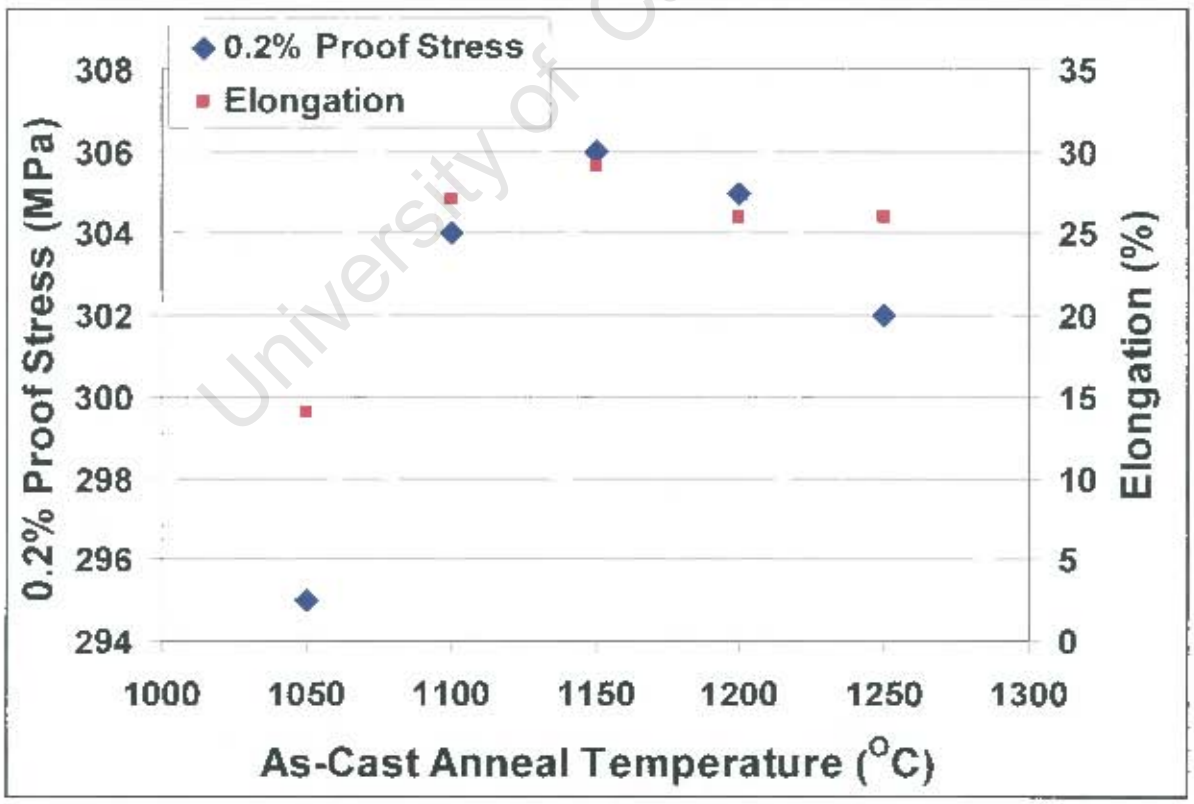

Figure 5.22: Effect of the as-cast reheat temperature on the proof and elongation of type 441 material.

6 Discussion

The methodology used to increase the creep resistance in steels and more specifically stainless steels is either by solid solution strengthening (molybdenum) or by the formation of precipitates (titanium and niobium) prior to or during service of the material. Niobium it appears can fulfil both of these roles initially as a solid solution strengthener and then as a precipitate by the formation of either carbo-nitrides or Laves phase at the service temperature. The complex relationship between these two thermodynamic requirements to obtain the optimum creep or sag resistance for this material appeared to be at the centre of this investigation. Initially, random samples were obtained of standard production material. The grain size and sag value was determined for all of these samples and it was observed that some form of relationship existed between these two and the gauge of the material (figure 6.1).

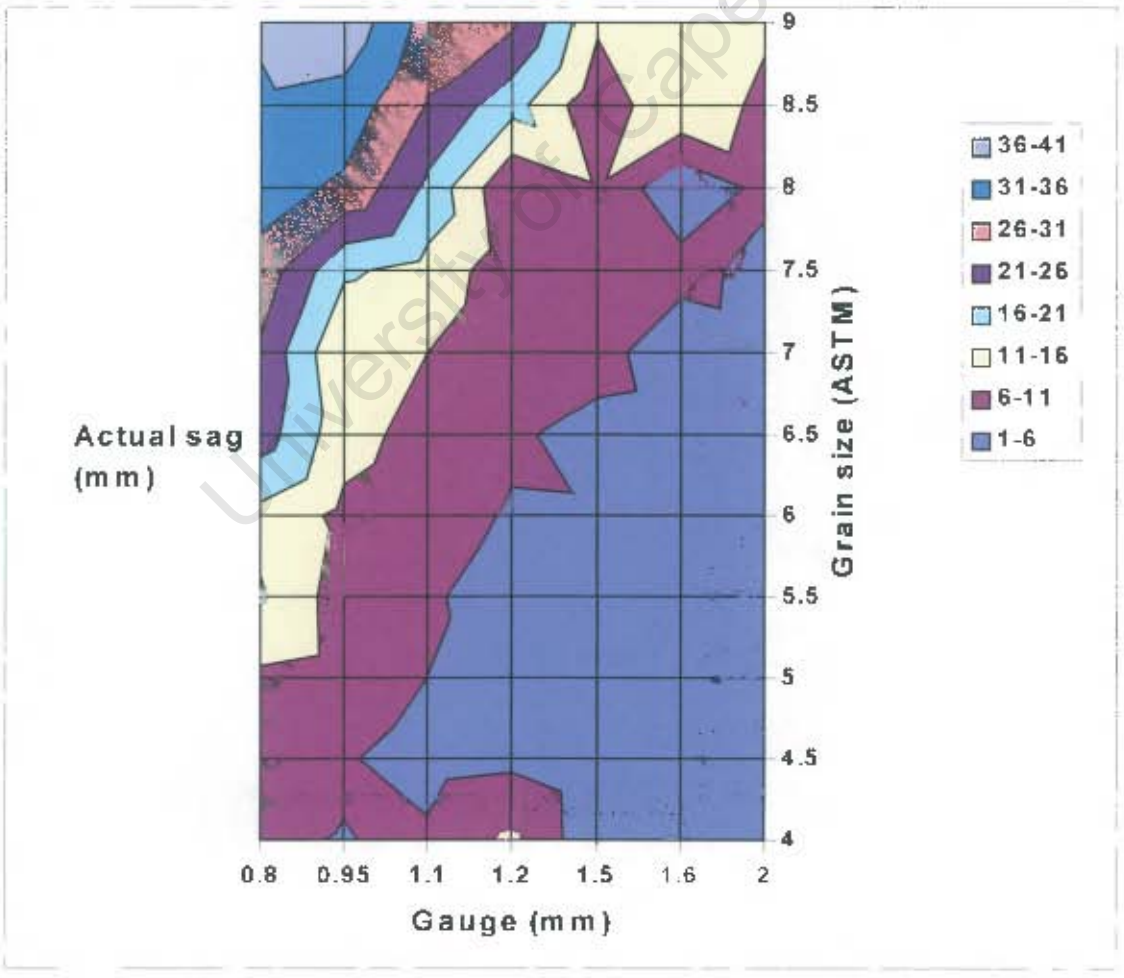

Figure 6.1: Topographical map of the sag obtained for production material for various gauges.

6.1 Statistical analysis of plant material

The statistical analysis of the sag obtained for randomly sampled material revealed that a strong correlation existed between the sag measured and the grain size of the material. Various attempts were made to incorporate some form of the calculated niobium in solution. In fact niobium had a detrimental effect on the sag resistance of the material. This could be argued to be related to the fact that as the amount of niobium increased in the material the amount of niobium in solution theoretically increased which in turn decreased the grain size due to solute drag. The processing parameters that may in-fact contribute to niobium in solution are the reheating and cooling cycles. In this respect the sag resistance was directly related to the inverse of the slab reheat temperature and final annealing temperature and directly proportional to the final line speed. The latter two parameters directly impact on the grain size, but were kept in the model as it was felt that they might in fact still play a role in the amount of niobium in solution. The interesting parameter is the reheat temperature and the assumption can be indirectly made that this parameter is directly related to the niobium in solution.

The final mathematical model was determined that related the sag value to:

- The gauge of the material tested
- The grain size (diameter) of the material in mm
- Final temperature of the strip during annealing (^{0}C)
- The velocity of the strip through the furnace m/sec
- The slab reheat furnace temperature (^{0}C)
- The mass per cent niobium in the steel

The influence of each of these parameters on the sag, as predicted by the model was plotted (figure 6.2). The greatest influence on the normalised sag value is seen as the grain size and the niobium content in the ranges investigated. One interesting aspect of this graphical representation is the fact that the influence of the grain size stabilises below an ASTM grain size number of approximately 6.5.

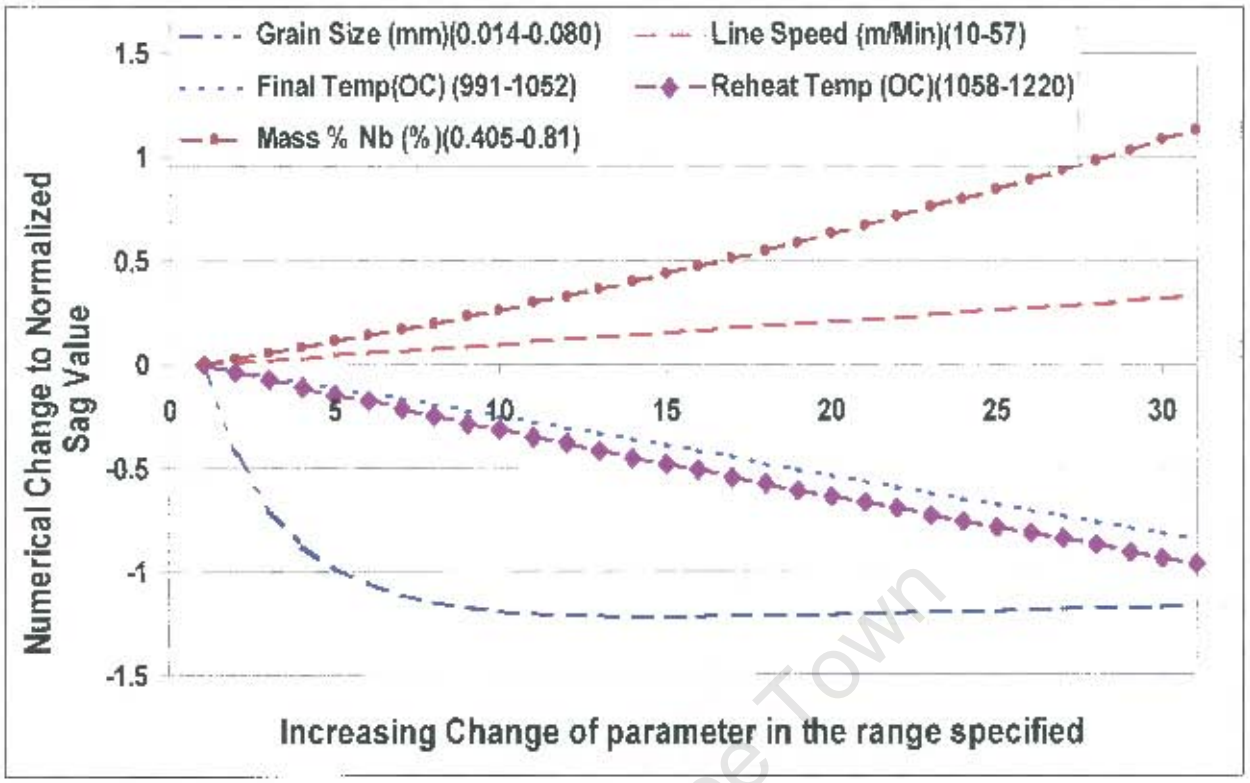

Figure 6.2: The effect of an increasing change in the parameters in the model on the normalised sag value.

6.2 Morphological development of precipitates during production

The interesting aspect of this part of the investigation was to see how and when the niobium precipitates out. A sample was taken of the molten metal (in the tundish) at approximately $1500^{O}C$ prior to casting. This sample exhibited fine precipitates of niobium; no titanium precipitates were evident at this stage. After casting, cruciform titanium precipitates with nodules of niobium precipitates attached primarily to the axis of the cruciform were observed. The classical cubic titanium carbo-nitride precipitates did not appear to be present. A sample after the reheat furnace was not investigated. The cubic precipitates appeared during hot rolling after the first couple of passes on the roughing mill. The cubic precipitates may in fact form during the reheat cycle as was confirmed with experimental work. A significant amount of niobium precipitates were still present on a central core of a predominantly titanium precipitate, presumably titanium carbo-nitride. These precipitates were crushed during cold rolling and formed stringers of titanium and niobium inclusions. During no stage

of the thermo-mechanical history did it appear as if a significant amount of niobium had been dissolved or that a significant amount of niobium precipitates had formed due to some thermo-mechanical process. Only the titanium carbo-nitrides appeared to grow in size from the slab sample to the hot band annealed material. The niobium precipitates also appeared to increase in size; however, this appeared negligible when compared to the titanium precipitates.

6.3 Experimental heat treatments

The permutations used during experimentation were initially limited to a matrix of acceptable processing parameters for the plant. Temperatures that exceeded 1100°C for example were not investigated for experiments involving hot and cold rolled material. The cold band material was initially annealed at various final temperatures from 925°C to 1100°C. The hot band material was initially limited to temperatures in the range 1000 °C to 1100 °C based on the observations for the cold band material. This was expanded to 925°C to 1100°C for simulation to investigate if the hot band material should be batch annealed and not line annealed, as is the current practice. Finally the slab reheat temperatures used in the experimentation were limited to the range normally used for stainless steels approximately 1050°C to 1250°C.

6.3.1 Cold band material

The most important finding from these experiments was that the grain size appeared to be the most significant parameter in determining the creep resistance of the material (figure 6.3). The experimental data indicates, that the material should be annealed at 1000°C as this gave the greatest window of increased sag resistance.

The difficulties associated with this from a production perspective is that there appears to be a point of inflection in the bulk activation energy (recovery, recrystallization and grain growth) at approximately 1000°C. This jump in activation energy is an order of magnitude larger; at temperatures below approximately 1000°C it is 1113kJ/mol, while above this temperature it is 112kJ/mol. This would entail significantly longer annealing times, which impacts on the productivity of the line. In

addition, the literature and the experimental work carried out on the cold rolled material (figure 5.1A) has shown that the precipitates do not appear to form a significantly larger area fraction at final annealing temperatures at 1050°C and above. This reportedly increases the sag resistance. This is further substantiated in the later work (table 5.6) when the hot band material was solution treated at various temperatures and it was found that the sag resistance increased as the simulated batch anneal temperature increased. In addition it has been shown that should the laves phase form during the processing history prior to cold band annealing, this would probably be rapidly taken up into solution should the material be annealed in the temperature range 1000 °C to 1100 °C (figure 5.11).

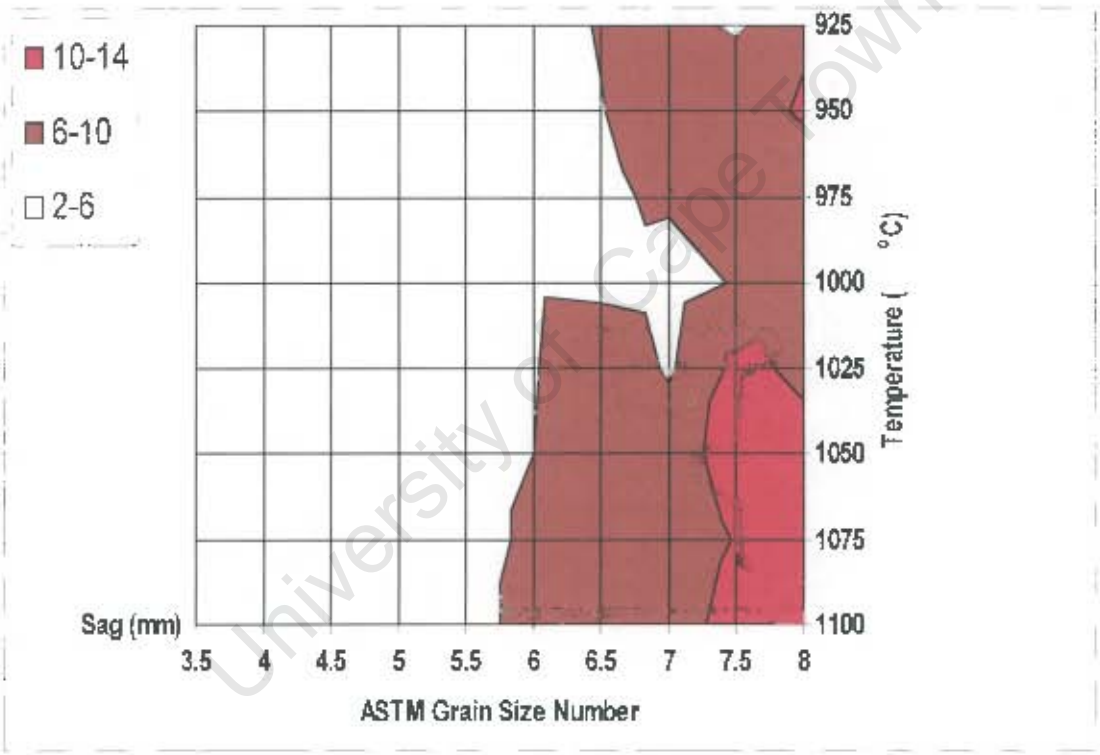

Figure 6.3: Topographical map of the sag obtained after various heat treatments on the final material.

The experimental data obtained for the sag resistance after various anneals on cold rolled material was subjected to statistical analysis. It was found that the affect of the final annealing parameters on the sag resistance of the material could be mathematically formulated as:

$$Sag = 2.87 + 0.00235*G^{-2}\ (mm) + 30056.04*t^{-2} \quad \text{----------(Equation 6.2)}$$

Where:

G = The grain size (diameter) of the material in mm

t = Time in furnace (seconds)

This means that the sag resistance of the material is inversely proportional to both the grain size of the material and the time the material spent in the furnace during final annealing. The interesting aspect of this relationship is that it was found that the grain size obtained during final annealing was more a function of annealing temperature and niobium in solution than the time at temperature. The function of the time resident in the furnace has an influence on the grain structure; however, in this analysis it appears to affect the sag value to a greater degree. This could possibly be related back to the initial analysis of the plant material where the sag resistance was found to be directly related to the speed of the strip through the furnace. The higher the speed the less the resident time of the strip in the furnace, speed is thus inversely proportional to the resident time. It can thus be said that the sag measured in production material is inversely related to the resident time in the furnace.

The ageing treatments applied to the cold rolled material after final annealing appeared to increase the sag resistance of the material slightly. This increase occurred from approximately 8 to over 120 minutes depending on the ageing temperature (950^{O}C too 700^{O}C). This slight increase (between 10 to 30 percent) did not appear significant enough to pursue this line of investigation further.

It would thus appear that the final cold band annealing temperature for type 441 material should be between 1000^{O}C and 1100^{O}C. An aim temperature of 1050 ^{O}C with a resident time in the furnace to obtain a maximum ASTM grain size number of 6.5 would give the optimum value for sag resistance.

6.3.2 Hot band material

The sag resistance of the material appeared to increase as the hot bands' anneal temperature (2 hours in the furnace) was increased. Initially it could be speculated that the increase in this value is due to an increase in the amount of niobium in solution prior to final annealing. This appeared to be substantiated by tensile tests which

showed an increase in the proof stress with increasing hot band anneal temperature (figure 5.15). The down side of this heat treatment is that it significantly impacts on the elongation of the material and possibly on the formability.

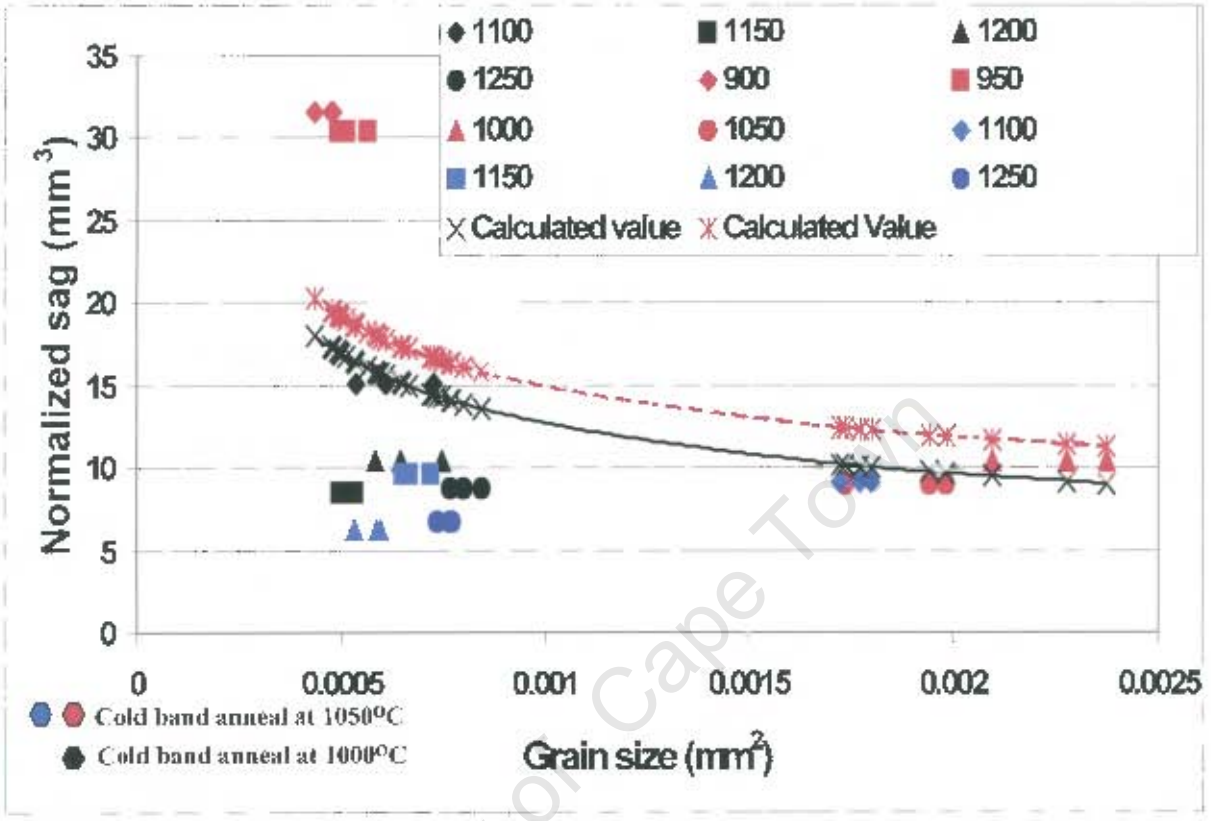

Figure 6.4 Effect of the hot band anneal temperature on the sag resistance of the material for different grain sizes.

The increasing hot band anneal temperature on the sag resistance is only really seen when the sag resistance measured for the samples annealed at the various temperatures is plotted against the grain size obtained after final annealing (figure 6.4). The average grain size of the material hot band annealed at 1100 °C to 1250 °C had a bimodal grains size structure in the final material. This could have positively influenced the sag resistance due to the significantly larger grains present in such a structure. Nevertheless, if it is assumed in the present discussion that the average grain size is a function of the degree of sagging in the material. It is interesting to note that the materials annealed from 1000°C to 1100°C (final anneal at 1050°C) appeared to have the same recrystallization and grain growth characteristics as the plant annealed material as the grain size obtained was similar to that predicted by the model. The hot band materials annealed at 900 °C and 950 °C exhibited a finer grain

structure. This is probably due to the significant number of precipitates that formed at these low annealing temperatures after two hours (figure 5.1b) and caused particle inhibited grain growth. This effect probably did not occur in the plant material annealed at 950^{O}C and subsequently tested in the laboratory as insufficient time was spent in the furnace for a significant amount of particles to form. It would also be expected to see some increase in the proof stress of the material at these two temperatures due to the Hall Petch relationship. This, however, was not observed. In addition the samples hot band annealed at temperatures 900 °C and 950 °C showed the worst sag resistance (as would be expected from the cold band analysis) due to the fine grain size. The particularly interesting aspect of the material annealed at approximately 1100^{O}C and above was that the grain size appeared to decrease. The only plausible explanation for this is that more niobium has gone into solution due to these higher temperatures and grain growth has been retarded due to solute drag. The fact that there is more niobium in solution appears to be substantiated by the increase in proof stress due to solid solution strengthening. The higher percent niobium in solid solution caused an increase in the sag resistance of the material. This can be seen as a sag drop in sag from about 16mm (material annealed at 900 °C and 950 °C) to approximately 3-5mm for material with the same grain size. In addition the sag was similar for material annealed at 1100 °C and above and with an ASTM grain size number of approximately 7.2 compared to material hot band annealed between 1000 °C and 1100 °C with an ASTM grain size of approximately 5.7 (figure 6.4). The calculated normalised sag values (for a gauge of 1.45mm) were determined using equation 6.2 above and plotted on figure 6.4, from the following can be seen and corroborates the above statements;

- The material hot band annealed at 950^{O}C is significantly above the calculated sag value and thus does not follow the predicted values obtained for typical plant material.
- The material hot band annealed at 1000 °C to 1100 °C appears to fit the predicted values
- The material hot band annealed at 1150 °C and above has a significantly lower sag value than is predicted for the material.

A significant increase in sag resistance could be obtained should the batch anneal route be chosen solely for creep (sag) resistance. It would then appear that the material would require a heat treatment at 1150 °C or above. The down side is that a longer anneal at final processing would probably be required and also a slight loss in elongation which would negatively impact on the formability of the material.

6.3.3 As- cast material

The amount of niobium precipitates appeared to decrease in the as-cast material as the reheat annealing temperature was increased. Theoretically, therefore, more niobium should be in solution after the higher annealing temperatures. It appears as if this higher percent of niobium in solution persisted throughout the simulated thermo-mechanical processing of this material as the sag values appeared to show a relatively higher degree of sag resistance when compared to the calculated values expected (figure 6.5). It is interesting to note that the material with sag values similar to the predicted values for this material was heat treated at a similar reheat temperature as is used in production, namely approximately 1100^{O}C. The material annealed at 1050^{O}C should theoretically have shown a similar or worse sag value to that annealed at 1100^{O}C due to the fact that niobium appears to have come out of solution at this temperature (figure 5.16). The grain size, however, of this material for a similar anneal is finer or similar to the materials exhibiting the increase in sag resistance. It could be postulated from the results of the hot band anneals above that either a significantly higher number of precipitates were present or that a significantly higher percentage of niobium is in solution to account for this decrease in grain size. Both of these scenarios could possibly be present in the material at the 1050^{O}C anneal. The probability exists that the 1050^{O}C has insufficient driving force to cause the diffusion of atoms in solid solution to pre-existing precipitates and that the material may in fact form a larger amount of smaller precipitates along with the pre-existing precipitates in the material after casting. The end result is a material with finer precipitates which are more uniformly distributed throughout the matrix and which on final annealing may be more prone to dissolution.

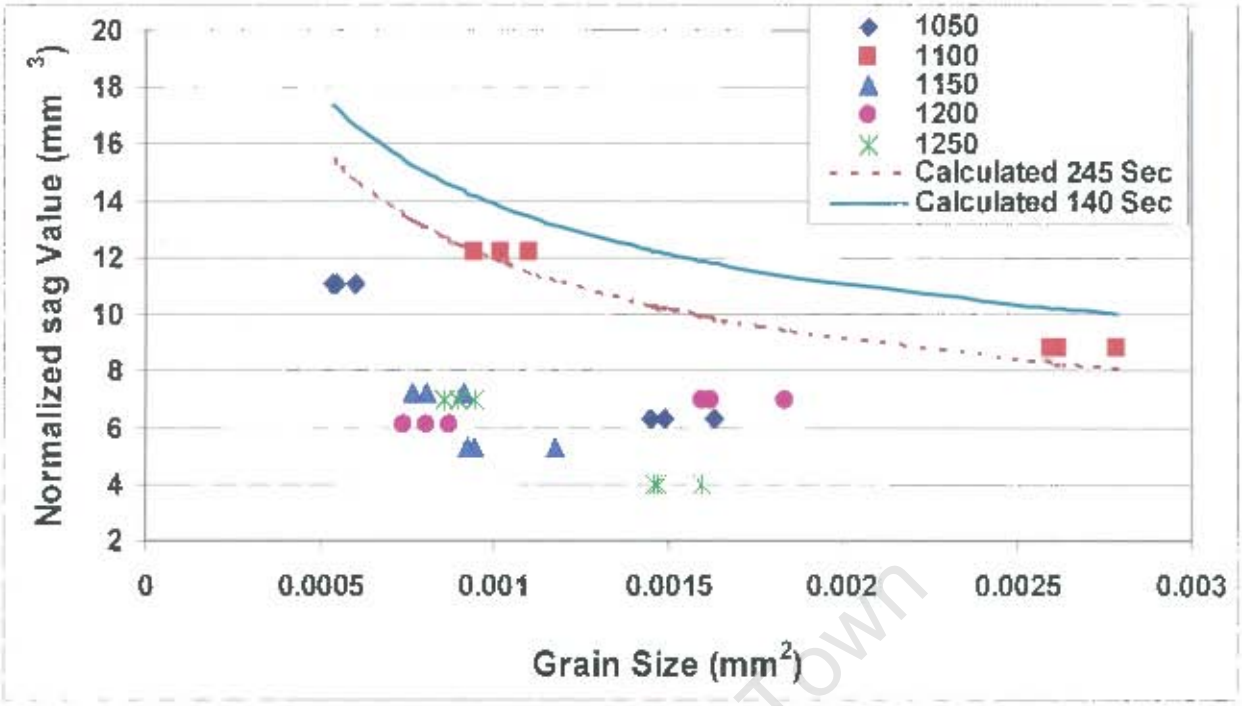

Figure 6.5 Effect of the as cast anneal temperature on the sag resistance of the material for different grain sizes.

Although the anneal at 1050 °C appears to be a ideal option it may in fact be that the plant can not roll material from these low reheat temperatures due to load limitations on the mill. The alternative is that the material must be annealed at least at 1150 °C or above to increase the amount of niobium in solution prior to the material being processed further.

7 Conclusions

This work indicates that a longer annealing time improves the sag resistance of the material. The combination of longer and higher temperatures on the hot band and on the final anneals appears to be beneficial to the sag resistance of the material. This translates directly into a grain size and niobium in solution relationship with the sag resistance of the material. This relationship with grain size on the final cold rolled material has been proven via experimental and plant results. Analysis by the stat-graphics package has indicated that the sag resistance is conclusively related to the final grain size in the material on final annealing. This relationship can be mathematically formulated for the final anneal as:

$Sag = 2.87 + 0.00235*G^{-2}$ (mm) $+ 30056.04*t^{-2}$

Where:

G = The grain size (diameter) of the material in mm

t = Time in furnace (seconds)

It was found that with production material the effect of grain size is only significant up to approximately a grain size ASTM number of approximately 6.5 (mean linear intercept length of 0.0336mm). The contribution to the sag value from a modelling perspective flattens out at a coarser grain size (smaller ASTM number). This, therefore, appears to be a critical grain size should the present processing parameters be adhered to in order to obtain a significant increase in sag resistance.

The increasing contribution of each parameter to the model is (from least significant to most):

- Final annealing line speed
- Final annealing temperature
- Reheat temperature
- Total mass percent niobium in the steel and
- Final grain size.

Experimental work on final cold rolled material has shown that there appears to be a change in the "bulk" activation energy (recovery, recrystallization and grain growth)

from below approximately 1000^{O}C to that above this temperature. These values were 1113 kJ/mol and 112kJ /mol respectively. The "bulk" activation energy was determined as material is generally annealed in production plants from cold rolled material to obtain a final grain size. The annealing speed would thus be significantly slower at temperatures below 1000^{O}C if a final grain size is required than it would be above 1000^{O}C.

The sag resistance of type 441 material does not appear to be significantly increased by ageing heat treatments on final annealed material.

The sag resistance of the material can be significantly increased with a hot band anneal at a temperature of 1150^{o}C and above. This is due, it appears, to a greater degree of solid solution strengthening by the niobium. The elongation of the material, however, annealed at these higher temperatures is negatively affected. The optimum results as far as sag and elongation properties are concerned is to anneal the hot band between 1000^{o}C and 1100^{O}C followed by a similar heat treatment at 1050 ^{o}C on the cold band material to obtain an ASTM grain size of approximately 6.5 or less.

The as-cast material appeared to increase in sag resistance at temperatures below and above the reheat temperature of approximately 1100^{O}C. It would appear at this stage from a processing perspective that the material should be reheated at a temperature of approximately 1150^{O}C. This temperature should be sufficient to cause the maximum amount of niobium to go in to solution. This temperature is also not significantly higher than the present practice of reheating at approximately 1100 ^{o}C. The formation of laves phase should, therefore, be avoided by the fast laminar cooling after hot rolling to below approximately 600^{O}C. The processing parameters would, however, need some modification to take account of the higher mass percent niobium in solution. The sag values should, however, not be significantly altered by the slightly larger grain size, but could be improved upon (by assuming that the same model would apply to final annealed material with a higher niobium content) should the grain size be limited to a maximum ASTM number of 6.5. The longer anneal on the final material may be critical to ensure that maximum dissolution of the niobium has occurred both from an elongation and sag resistance perspective.

The optimum processing parameters for maximum sag resistance, with some consideration of the final elongation, would thus be:

- A reheat temperature of approximately 1150^{O}C
- Hot band anneal within the range 1000 °C to 1100 °C
- Cold band anneal within the range 1000 °C to 1100 °C to obtain a maximum ASTM grain size number of approximately 6.5.

BIBLIOGRAPHY

1. K.C. Barraclough, *Sheffield and the development of stainless steel*, Ironmaking and Steelmaking, **Vol. 16, No. 4**, p253-265, 1989.
2. W. D. Edsall, *Stainless steel for automotive exhaust systems*, Chromium Review **No. 9**, p1-4, 9th December 1988.
3. F.B. Pickering, *Physical metallurgical development of stainless steels*, Perspectives in metallurgical developments, p2-28, 1984.
4. J. Beddoes and J.G. Parr, *Introduction to Stainless Steels*, 3rd Edition, ASM International, Materials Park, OH 44073-0002, First Printing June 1999.
5. *Properties and Selection: Stainless Steels, Tool Materials and Special-Purpose Metals*, Volume 3, Metals Handbook, Ninth edition, American Society of Metals, 1980.
6. J Olsson and M. Liljas, *60 Years of Duplex Stainless Steel Applications*, National Association of Corrosion Engineers annual Conference, Paper no **395**, 1994.
7. Collin Barns and John Tarbotton, Private Communication, Columbus Stainless, 2001.
8. A. Hocking, *The Chrome connection, Commemorative History of Middelburg Steel & Alloys*, Hollards South Africa, ISBN 0-620-16077-2, 1992.
9. *Metallography, Structures and Phase Diagrams*, Volume 8, Metals Handbook, Eighth edition, American Society of Metals, September 1973.
10. Scientific Editors – P. Lacombe, B. Baroux, G. Beranger, Translated by- J.H.Davidson and J.B. Lindquest, Stainless Steels Les Editions De Physique Les Ulis, France, ISBN 2-86883-189-3, 1993.
11. F.B. Pickering, *Relationship between Microstructure and Properties in Stainless Steels*, Micon **78**, ASTM STP 672, p263-295, 1979.
12. F.B.Pickering, *Physical Metallurgy of stainless steel developments*, International Metals Reviews, **Review 211**, p227-268, December 1976.
13. L.Colombier and J.Hochmann, Translated by Scripta Technica Ltd, *Stainless and heat Resisting Steels*, Edward Arnold (Publishers) Ltd, Printed in Great Britain by Fletcher & Son Ltd. Norwich, 1967.
14. R.A. Lula, from an introduction to stainless steel, by J.G Parr and A.Hanson, Stainless Steel, American society of Metals, ISBN 0-87170-208-8, Cairns Publication Services, Inc, USA, Fifth printing Feb 1993,

15. Y. Hosoi and N. Wade, *Improvement of Creep properties and cavity formation of modified Type 316 austenitic stainless steel by micro alloying with Phosphorus and Carbon*, International Conference on Creep and Fracture Engineering materials and Structures, p763-773, 1984.
16. *Stainless Steel Type 441, AL441HP™ Alloy*, Technical Data Blue Sheet, Allegheny Ludlum Corporation, Pittsburgh, PA, p1-6, 1999.
17. Z. Kubon and V. Foldyna, *The Effect of Nb, V, N and Al on the creep rupture strength of 9-12% Cr steel*, Steel Research **66, No9**, p389-393, 1995.
18. J. Wadsworth, S.R.Keown and J.H.Woodhead, *The effect of niobium carbide precipitation on the density changes and creep properties of Type 347 austenitic stainless steels*, Metal Science, vol **10**, p105-112, March 1976.
19. K.J.Irvine, J.D. Murray and F.B.Pickering, *Structural aspects of Creep-Resisting Steel*, I.S.I Special Report **No. 70**, p246-275, 1961.
20. K. Miyakusu, Y. Uematsu and K. Hoshino, *Effect of Alloying elements on Strain Hardening Exponent of Ferritic Stainless Steel*, Transactions ISIJ, **Vol. 26**, 1986.
21. K.Miyata, Y. Sawaragi, H.Okada, F.Masuyama, T.Yokoyama and N.Komoi, *Microstructural Evolution of a 12Cr-2W-Cu-V-Nb Steel during three-year Service Exposure*, ISIJ International, **Vol. 40, No 11**, p1156-1163, 2000.
22. A.J. De Ardo, *The role of Niobium in modern Ferritic Stainless Steels*, International Symposium on Tantulum and Niobium, Germany, p113-126, 24-28 Sept 1995.
23. M. Barteri and M.G. Mecozzi, *Low cost weldable Ferritic stainless steel for hot end of automotive exhaust gas systems*, International congress- Stainless steel '99 Science and market, 3rd European congress, **Vol1**, p75-84, 1999.
24. N. Fujita, E. Sato, K. Ohmura, and A. Yamamoto, *Development of Ferritic stainless steel YUS450 with High Heat Resistance for Automotive Exhaust System Components*, Nippin Steel Technical Report **No 71**, p25-30, October 1996.
25. T. Sawatani, S. Minamino and H. Morikawa, *Effect of Laves Phase on the properties of Ti and Nb Stabilised low C, N-19%CR-2%Mo Stainless Steel Sheets*, Transactions ISIJ, **Vol. 22**, p172-180, 1982.
26. L.Bin, L. Shiying and W. Xinzeng, *Study on Mechanism of Brittle Cracking for High Purity Cr18Mo2 Ferritic Stainless Steel*, 21st Century Steel Industry of Russia and CIS, **3**, p206-210, 1994.

27. M. Koike, Y. Hayashi and M. Ogaya, *Development of Niobium- stabilised Ferritic stainless steel sheets with extra clean surface and good drawability*, New development stainless steel technologies conference proceedings, p263-268, 17-21 Sept 1984.
28. V. Albino Rodriques, R. Claret, R, da Silva, J. Nicacio. da Silva, J. Antanio and N. de Carvalco, *Process for the Production of Ferritic Stainless Steel, Innovation in Stainless Steel*, Florence, Italy, p2.353-2.358, 1993.
29. Y.Xu, C. I. Garcia, I.A. Franson and A.J.DeArdo, *Annealing behaviour and formability of Ferritic stainless Steel*, International symposium on Low- Carbon Steels for the 90's, Edited by R. Asfahani and G. Tither, The Minerals, Metals and Materials Society, p397-404, 1993.
30. S. D. Washko and J. F. Grubb, *The effect of Niobium and Titanium dual Stabilisation on the Weldability of 11% Chromium Ferritic Stainless Steel*, Proceedings of International Conference on Stainless Steels, Chiba, ISIJ, p1062-1068, 1991.
31. M.Hua, G.I. Garcia, A.J. DeArdo, G. Tither, *Dual- Stabilised Ferritic Stainless steels for demanding applications such as Automotive exhaust systems*, I&SM, p41-44, April 1997.
32. A.J. De Ardo, *Influence of Niobium and Tantalum on Stainless Steel*, Basic Metals Processing Research institute, p435-462.
33. S.R. Keown, *Niobium in Stainless Steels, Niobium Technical Report*, NbTR – 09/86, ISSN 0101 – 5963, p1-31, 1986.
34. R.F. Steigerwald, H.J. Dundas, J.D. Redmond and R.M. Davidson, *The Physical Metallurgy of Fe-Cr-Mo Ferritic Stainless Steels*, Metallurgist and Material Technologist, p57-71, April 1978.
35. R.D. Campbell, *Ferritic Stainless Steel Welding Metallurgy*, Key engineering Materials, Copyright Trans Tech Publications, Switzerland, **69 &70**, p167- 216, 1992.
36. G. E. Dieter, *Mechanical metallurgy*, Third Edition, McGraw - Hill Book Company, ISBN 0-07-100406-08, 1988.
37. D. S. Clark and W. R. Varney, *Physical Metallurgy for Engineers*, 2nd Edition, D.Van Nostrand Company, ISBN 0-442-01570-4, p350-351, 1962.
38. G.Bernosconi and G. Piatti, Creep of Engineering Materials and Structures, Applied Science Publishers. LTD, England, ISBN 0-85334-878-2, 1979.

39. J. Glen and J.D. Murray, *Metallurgical aspects of creep in Carbon and Low-alloy steels*, Special Report **Part 69**, p40-53, 1961.

40. Y. Uematsu, N. Hiramatsu and S. Nakamura, *Heat resisting Ferritic stainless steel excellent in low temperature toughness, Weldability and heat resistance*, United States Patent 5,302,214, p1-12, Apr. 12 1994.

41. N. Fujita, K.Ohmura, M.Kikuchi, T. Sizuki, S. Funaki and I. Hiroshiga, *Effect of Nb on high Temperature Properties for Ferritic Stainless Steel*, Innovation Stainless Steel, Florence, Italy, p2.197-2.202, 11-14 October 1993.

42. P.R.Borneman, *Alloying effects of reactive elements in Ferritic Stainless steels*, Conference Proceedings – Speciality Steels and Hard Materials, p307-314, 8-12 November 1982.

43. J.N. Johnson, *Influence of Columbium on 870°C creep properties of 18% chromium Ferritic stainless steels*, International congress and exposition, Society of Automotive Engineers, Inc, **810035**, Feb 1981.

44. J.H. Woodhead and A. G. Quarrell, *The role of carbides in low – alloy creep – resisting steels*, Department of Metallurgy, University of Sheffield, Silk and Terry Ltd., London and Birmingham.

45. I. Yamauchi, T. Sakamoto, T. Zaizen and A. Takahashi, *Corrosion Resistance of Ferritic Stainless Steel Welds*, Transactions ISIJ, **Vol23**, pB298, 1983.

46. C.A.C Sousa and S.E. Kuri, *Relationship between Niobium content and pitting corrosion resistance in Ferritic Stainless Steel*, Materials Letters **25**, 1995.

47. S. Akiyama, S. Kiya, K. Yokoyama, K. Hiahara and H. Hoshi, *Development of an improved Corrosion resistant Ferritic stainless steel "AR-FC-3"*, The Charles Hatchet Award Paper, p3-17, 1989.

48. B. Baroux, P. Pedarre and J. Decroix, *Metallurgical aspects of corrosion resistance of stabilised 17%Cr stainless steel*, The institute of metals – Stainless Steel 87, York, p138-143, September 1987.

49. Ivan A. Franson and J. D. Fritz, *Stabilisation requirements for T409 (UNS S40900) Ferritic Stainless Steel*, Society of Automotive Engineers, Inc, p155-161, 1997.

50. J.D. Gates and R. A. Jago, *Effect of Nitrogen contamination on intergranular corrosion of stabilised Ferritic stainless steels*, Materials Science and Technology, **Vol. 3**, p450-454, June 1987.

51. M. Onoyama, M. Tsuji, H. Abo, H. Ogawa and S. Aokil, *Development and application of corrosion resistant Ferritic stainless Steels, YUS 434D, YUS 190, YUS 190L and 25Cr-5Ni-4Mo-Nb Steel*, Nippon Steel Technical report **No.12**, p 29-38, December 1978.
52. H. Fujimura and S. Tsuge, *Effect of C, Ti, Nb on the recrystallization behaviour after hot deformation in 16% Cr Ferritic stainless steel*, International congress- Stainless steel '99 Science and Market, 3rd European congress, p67-76, 1999.
53. Y. Kato, Y.Yazawa, T. Yokota, T. Ujiro and S. Satoh, *Effect of steel chemistry on the ridging property of Ferritic stainless steels*, Technical Research Lab, Kawasaki Steel Corp.
54. S. R. Mediratta and V. Ramaswamy, *Physical Metallurgy of Ferritic stainless Steel*, Tool and Alloy Steels, **Vol. 10, No12**, p451-461, December 1976.
55. J. B. Hill, *Meeting North American demands for stainless exhaust systems*, Steel Times International, p35, July 1993.
56. R Ashworth, D. Dulieu and K.J. King, *Materials requirement for modern exhaust systems*, Steel Times International, p36-38, July 1993.
57. J. Lagier, P. Rombeaux, J. Ragot, P. Vaugeois, *Ferritic Stainless Steels in Exhaust systems*, Innovation Stainless steel, Florence, Italy, p1.159-1.164, 11-14 October 1993.
58. K. Ishii, A. Miyazaki and S. Satoh, *Stainless steels for Automotive Exhaust System*, Kawasaki Steel Technical Report **No40**, p39-41, May 1999.
59. S. Gallo, W.Nicodemi and G.Pontini, *Comparison of Technologies for stainless applications to I.C Engines exhaust manifolds*, International congress- Stainless steel '99 Science and market, 3rd European congress, **Vol1**, p95-103, 1999.
60. T.Lyman et all, *Metallography, Atlas of Microstructures of Industrial Alloys*, Volume 7, Metals Handbook, Eighth edition, American Society of Metals, Library of Congress catalogue card Number: 27-12046, pp.132, 1972
61. ASTM Committee E-4, *Standard Methods for Determining Average Grain Size*, Designation: E112 –96, Annual Book of ASTM Standards, Section 3, **Volume 03/01**, ASTM, ISBN 0-8031-2766-9, 2000.
62. J.M. Juran and F.M. Gryna, *Quality Planning and analysis, from product development through use*: McGraw-Hill Book Company, ISBN 0-07-033178-2, p67-68, 1980.

63. M.Barteri, F. Fazio and F. Fortunati, *Gli Acciai inossidabili nei sistemi di scarico degli autoveicoli*, La metallurgia italiana, p33, 1999.
64. D.Peckner and I.M. Bernstein, Handbook of Stainless Steels, McGraw-Hill Book Company, ISBN 0-07-049147-X, 1977.
65. J. A. Douthett, *Oxidation Resistant 12% Cr Automotive Stainless Steel, International congress and exposition*, Society of Automotive Engineers, **810036**, p1-12, 1981.
66. E.Popov, *Mechanics of Materials*, 2nd Edition, Prentice-Hall, Inc, ISBN 0-13-571158-4, p135-140, 1978
67. W.A.Nash, Schaum's Outline Series, Theory and Problems of Strength of Materials, 2nd Edition, p. 143-146, 1977, McGraw-Hill Book Company, ISBN 0-07-084366-X
68. F.R.N. Nabarro and H. L. de Villiers, *The Physics of Creep, Creep and Creep-resistant Alloys*, Taylor and Francis Ltd., ISBN 085066 852 2, p. 53 to 60, 1995.
69. *Temperature-Electromotive Force (EMF) Tables for Standardised Thermocouples – E230*, ASTM Annual Book of ASTM Standards, **Volume 14.03**.
70. Private Communication – C. M.P. Frost and J.P. Wessels, *Heating Up Rate Of Stainless Steel, Columbus Internal Report*, p2, 29 January 1997.
71. M. Tamura, K. Ikeda, H.Esaka and K. Shinozuka, *Precipitation Behaviour of NbC in 9%Cr1%Mo0.2%VNb Steel*, ISIJ International, **Vol.41, No8**, p908-914 2001.
72. V.Kuzucu, M.Aksoy, M.H. Korkut and M.M. Yildirim, *The effect of Niobium on the microstructure of Ferritic Stainless Steel*, Materials Science and Engineering **A230**, p75-80, 1997.
73. G.M.Clarke and D.Cooke, *A Basic Course in Statistics*, 2nd Edition, Edward Arnold Publishers) Ltd, ISBN 0-7131-3496-8, 1986
74. *Statgraphics Plus Reference Manual*, Version 6, Manugistics, Inc, 1992.
75. M. Suehiro, *An Analysis of the solute Drag Effect of Nb on recrystallization of Ultra Low Carbon Steel*, ISIJ International, **Vol. 38, No 6**, p547-552, 1998.
76. Y.Li, Y. Li and R.J. Fruehan, *Formation of Titanium Carbonitride from Hot Metal*, ISIJ International, **Vol. 41, No12**, p1417-1422, 2001.
77. P.Cotterill and P.R.Mould, *Recrystallization and Grain Growth in Metals*, Surrey University Press, ISBN 0 903384 11 6, p275 - 281, 1976.
78. P.Cotterill and P.R.Mould, *Recrystallization and Grain Growth in Metals*, Surrey University Press, ISBN 0 903384 11 6, p115-119, p153-155, 1976.

Appendix 1

Database used in the analysis of processing parameters and chemistry on the sag resistance of 441 material.

MPO	sag (mm)	Calculated Grain Size (mm)	Normalized Sag (mm3)	ASTM Grain Size no.	Final Gauge	Average Sag	Hot band Gauge	Discharge Temp (oC)
3110144	2.5	0.0336	6.0	6.5	1.55	2.7	5.07	1220
3110144	2.5	0.0336	6.0	6.5	1.55	2.7	5.07	1220
3110144	3	0.0336	7.2	6.5	1.55	2.7	5.07	1220
3115260	29	0.0168	25.7	8.5	0.942	29	3.511	1216
3117302	39	0.0141	35.4	9	0.953	39.7	3.498	1220
3117302	39	0.0141	35.4	9	0.953	39.7	3.498	1220
3117302	41	0.0141	37.2	9	0.953	39.7	3.498	1220
3117470	16.5	0.0168	22.8	8.5	1.175	17	3.496	1219
3117470	17	0.0168	23.5	8.5	1.175	17	3.496	1219
3117470	17.5	0.0168	24.2	8.5	1.175	17	3.496	1219
3122172	1.5	0.0200	3.7	8	1.578	2	4.999	1216
3122172	2.5	0.0200	6.2	8	1.578	2	4.999	1216
3122172	6.5	0.0238	16.2	7.5	1.578	6.5	4.999	1216
3122173	4.5	0.0200	10.7	8	1.541	5.3	5	1216
3122173	6	0.0200	14.2	8	1.541	5.3	5	1216
3122180	5	0.0200	7.1	8	1.19	6.3	5	1217
3122180	7.5	0.0200	10.6	8	1.19	6.3	5	1217
3122181	2	0.0336	5.1	6.5	1.6	2.1	4.999	1213
3122181	2.2	0.0336	5.6	6.5	1.6	2.1	4.999	1213
3122182	1	0.0429	2.4	5.8	1.559	1.3	5	1214
3122182	1.5	0.0429	3.6	5.8	1.559	1.3	5	1214
3122183	1.5	0.0283	3.8	7	1.591	2.3	4.999	1215
3122183	3	0.0283	7.6	7	1.591	2.3	4.999	1215
3122184	1.5	0.0444	3.4	5.7	1.5	1.5	4.999	1215
3122184	1.5	0.0444	3.4	5.7	1.5	1.5	4.999	1215
3124261	0.5	0.0800	1.2	4	1.55	2.3	5.002	1089
3124261	2	0.0800	4.8	4	1.55	2.3	5.002	1089
3124261	4.5	0.0800	10.8	4	1.55	2.3	5.002	1089
3124262	7.5	0.0238	16.9	7.5	1.5	7.8	5.004	1089
3124262	8	0.0238	18.0	7.5	1.5	7.8	5.004	1089
3124263	7	0.0606	6.3	4.8	0.948	7.2	3.5	1093
3124263	7	0.0606	6.3	4.8	0.948	7.2	3.5	1093
3124263	7.5	0.0606	6.7	4.8	0.948	7.2	3.5	1093
3124264	4.5	0.0734	5.7	4.25	1.125	5	3.503	1092
3124264	5	0.0734	6.3	4.25	1.125	5	3.503	1092
3124264	5.5	0.0734	7.0	4.25	1.125	5	3.503	1092
3124270	5.5	0.0141	12.5	9	1.508	7.2	5.003	1091
3124270	7.5	0.0141	17.1	9	1.508	7.2	5.003	1091
3124270	8.5	0.0141	19.3	9	1.508	7.2	5.003	1091
3124271	2.8	0.0566	3.6	5	1.13	3.3	3.499	1088
3124271	3	0.0566	3.8	5	1.13	3.3	3.499	1088
3124271	4	0.0566	5.1	5	1.13	3.3	3.499	1088
3124274	2.5	0.0566	5.8	5	1.52	3.7	5.002	1090

MPO	sag (mm)	Calculated Grain Size (mm)	Normalized Sag (mm3)	ASTM Grain Size no.	Final Gauge	Average Sag	Hot band Gauge	Discharge Temp (oC)
3124274	3	0.0566	6.9	5	1.52	3.7	5.002	1090
3124274	5.5	0.0566	12.7	5	1.52	3.7	5.002	1090
3125353	4	0.0308	9.0	6.75	1.504	4.8	4.996	1095
3125353	5.5	0.0308	12.4	6.75	1.504	4.8	4.996	1095
3125354	3	0.0566	6.6	5	1.48	3.2	4.993	1097
3125354	3	0.0566	6.6	5	1.48	3.2	4.993	1097
3125354	3.5	0.0566	7.7	5	1.48	3.2	4.993	1097
3125360	11	0.0283	10.3	7	0.967	12.5	3.497	1093
3125360	14	0.0283	13.1	7	0.967	12.5	3.497	1093
3125361	15.5	0.0283	13.4	7	0.931	17	3.496	1093
3125361	18.5	0.0283	16.0	7	0.931	17	3.496	1093
3125362	1.5	0.0336	5.6	6.5	1.94	1.8	5.987	1094
3125362	2	0.0336	7.5	6.5	1.94	1.8	5.987	1094
3125364	4	0.0566	9.1	5	1.511	4.2	4.993	1092
3125364	4	0.0566	9.1	5	1.511	4.2	4.993	1092
3125364	4.5	0.0566	10.3	5	1.511	4.2	4.993	1092
3126383	15	0.0200	13.5	8	0.947	15.5	3.499	1096
3126383	16	0.0200	14.3	8	0.947	15.5	3.499	1096
3126384	12	0.0238	11.1	7.5	0.96	12	3.496	1097
3126384	12	0.0238	11.1	7.5	0.96	12	3.496	1097
3126391	4.5	0.0400	10.4	6	1.52	6.2	4.994	1095
3126391	7	0.0400	16.2	6	1.52	6.2	4.994	1095
3126391	7	0.0400	16.2	6	1.52	6.2	4.994	1095
3126392	8.5	0.0400	7.5	6	0.938	9.8	3.496	1093
3126392	10	0.0400	8.8	6	0.938	9.8	3.496	1093
3126392	11	0.0400	9.7	6	0.938	9.8	3.496	1093
3126394	12	0.0800	17.3	4	1.2	12	3.495	1096
3126394	12	0.0800	17.3	4	1.2	12	3.495	1096
3127730	5	0.0400	7.2	6	1.2	6.3	3.164	1115
3127730	7.5	0.0400	10.8	6	1.2	6.3	3.164	1115
3127732	10.5	0.0283	9.7	7	0.96	11.8	3.153	1109
3127732	13	0.0283	12.0	7	0.96	11.8	3.153	1109
3127732	12.5	0.0336	11.5	6.5	0.96	13.3	3.153	1109
3127732	14	0.0336	12.9	6.5	0.96	13.3	3.153	1109
3129511	6.5	0.0238	15.6	7.5	1.55	6.5	4.998	1095
3130461	3	0.0400	7.2	6	1.55	3.5	5	1098
3130461	4	0.0400	9.6	6	1.55	3.5	5	1098
3130463	15	0.0476	9.8	5.5	0.81	15	2.796	1102
3130464	24	0.0230	15.4	7.6	0.8	24	3.495	1095
3130464	27	0.0238	17.3	7.5	0.8	27	3.495	1095
3130471	4	0.0400	5.8	6	1.2	5	3.496	1106
3130471	6	0.0400	8.6	6	1.2	5	3.496	1106
3131190	3.5	0.0283	14.0	7	2	3.8	6.004	1104
3131190	4	0.0283	16.0	7	2	3.8	6.004	1104
3131191	16	0.0283	10.3	7	0.803	16	2.799	1098
3131192	12.5	0.0400	8.0	6	0.8	13.8	2.799	1097
3131192	14	0.0400	9.0	6	0.8	13.8	2.799	1097

MPO	sag (mm)	Calculated Grain Size (mm)	Normalized Sag (mm3)	ASTM Grain Size no.	Final Gauge	Average Sag	Hot band Gauge	Discharge Temp (oC)
3131192	15	0.0400	9.6	6	0.8	13.8	2.799	1097
3131193	4	0.0336	9.8	6.5	1.566	5.2	5.001	1096
3131193	5.5	0.0336	13.5	6.5	1.566	5.2	5.001	1096
3131193	6	0.0336	14.7	6.5	1.566	5.2	5.001	1096
3131201	10.5	0.0168	26.9	8.5	1.6	10.5	5.003	1100
3131203	4	0.0566	6.4	5	1.264	4.5	4.502	1094
3131203	5	0.0566	8.0	5	1.264	4.5	4.502	1094
3131204	11	0.0283	10.3	7	0.97	11	3.499	1097
3132020	4	0.0283	9.3	7	1.527	4	5.003	1100
3132020	4	0.0283	9.3	7	1.527	4	5.003	1100
3132021	6	0.0283	5.3	7	0.94	6.8	3.5	1098
3132021	7.5	0.0283	6.6	7	0.94	6.8	3.5	1098
3132023	1.5	0.0336	3.4	6.5	1.512	2.3	4.506	1110
3132023	3	0.0336	6.9	6.5	1.512	2.3	4.506	1110
3132024	7	0.0174	16.8	8.4	1.55	7.5	5.004	1105
3132024	8	0.0174	19.2	8.4	1.55	7.5	5.004	1105
3132031	4.5	0.0400	10.8	6	1.55	5.3	5.001	1099
3132031	6	0.0400	14.4	6	1.55	5.3	5.001	1099
3132034	2.5	0.0400	6.1	6	1.562	3.8	5.001	1093
3132034	5	0.0400	12.2	6	1.562	3.8	5.001	1093
3132870	6.5	0.0336	10.4	6.5	1.265	6.8	4.494	1098
3132870	7	0.0336	11.2	6.5	1.265	6.8	4.494	1098
3132870	2	0.0386	3.2	6.1	1.265	2.8	4.494	1098
3132870	3	0.0386	4.8	6.1	1.265	2.8	4.494	1098
3132870	3.5	0.0386	5.6	6.1	1.265	2.8	4.494	1098
3135000	10	0.0566	9.2	5	0.958	10.5	3.502	1088
3135000	11	0.0566	10.1	5	0.958	10.5	3.502	1088
3135001	10	0.0200	22.5	8	1.5	10	5.015	1090
3135002	6.5	0.0283	14.2	7	1.48	6.5	5.006	1090
3135003	7.5	0.0283	16.3	7	1.473	7.8	5.007	1088
3135003	8	0.0283	17.4	7	1.473	7.8	5.007	1088
3135004	8.5	0.0200	18.6	8	1.48	8.5	5.006	1091
3135011	7.5	0.0200	16.4	8	1.48	7.5	4.506	1088
3135610	14	0.0200	30.7	8	1.48	14	5.01	1091
3135611	16.5	0.0141	35.2	9	1.46	16.5	4.506	1089
3135611	16.5	0.0141	35.2	9	1.46	16.5	4.506	1089
3135612	8	0.0238	18.2	7.5	1.51	8.3	4.504	1090
3135612	8.5	0.0238	19.4	7.5	1.51	8.3	4.504	1090
3135613	15.5	0.0168	22.3	8.5	1.2	15.5	3.502	1093
3135622	8	0.0283	17.4	7	1.473	8	4.506	1090
3135623	12	0.0283	10.9	7	0.954	12	3.501	1094
3151143	12	0.0273	15.6	7.1	1.14	12.5	3.5	1117
3151143	12.5	0.0273	16.2	7.1	1.14	12.5	3.5	1117
3151143	13	0.0273	16.9	7.1	1.14	12.5	3.5	1117
3151192	11	0.0325	10.1	6.6	0.96	12.5	3.502	1095
3151192	12.5	0.0325	11.5	6.6	0.96	12.5	3.502	1095
3151192	14	0.0325	12.9	6.6	0.96	12.5	3.502	1095

MPO	sag (mm)	Calculated Grain Size (mm)	Normalized Sag (mm3)	ASTM Grain Size no.	Final Gauge	Average Sag	Hot band Gauge	Discharge Temp (oC)
3151193	5	0.0264	11.4	7.2	1.513	5.3	4.999	1096
3151193	5.5	0.0264	12.6	7.2	1.513	5.3	4.999	1096
3151193	5.5	0.0264	12.6	7.2	1.513	5.3	4.999	1096
3181322	45	0.0400	27.5	6	0.782	45	3.006	1058
3182872	31	0.0336	27.5	6.5	0.942	31	4.521	1137
3183330	45	0.0476	10.8	5.5	0.489	45	2.51	1066
3185001	20	0.0336	17.2	6.5	0.927	20	4.519	1073
3185802	7	0.0566	9.7	5	1.179	8.1	4.523	1059
3185802	9.1	0.0566	12.6	5	1.179	8.1	4.523	1059
3185804	8	0.0400	7.2	6	0.947	9	4.521	1060
3185804	10	0.0400	9.0	6	0.947	9	4.521	1060
3185811	31	0.0459	19.1	5.6	0.784	31	3.008	1063
3186291	14.5	0.0336	32.6	6.5	1.499	14.5	6.323	1075
3186293	29	0.0283	17.8	7	0.784	29	3.011	1059
3189242	12	0.0255	16.1	7.3	1.159	12	3.018	1063
3189243	21	0.0581	17.0	4.925	0.9	21	2.506	1060
3191661	6	0.0400	13.3	6	1.49	6	6.313	1095
3191662	6	0.0414	13.3	5.9	1.49	6	6.313	1088
3191663	6	0.0230	13.3	7.6	1.49	6	6.315	1092
3191663	5.5	0.0283	12.2	7	1.49	5.5	6.315	1092
3191664	7.5	0.0400	17.0	6	1.505	7.5	6.323	1095
3192851	17	0.0566	9.8	5	0.76	17.8	2.504	1097
3192851	17.5	0.0566	10.1	5	0.76	17.8	2.504	1097
3192851	19	0.0566	11.0	5	0.76	17.8	2.504	1097
3192852	8	0.0336	17.5	6.5	1.48	8	6.308	1095
3192860	62	0.0476	14.2	5.5	0.478	62	2.504	1096
3192864	12.5	0.0400	11.0	6	0.94	12.8	4.517	1089
3192864	13	0.0400	11.5	6	0.94	12.8	4.517	1089
3192870	9.5	0.0400	13.7	6	1.2	9.5	4.516	1096
3192873	10	0.0476	9.0	5.5	0.95	10.5	4.524	1096
3192873	11	0.0476	9.9	5.5	0.95	10.5	4.524	1096
3192880	7	0.0400	9.9	6	1.19	7	4.52	1098
3192881	14	0.0400	12.9	6	0.96	14	4.515	1097
3192882	3.5	0.0476	7.5	5.5	1.46	3.8	6.312	1090
3192882	4	0.0476	8.5	5.5	1.46	3.8	6.312	1090
3192882	4	0.0476	8.5	5.5	1.46	3.8	6.312	1090
3192883	3.5	0.0400	7.6	6	1.47	4.5	6.312	1094
3192883	4.5	0.0400	9.7	6	1.47	4.5	6.312	1094
3192883	5.5	0.0400	11.9	6	1.47	4.5	6.312	1094
3192884	7.5	0.0283	9.4	7	1.12	7.5	4.528	1090

MPO	Max Last Pass Temp (oC)	Ave Last pass Temp (oC)	Down Coil Temp (oC)	Hot Band Line Speed	Hot Band time at temp	Hot Band Strip Temp (oC)	Final Line Speed	Final Time at Temp	Final Strip Temp (oC)
3110144	894	869	519	9	22	919	29	8	991
3110144	894	869	519	9	22	919	29	8	991
3110144	894	869	519	9	22	919	29	8	991
3115260	923	894	705	16	92	955	34	38	1000
3117302	956	931	744	16	69	949	35	48	1001
3117302	956	931	744	16	69	949	35	48	1001
3117302	956	931	744	16	69	949	35	48	1001
3117470	960	928	727	16	75	950	13	73	1000
3117470	960	928	727	16	75	950	13	73	1000
3117470	960	928	727	16	75	950	13	73	1000
3122172	960	931	689	12	29	944	24	40	1000
3122172	960	931	689	12	29	944	24	40	1000
3122172	960	931	689	12	29	944	24	40	1000
3122173	959	933	710	12	22	947	21	88	1000
3122173	959	933	710	12	22	947	21	88	1000
3122180	945	917	685	12	26	947	30	20	998
3122180	945	917	685	12	26	947	30	20	998
3122181	956	928	680	12	20	946	20	56	1000
3122181	956	928	680	12	20	946	20	56	1000
3122182	957	928	693	12	21	946	13		1000
3122182	957	928	693	12	21	946	13		1000
3122183	953	925	681	12	30	947	19		1000
3122183	953	925	681	12	30	947	19		1000
3122184	954	926	685	12	29	947	14		996
3122184	954	926	685	12	29	947	14		996
3124261	904	880	605	16	19	948	24	40	1050
3124261	904	880	605	16	19	948	24	40	1050
3124261	904	880	605	16	19	948	24	40	1050
3124262	943	924	630	16	3	938	36	14	1018
3124262	943	924	630	16	3	938	36	14	1018
3124263	908	879	555	19	33	947	36	25	1050
3124263	908	879	555	19	33	947	36	25	1050
3124263	908	879	555	19	33	947	36	25	1050
3124264	915	889	584	19	21	947			
3124264	915	889	584	19	21	947			
3124264	915	889	584	19	21	947			
3124270	898	872	582	16	20	944	18	42	1048
3124270	898	872	582	16	20	944	18	42	1048
3124270	898	872	582	16	20	944	18	42	1048
3124271	909	886	598	20	15	947	22	47	1051
3124271	909	886	598	20	15	947	22	47	1051
3124271	909	886	598	20	15	947	22	47	1051
3124274	902	875	570	15	34	945	29	16	1049
3124274	902	875	570	15	34	945	29	16	1049
3124274	902	875	570	15	34	945	29	16	1049
3125353	916	891	656	14	3	941	28	12	1048
3125353	916	891	656	14	3	941	28	12	1048

MPO	Max Last Pass Temp (oC)	Ave Last pass Temp (oC)	Down Coil Temp (oC)	Hot Band Line Speed	Hot Band time at temp	Hot Band Strip Temp (oC)	Final Line Speed	Final Time at Temp	Final Strip Temp (oC)
3125354	910	887	635	12	24	949	19	92	1052
3125354	910	887	635	12	24	949	19	92	1052
3125354	910	887	635	12	24	949	19	92	1052
3125360	905	882	601	14		951	38	17	1020
3125360	905	882	601	14		951	38	17	1020
3125361	906	885	615	14	68	949	14		1019
3125361	906	885	615	14	68	949	14		1019
3125362	925	909	692	10	1	934	27	19	1033
3125362	925	909	692	10	1	934	27	19	1033
3125364	895	873	641	13	8	944	13	22	
3125364	895	873	641	13	8	944	13	22	
3125364	895	873	641	13	8	944	13	22	
3126383	913	893	630	11		949	34	20	1019
3126383	913	893	630	11		949	34	20	1019
3126384	914	893	598	9		950			
3126384	914	893	598	9		950			
3126391	906	880	655	10	31	947			
3126391	906	880	655	10	31	947			
3126391	906	880	655	10	31	947			
3126392	912	889	618	11	90	952	39	24	1020
3126392	912	889	618	11	90	952	39	24	1020
3126392	912	889	618	11	90	952	39	24	1020
3126394	914	887	598	11		1055	10	64	1000
3126394	914	887	598	11		1055	10	64	1000
3127730	933	900	640	24	24	946	32	64	1023
3127730	933	900	640	24	24	946	32	64	1023
3127732	922	900	742	19		955	57	12	1021
3127732	922	900	742	19		955	57	12	1021
3127732	922	900	742	19		955	57	12	1021
3127732	922	900	742	19		955	57	12	1021
3129511	915	888	677	17	19	928	33	64	1022
3130461	915	888	738	18		929	32	65	1024
3130461	915	888	738	18		929	32	65	1024
3130463	912	885	696	20	92	962	50	43	1027
3130464	922	890	706	17		960	57	33	1020
3130464	922	890	706	17		960	57	33	1020
3130471	922	896	720	19	41	944	36	57	1022
3130471	922	896	720	19	41	944	36	57	1022
3131190	929	910	698	15	1	923	24	38	1019
3131190	929	910	698	15	1	923	24	38	1019
3131191	906	875	645	20		759	41	55	1033
3131192	903	872	640	19	87	949	53	40	1023
3131192	903	872	640	19	87	949	53	40	1023
3131192	903	872	640	19	87	949	53	40	1023
3131193	909	884	694	16	4	938	30	72	1024
3131193	909	884	694	16	4	938	30	72	1024
3131193	909	884	694	16	4	938	30	72	1024

MPO	Max Last Pass Temp (oC)	Ave Last pass Temp (oC)	Down Coil Temp (oC)	Hot Band Line Speed	Hot Band time at temp	Hot Band Strip Temp (oC)	Final Line Speed	Final Time at Temp	Final Strip Temp (oC)
3131201	906	882	699	17	4	939	39	3	1011
3131203	902	880	691	17	12	940	34	61	1025
3131203	902	880	691	17	12	940	34	61	1025
3131204	910	885	679	21	11	937	49	34	1021
3132020	903	878	686	18	1	938	28	78	1023
3132020	903	878	686	18	1	938	28	78	1023
3132021	915	888	655	24	12	939	41	53	1026
3132021	915	888	655	24	12	939	41	53	1026
3132023	912	886	673	19	6	938	28	78	1024
3132023	912	886	673	19	6	938	28	78	1024
3132024	905	879	682	14	48	940	29	61	1021
3132024	905	879	682	14	48	940	29	61	1021
3132031	902	877	666	18	1	937	31	60	1021
3132031	902	877	666	18	1	937	31	60	1021
3132034	898	873	659	18	2	937	28	77	1023
3132034	898	873	659	18	2	937	28	77	1023
3132870	902	860	618	20	10	925	27	72	1025
3132870	902	860	618	20	10	925	27	72	1025
3132870	902	860	618	20	10	925	27	72	1025
3132870	902	860	618	20	10	925	27	72	1025
3132870	902	860	618	20	10	925	27	72	1025
3135000	925	892	661	22	11	947	43	41	1035
3135000	925	892	661	22	11	947	43	41	1035
3135001	910	883	658	19	2	926	38	7	1015
3135002	912	887	658	20		917	41	4	1017
3135003	909	883	667	20		926	41	6	1019
3135003	909	883	667	20		926	41	6	1019
3135004	913	888	676	21	1	932	41	1	1012
3135011	919	893	681	21	2	924	38	7	1015
3135610	915	884	649	20		915			
3135611	923	894	652				41	4	1016
3135611	923	894	652				41	4	1016
3135612	919	891	649				40	2	1013
3135612	919	891	649				40	2	1013
3135613	931	900	670	27	13	949	46	26	1023
3135622	918	888	643				41	2	1013
3135623	924	895	675	14		969	32	73	1033
3151143	905	880		14	61	942	42	51	1020
3151143	905	880		14	61	942	42	51	1020
3151143	905	880		14	61	942	42	51	1020
3151192	912	882	586	18	30	953	48	44	1020
3151192	912	882	586	18	30	953	48	44	1020
3151192	912	882	586	18	30	953	48	44	1020
3151193	891	870	656	13	16	939	30	54	1020
3151193	891	870	656	13	16	939	30	54	1020
3151193	891	870	656	13	16	939	30	54	1020
3181322	866	839		19	15	943	44	44	1021

MPO	Max Last Pass Temp (oC)	Ave Last pass Temp (oC)	Down Coil Temp (oC)	Hot Band Line Speed	Hot Band time at temp	Hot Band Strip Temp (oC)	Final Line Speed	Final Time at Temp	Final Strip Temp (oC)
3182872	929	907	623	17	6	942	29	57	1022
3183330	909	887	558	18	28	949	41	57	1020
3185001	911	888	727	13	32	946	44	33	1021
3185802	910	886	668				20	69	1020
3185802	910	886	668				20	69	1020
3185804	906	883	642	18	20	1050	44	20	1023
3185804	906	883	642	18	20	1050	44	20	1023
3185811	875	848	493				42	21	1019
3186291	900	880	701	11	59	947			
3186293	873	846	512				45	33	1026
3189242	861	835	489	16		1051			
3189243	853	829	529	18		1051	33	27	1021
3191661	864	847	641	11	9	1028	31	38	1020
3191662	856	841	559				32	62	1023
3191663	858	842	549				35	12	1018
3191663	858	842	549				35	12	1018
3191664	872	855	564	11	21	909	31	23	1019
3192851	871	851	559	24	25	1049	54	14	1052
3192851	871	851	559	24	25	1049	54	14	1052
3192851	871	851	559	24	25	1049	54	14	1052
3192852	877	861	651				28	13	1037
3192860	869	844	538				42	27	1050
3192864	881	867	667				49	9	1051
3192864	881	867	667				49	9	1051
3192870	882	868	619				37	10	1050
3192873	883	870	637	17	34	1047	50	6	1049
3192873	883	870	637	17	34	1047	50	6	1049
3192880	871	855	644	17	93	1071	39	6	1047
3192881	889	876	609				49	6	1049
3192882	877	863	676	14	22	1049	30	15	1051
3192882	877	863	676	14	22	1049	30	15	1051
3192882	877	863	676	14	22	1049	30	15	1051
3192883	876	861	677	14	20	1049			
3192883	876	861	677	14	20	1049			
3192883	876	861	677	14	20	1049			
3192884	884	871	605	19	29	1050	41	9	1051

MPO	C	S	Mn	Si	Ti	Mo	Cr	Nb	Al	B	N	O	Calcul reheat Nb	Calcul Down Coil Nb	Cold Red (%)
3110144	0.016	0.0045	0.5	0.5	0.249	0.03	17.9	0.437	0.007	0.0006	0.0201	0.0077	0.226	0.158	69.4
3110144	0.016	0.0045	0.5	0.5	0.249	0.03	17.9	0.437	0.007	0.0006	0.0201	0.0077	0.226	0.158	69.4
3110144	0.016	0.0045	0.5	0.5	0.249	0.03	17.9	0.437	0.007	0.0006	0.0201	0.0077	0.226	0.158	69.4
3115260	0.021	0.0083	0.44	0.47	0.18	0.03	17.8	0.553	0.004	0.0007	0.0185	0.0097	0.297	0.248	73.2
3117302	0.015	0.0038	0.54	0.54	0.253	0.04	17.9	0.77	0.006	0.0008	0.0186	0.0107	0.539	0.510	72.8
3117302	0.015	0.0038	0.54	0.54	0.253	0.04	17.9	0.77	0.006	0.0008	0.0186	0.0107	0.539	0.510	72.8
3117302	0.015	0.0038	0.54	0.54	0.253	0.04	17.9	0.77	0.006	0.0008	0.0186	0.0107	0.539	0.510	72.8
3117470	0.016	0.0024	0.5	0.5	0.202	0.05	17.9	0.81	0.005	0.0007	0.0232	0.0077	0.535	0.507	66.4
3117470	0.016	0.0024	0.5	0.5	0.202	0.05	17.9	0.81	0.005	0.0007	0.0232	0.0077	0.535	0.507	66.4
3117470	0.016	0.0024	0.5	0.5	0.202	0.05	17.9	0.81	0.005	0.0007	0.0232	0.0077	0.535	0.507	66.4
3122172	0.017	0.0035	0.47	0.52	0.193	0.02	18	0.517	0.005	0.0006	0.019	0.0095	0.289	0.239	68.4
3122172	0.017	0.0035	0.47	0.52	0.193	0.02	18	0.517	0.005	0.0006	0.019	0.0095	0.289	0.239	68.4
3122172	0.017	0.0035	0.47	0.52	0.193	0.02	18	0.517	0.005	0.0006	0.019	0.0095	0.289	0.239	68.4
3122173	0.017	0.0035	0.47	0.52	0.193	0.02	18	0.517	0.005	0.0006	0.019	0.0095	0.289	0.239	69.2
3122173	0.017	0.0035	0.47	0.52	0.193	0.02	18	0.517	0.005	0.0006	0.019	0.0095	0.289	0.239	69.2
3122180	0.023	0.0035	0.47	0.66	0.177	0.02	17.9	0.479	0.005	0.0007	0.0199	0.0079	0.216	0.147	76.2
3122180	0.023	0.0035	0.47	0.66	0.177	0.02	17.9	0.479	0.005	0.0007	0.0199	0.0079	0.216	0.147	76.2
3122181	0.023	0.0035	0.47	0.66	0.177	0.02	17.9	0.479	0.005	0.0007	0.0199	0.0079	0.213	0.147	68.0
3122181	0.023	0.0035	0.47	0.66	0.177	0.02	17.9	0.479	0.005	0.0007	0.0199	0.0079	0.213	0.147	68.0
3122182	0.023	0.0035	0.47	0.66	0.177	0.02	17.9	0.479	0.005	0.0007	0.0199	0.0079	0.214	0.147	68.8
3122182	0.023	0.0035	0.47	0.66	0.177	0.02	17.9	0.479	0.005	0.0007	0.0199	0.0079	0.214	0.147	68.8
3122183	0.023	0.0035	0.47	0.66	0.177	0.02	17.9	0.479	0.005	0.0007	0.0199	0.0079	0.215	0.147	68.2
3122183	0.023	0.0035	0.47	0.66	0.177	0.02	17.9	0.479	0.005	0.0007	0.0199	0.0079	0.215	0.147	68.2
3122184	0.023	0.0035	0.47	0.66	0.177	0.02	17.9	0.479	0.005	0.0007	0.0199	0.0079	0.215	0.147	70.0
3122184	0.023	0.0035	0.47	0.66	0.177	0.02	17.9	0.479	0.005	0.0007	0.0199	0.0079	0.215	0.147	70.0
3124261	0.021	0.0019	0.55	0.5	0.183	0.03	17.9	0.494	0.007	0.0007	0.0236	0.0034	0.167	0.149	69.0
3124261	0.021	0.0019	0.55	0.5	0.183	0.03	17.9	0.494	0.007	0.0007	0.0236	0.0034	0.167	0.149	69.0
3124261	0.021	0.0019	0.55	0.5	0.183	0.03	17.9	0.494	0.007	0.0007	0.0236	0.0034	0.167	0.149	69.0
3124262	0.021	0.0019	0.55	0.5	0.183	0.03	17.9	0.494	0.007	0.0007	0.0236	0.0034	0.167	0.149	70.0
3124262	0.021	0.0019	0.55	0.5	0.183	0.03	17.9	0.494	0.007	0.0007	0.0236	0.0034	0.167	0.149	70.0
3124263	0.021	0.0019	0.55	0.5	0.183	0.03	17.9	0.494	0.007	0.0007	0.0236	0.0034	0.168	0.149	72.9
3124263	0.021	0.0019	0.55	0.5	0.183	0.03	17.9	0.494	0.007	0.0007	0.0236	0.0034	0.168	0.149	72.9
3124263	0.021	0.0019	0.55	0.5	0.183	0.03	17.9	0.494	0.007	0.0007	0.0236	0.0034	0.168	0.149	72.9
3124264	0.021	0.0019	0.55	0.5	0.183	0.03	17.9	0.494	0.007	0.0007	0.0236	0.0034	0.168	0.149	67.9
3124264	0.021	0.0019	0.55	0.5	0.183	0.03	17.9	0.494	0.007	0.0007	0.0236	0.0034	0.168	0.149	67.9
3124264	0.021	0.0019	0.55	0.5	0.183	0.03	17.9	0.494	0.007	0.0007	0.0236	0.0034	0.168	0.149	67.9
3124270	0.016	0.001	0.55	0.54	0.172	0.02	17.9	0.439	0.006	0.0006	0.0276	0.0078	0.126	0.102	69.9
3124270	0.016	0.001	0.55	0.54	0.172	0.02	17.9	0.439	0.006	0.0006	0.0276	0.0078	0.126	0.102	69.9
3124270	0.016	0.001	0.55	0.54	0.172	0.02	17.9	0.439	0.006	0.0006	0.0276	0.0078	0.126	0.102	69.9
3124271	0.016	0.001	0.55	0.54	0.172	0.02	17.9	0.439	0.006	0.0006	0.0276	0.0078	0.126	0.102	67.7
3124271	0.016	0.001	0.55	0.54	0.172	0.02	17.9	0.439	0.006	0.0006	0.0276	0.0078	0.126	0.102	67.7
3124271	0.016	0.001	0.55	0.54	0.172	0.02	17.9	0.439	0.006	0.0006	0.0276	0.0078	0.126	0.102	67.7
3124274	0.016	0.001	0.55	0.54	0.172	0.02	17.9	0.439	0.006	0.0006	0.0276	0.0078	0.126	0.102	69.6
3124274	0.016	0.001	0.55	0.54	0.172	0.02	17.9	0.439	0.006	0.0006	0.0276	0.0078	0.126	0.102	69.6
3124274	0.016	0.001	0.55	0.54	0.172	0.02	17.9	0.439	0.006	0.0006	0.0276	0.0078	0.126	0.102	69.6
3125353	0.015	0.0051	0.54	0.49	0.217	0.03	18	0.604	0.006	0.0007	0.0172	0.0082	0.364	0.355	69.9
3125353	0.015	0.0051	0.54	0.49	0.217	0.03	18	0.604	0.006	0.0007	0.0172	0.0082	0.364	0.355	69.9

MPO	C	S	Mn	Si	Ti	Mo	Cr	Nb	Al	B	N	O	Calcul reheat Nb	Calcul Down Coil Nb	Cold Red (%)
3125354	0.015	0.0051	0.54	0.49	0.217	0.03	18	0.604	0.006	0.0007	0.0172	0.0082	0.364	0.355	70.4
3125354	0.015	0.0051	0.54	0.49	0.217	0.03	18	0.604	0.006	0.0007	0.0172	0.0082	0.364	0.355	70.4
3125354	0.015	0.0051	0.54	0.49	0.217	0.03	18	0.604	0.006	0.0007	0.0172	0.0082	0.364	0.355	70.4
3125360	0.02	0.0047	0.6	0.5	0.179	0.03	17.8	0.423	0.006	0.0007	0.02	0.0081	0.137	0.114	72.3
3125360	0.02	0.0047	0.6	0.5	0.179	0.03	17.8	0.423	0.006	0.0007	0.02	0.0081	0.137	0.114	72.3
3125361	0.02	0.0047	0.6	0.5	0.179	0.03	17.8	0.423	0.006	0.0007	0.02	0.0081	0.137	0.113	73.4
3125361	0.02	0.0047	0.6	0.5	0.179	0.03	17.8	0.423	0.006	0.0007	0.02	0.0081	0.137	0.113	73.4
3125362	0.02	0.0047	0.6	0.5	0.179	0.03	17.8	0.423	0.006	0.0007	0.02	0.0081	0.137	0.114	67.6
3125362	0.02	0.0047	0.6	0.5	0.179	0.03	17.8	0.423	0.006	0.0007	0.02	0.0081	0.137	0.114	67.6
3125364	0.02	0.0047	0.6	0.5	0.179	0.03	17.8	0.423	0.006	0.0007	0.02	0.0081	0.137	0.114	69.7
3125364	0.02	0.0047	0.6	0.5	0.179	0.03	17.8	0.423	0.006	0.0007	0.02	0.0081	0.137	0.114	69.7
3125364	0.02	0.0047	0.6	0.5	0.179	0.03	17.8	0.423	0.006	0.0007	0.02	0.0081	0.137	0.114	69.7
3126383	0.018	0.0013	0.55	0.55	0.184	0.02	18.2	0.482	0.005	0.0006	0.0178	0.0068	0.220	0.205	72.9
3126383	0.018	0.0013	0.55	0.55	0.184	0.02	18.2	0.482	0.005	0.0006	0.0178	0.0068	0.220	0.205	72.9
3126384	0.018	0.0013	0.55	0.55	0.184	0.02	18.2	0.482	0.005	0.0006	0.0178	0.0068	0.220	0.205	72.5
3126384	0.018	0.0013	0.55	0.55	0.184	0.02	18.2	0.482	0.005	0.0006	0.0178	0.0068	0.220	0.205	72.5
3126391	0.017	0.001	0.69	0.54	0.16	0.03	18	0.472	0.005	0.0006	0.0234	0.0059	0.178	0.160	69.6
3126391	0.017	0.001	0.69	0.54	0.16	0.03	18	0.472	0.005	0.0006	0.0234	0.0059	0.178	0.160	69.6
3126391	0.017	0.001	0.69	0.54	0.16	0.03	18	0.472	0.005	0.0006	0.0234	0.0059	0.178	0.160	69.6
3126392	0.017	0.001	0.69	0.54	0.16	0.03	18	0.472	0.005	0.0006	0.0234	0.0059	0.178	0.160	73.2
3126392	0.017	0.001	0.69	0.54	0.16	0.03	18	0.472	0.005	0.0006	0.0234	0.0059	0.178	0.160	73.2
3126392	0.017	0.001	0.69	0.54	0.16	0.03	18	0.472	0.005	0.0006	0.0234	0.0059	0.178	0.160	73.2
3126394	0.017	0.001	0.69	0.54	0.16	0.03	18	0.472	0.005	0.0006	0.0234	0.0059	0.178	0.160	65.7
3126394	0.017	0.001	0.69	0.54	0.16	0.03	18	0.472	0.005	0.0006	0.0234	0.0059	0.178	0.160	65.7
3127730	0.016	0.0017	0.56	0.47	0.174	0.04	17.8	0.438	0.005	0.0006	0.0195	0.0107	0.186	0.163	62.1
3127730	0.016	0.0017	0.56	0.47	0.174	0.04	17.8	0.438	0.005	0.0006	0.0195	0.0107	0.186	0.163	62.1
3127732	0.016	0.0017	0.56	0.47	0.174	0.04	17.8	0.438	0.005	0.0006	0.0195	0.0107	0.185	0.163	69.6
3127732	0.016	0.0017	0.56	0.47	0.174	0.04	17.8	0.438	0.005	0.0006	0.0195	0.0107	0.185	0.163	69.6
3127732	0.016	0.0017	0.56	0.47	0.174	0.04	17.8	0.438	0.005	0.0006	0.0195	0.0107	0.185	0.163	69.6
3127732	0.016	0.0017	0.56	0.47	0.174	0.04	17.8	0.438	0.005	0.0006	0.0195	0.0107	0.185	0.163	69.6
3129511	0.019	0.003	0.51	0.51	0.189	0.02	17.9	0.601	0.003	0.0006	0.0187	0.0082	0.320	0.309	69.0
3130461	0.02	0.0022	0.53	0.58	0.175	0.04	18.1	0.473	0.007	0.0005	0.0222	0.0087	0.167	0.147	69.0
3130461	0.02	0.0022	0.53	0.58	0.175	0.04	18.1	0.473	0.007	0.0005	0.0222	0.0087	0.167	0.147	69.0
3130463	0.02	0.0022	0.53	0.58	0.175	0.04	18.1	0.473	0.007	0.0005	0.0222	0.0087	0.168	0.147	71.0
3130464	0.02	0.0022	0.53	0.58	0.175	0.04	18.1	0.473	0.007	0.0005	0.0222	0.0087	0.166	0.147	77.1
3130464	0.02	0.0022	0.53	0.58	0.175	0.04	18.1	0.473	0.007	0.0005	0.0222	0.0087	0.166	0.147	77.1
3130471	0.016	0.0031	0.48	0.55	0.207	0.05	18	0.441	0.006	0.0006	0.024	0.01	0.156	0.132	65.7
3130471	0.016	0.0031	0.48	0.55	0.207	0.05	18	0.441	0.006	0.0006	0.024	0.01	0.156	0.132	65.7
3131190	0.013	0.0023	0.46	0.55	0.19	0.09	18	0.466	0.006	0.0006	0.02	0.0085	0.227	0.211	66.7
3131190	0.013	0.0023	0.46	0.55	0.19	0.09	18	0.466	0.006	0.0006	0.02	0.0085	0.227	0.211	66.7
3131191	0.013	0.0023	0.46	0.55	0.19	0.09	18	0.466	0.006	0.0006	0.02	0.0085	0.226	0.211	71.3
3131192	0.013	0.0023	0.46	0.55	0.19	0.09	18	0.466	0.006	0.0006	0.02	0.0085	0.226	0.211	71.4
3131192	0.013	0.0023	0.46	0.55	0.19	0.09	18	0.466	0.006	0.0006	0.02	0.0085	0.226	0.211	71.4
3131192	0.013	0.0023	0.46	0.55	0.19	0.09	18	0.466	0.006	0.0006	0.02	0.0085	0.226	0.211	71.4
3131193	0.013	0.0023	0.46	0.55	0.19	0.09	18	0.466	0.006	0.0006	0.02	0.0085	0.226	0.211	68.7
3131193	0.013	0.0023	0.46	0.55	0.19	0.09	18	0.466	0.006	0.0006	0.02	0.0085	0.226	0.211	68.7
3131193	0.013	0.0023	0.46	0.55	0.19	0.09	18	0.466	0.006	0.0006	0.02	0.0085	0.226	0.211	68.7

MPO	C	S	Mn	Si	Ti	Mo	Cr	Nb	Al	B	N	O	Calcul reheat Nb	Calcul Down Coil Nb	Cold Red (%)
3131201	0.017	0.0022	0.48	0.51	0.168	0.07	18	0.442	0.006	0.0006	0.0166	0.006	0.200	0.182	68.0
3131203	0.017	0.0022	0.48	0.51	0.168	0.07	18	0.442	0.006	0.0006	0.0166	0.006	0.198	0.182	71.9
3131203	0.017	0.0022	0.48	0.51	0.168	0.07	18	0.442	0.006	0.0006	0.0166	0.006	0.198	0.182	71.9
3131204	0.017	0.0022	0.48	0.51	0.168	0.07	18	0.442	0.006	0.0006	0.0166	0.006	0.199	0.182	72.3
3132020	0.02	0.0045	0.48	0.53	0.208	0.06	17.9	0.493	0.005	0.0005	0.0158	0.0065	0.231	0.216	69.5
3132020	0.02	0.0045	0.48	0.53	0.208	0.06	17.9	0.493	0.005	0.0005	0.0158	0.0065	0.231	0.216	69.5
3132021	0.02	0.0045	0.48	0.53	0.208	0.06	17.9	0.493	0.005	0.0005	0.0158	0.0065	0.231	0.216	73.1
3132021	0.02	0.0045	0.48	0.53	0.208	0.06	17.9	0.493	0.005	0.0005	0.0158	0.0065	0.231	0.216	73.1
3132023	0.02	0.0045	0.48	0.53	0.208	0.06	17.9	0.493	0.005	0.0005	0.0158	0.0065	0.233	0.216	66.4
3132023	0.02	0.0045	0.48	0.53	0.208	0.06	17.9	0.493	0.005	0.0005	0.0158	0.0065	0.233	0.216	66.4
3132024	0.02	0.0045	0.48	0.53	0.208	0.06	17.9	0.493	0.005	0.0005	0.0158	0.0065	0.232	0.216	69.0
3132024	0.02	0.0045	0.48	0.53	0.208	0.06	17.9	0.493	0.005	0.0005	0.0158	0.0065	0.232	0.216	69.0
3132031	0.02	0.0022	0.41	0.47	0.134	0.05	17.9	0.479	0.004	0.0004	0.0197	0.0109	0.190	0.172	69.0
3132031	0.02	0.0022	0.41	0.47	0.134	0.05	17.9	0.479	0.004	0.0004	0.0197	0.0109	0.190	0.172	69.0
3132034	0.02	0.0022	0.41	0.47	0.134	0.05	17.9	0.479	0.004	0.0004	0.0197	0.0109	0.189	0.172	68.8
3132034	0.02	0.0022	0.41	0.47	0.134	0.05	17.9	0.479	0.004	0.0004	0.0197	0.0109	0.189	0.172	68.8
3132870	0.015	0.0037	0.45	0.49	0.202	0.05	18.1	0.451	0.005	0.0005	0.0223	0.0076	0.181	0.163	71.9
3132870	0.015	0.0037	0.45	0.49	0.202	0.05	18.1	0.451	0.005	0.0005	0.0223	0.0076	0.181	0.163	71.9
3132870	0.015	0.0037	0.45	0.49	0.202	0.05	18.1	0.451	0.005	0.0005	0.0223	0.0076	0.181	0.163	71.9
3132870	0.015	0.0037	0.45	0.49	0.202	0.05	18.1	0.451	0.005	0.0005	0.0223	0.0076	0.181	0.163	71.9
3132870	0.015	0.0037	0.45	0.49	0.202	0.05	18.1	0.451	0.005	0.0005	0.0223	0.0076	0.181	0.163	71.9
3135000	0.022	0.001	0.52	0.55	0.147	0.03	18	0.405	0.007	0.0009	0.02	0.0081	0.108	0.080	72.6
3135000	0.022	0.001	0.52	0.55	0.147	0.03	18	0.405	0.007	0.0009	0.02	0.0081	0.108	0.080	72.6
3135001	0.022	0.001	0.52	0.55	0.147	0.03	18	0.405	0.007	0.0009	0.02	0.0081	0.108	0.080	70.1
3135002	0.022	0.001	0.52	0.55	0.147	0.03	18	0.405	0.007	0.0009	0.02	0.0081	0.108	0.080	70.4
3135003	0.022	0.001	0.52	0.55	0.147	0.03	18	0.405	0.007	0.0009	0.02	0.0081	0.108	0.080	70.6
3135003	0.022	0.001	0.52	0.55	0.147	0.03	18	0.405	0.007	0.0009	0.02	0.0081	0.108	0.080	70.6
3135004	0.022	0.001	0.52	0.55	0.147	0.03	18	0.405	0.007	0.0009	0.02	0.0081	0.109	0.080	70.4
3135011	0.02	0.0032	0.78	0.55	0.167	0.03	17.9	0.475	0.007	0.0008	0.0228	0.0043	0.162	0.144	67.2
3135610	0.014	0.007	0.54	0.49	0.181	0.02	17.9	0.591	0.005	0.0006	0.0157	0.0096	0.370	0.361	70.5
3135611	0.014	0.007	0.54	0.49	0.181	0.02	17.9	0.591	0.005	0.0006	0.0157	0.0096	0.369	0.361	67.6
3135611	0.014	0.007	0.54	0.49	0.181	0.02	17.9	0.591	0.005	0.0006	0.0157	0.0096	0.369	0.361	67.6
3135612	0.014	0.007	0.54	0.49	0.181	0.02	17.9	0.591	0.005	0.0006	0.0157	0.0096	0.370	0.361	66.5
3135612	0.014	0.007	0.54	0.49	0.181	0.02	17.9	0.591	0.005	0.0006	0.0157	0.0096	0.370	0.361	66.5
3135613	0.014	0.007	0.54	0.49	0.181	0.02	17.9	0.591	0.005	0.0006	0.0157	0.0096	0.370	0.361	65.7
3135622	0.014	0.0035	0.6	0.51	0.182	0.02	17.9	0.472	0.005	0.0007	0.0182	0.0083	0.236	0.223	67.3
3135623	0.014	0.0035	0.6	0.51	0.182	0.02	17.9	0.472	0.005	0.0007	0.0182	0.0083	0.237	0.223	72.8
3151143	0.018	0.0046	0.52	0.51	0.186	0.02	17.8	0.425	0.005	0.0006	0.0185	0.0085	0.169		67.4
3151143	0.018	0.0046	0.52	0.51	0.186	0.02	17.8	0.425	0.005	0.0006	0.0185	0.0085	0.169		67.4
3151143	0.018	0.0046	0.52	0.51	0.186	0.02	17.8	0.425	0.005	0.0006	0.0185	0.0085	0.169		67.4
3151192	0.015	0.0035	0.45	0.52	0.183	0.02	17.9	0.45	0.005	0.0007	0.0182	0.0076	0.209	0.193	72.6
3151192	0.015	0.0035	0.45	0.52	0.183	0.02	17.9	0.45	0.005	0.0007	0.0182	0.0076	0.209	0.193	72.6
3151192	0.015	0.0035	0.45	0.52	0.183	0.02	17.9	0.45	0.005	0.0007	0.0182	0.0076	0.209	0.193	72.6
3151193	0.015	0.0035	0.45	0.52	0.183	0.02	17.9	0.45	0.005	0.0007	0.0182	0.0076	0.209	0.193	69.7
3151193	0.015	0.0035	0.45	0.52	0.183	0.02	17.9	0.45	0.005	0.0007	0.0182	0.0076	0.209	0.193	69.7
3151193	0.015	0.0035	0.45	0.52	0.183	0.02	17.9	0.45	0.005	0.0007	0.0182	0.0076	0.209	0.193	69.7
3181322	0.016	0.0011	0.52	0.52	0.2	0.04	18.1	0.492	0.006	0.0007	0.0225	0.0088	0.204		74.0

MPO	C	S	Mn	Si	Ti	Mo	Cr	Nb	Al	B	N	O	Calcul reheat Nb	Calcul Down Coil Nb	Cold Red (%)
3182872	0.023	0.0047	0.63	0.48	0.163	0.03	17.8	0.517	0.006	0.0008	0.0251	0.0065	0.177	0.145	79.2
3183330	0.019	0.0036	0.6	0.55	0.196	0.02	17.8	0.505	0.005	0.0005	0.0249	0.0056	0.178	0.165	80.5
3185001	0.019	0.002	0.58	0.52	0.195	0.03	18.1	0.488	0.006	0.0006	0.0285	0.0061	0.138	0.121	79.5
3185802	0.014	0.0047	0.5	0.49	0.169	0.03	18	0.468	0.007	0.0008	0.03	0.007	0.142	0.128	73.9
3185802	0.014	0.0047	0.5	0.49	0.169	0.03	18	0.468	0.007	0.0008	0.03	0.007	0.142	0.128	73.9
3185804	0.014	0.0047	0.5	0.49	0.169	0.03	18	0.468	0.007	0.0008	0.03	0.007	0.142	0.128	79.1
3185804	0.014	0.0047	0.5	0.49	0.169	0.03	18	0.468	0.007	0.0008	0.03	0.007	0.142	0.128	79.1
3185811	0.017	0.0034	0.58	0.51	0.183	0.04	18.1	0.501	0.005	0.0007	0.0213	0.0069	0.215	0.205	73.9
3186291	0.017	0.0009	0.51	0.57	0.156	0.02	18	0.528	0.01	0.0009	0.0257	0.005	0.210	0.198	76.3
3186293	0.017	0.0009	0.51	0.57	0.156	0.02	18	0.528	0.01	0.0009	0.0257	0.005	0.208	0.198	74.0
3189242	0.015	0.0019	0.55	0.52	0.185	0.02	17.7	0.561	0.005	0.0008	0.0214	0.0068	0.287	0.280	61.6
3189243	0.015	0.0019	0.55	0.52	0.185	0.02	17.7	0.561	0.005	0.0008	0.0214	0.0068	0.287	0.280	64.1
3191661	0.02	0.0034	0.54	0.47	0.156	0.04	17.9	0.494	0.007	0.0007	0.0225	0.007	0.183	0.165	76.4
3191662	0.02	0.0034	0.54	0.47	0.156	0.04	17.9	0.494	0.007	0.0007	0.0225	0.007	0.182	0.165	76.4
3191663	0.02	0.0034	0.54	0.47	0.156	0.04	17.9	0.494	0.007	0.0007	0.0225	0.007	0.183	0.165	76.4
3191663	0.02	0.0034	0.54	0.47	0.156	0.04	17.9	0.494	0.007	0.0007	0.0225	0.007	0.183	0.165	76.4
3191664	0.02	0.0034	0.54	0.47	0.156	0.04	17.9	0.494	0.007	0.0007	0.0225	0.007	0.183	0.165	76.2
3192851	0.014	0.0002	0.54	0.47	0.245	0.02	17.7	0.562	0.006	0.0005	0.024	0.0054	0.280	0.268	69.6
3192851	0.014	0.0002	0.54	0.47	0.245	0.02	17.7	0.562	0.006	0.0005	0.024	0.0054	0.280	0.268	69.6
3192851	0.014	0.0002	0.54	0.47	0.245	0.02	17.7	0.562	0.006	0.0005	0.024	0.0054	0.280	0.268	69.6
3192852	0.014	0.0002	0.54	0.47	0.245	0.02	17.7	0.562	0.006	0.0005	0.024	0.0054	0.280	0.268	76.5
3192860	0.014	0.0011	0.54	0.51	0.144	0.03	17.8	0.57	0.005	0.0004	0.0229	0.0084	0.295	0.284	80.9
3192864	0.014	0.0011	0.54	0.51	0.144	0.03	17.8	0.57	0.005	0.0004	0.0229	0.0084	0.294	0.284	79.2
3192864	0.014	0.0011	0.54	0.51	0.144	0.03	17.8	0.57	0.005	0.0004	0.0229	0.0084	0.294	0.284	79.2
3192870	0.018	0.0001	0.57	0.58	0.177	0.03	17.8	0.6	0.006	0.0005	0.023	0.0035	0.294	0.283	73.4
3192873	0.018	0.0001	0.57	0.58	0.177	0.03	17.8	0.6	0.006	0.0005	0.023	0.0035	0.294	0.283	79.0
3192873	0.018	0.0001	0.57	0.58	0.177	0.03	17.8	0.6	0.006	0.0005	0.023	0.0035	0.294	0.283	79.0
3192880	0.014	0.0045	0.45	0.48	0.192	0.03	17.9	0.457	0.005	0.0004	0.02	0.0058	0.211	0.194	73.7
3192881	0.014	0.0045	0.45	0.48	0.192	0.03	17.9	0.457	0.005	0.0004	0.02	0.0058	0.210	0.194	78.7
3192882	0.014	0.0045	0.45	0.48	0.192	0.03	17.9	0.457	0.005	0.0004	0.02	0.0058	0.209	0.194	76.9
3192882	0.014	0.0045	0.45	0.48	0.192	0.03	17.9	0.457	0.005	0.0004	0.02	0.0058	0.209	0.194	76.9
3192882	0.014	0.0045	0.45	0.48	0.192	0.03	17.9	0.457	0.005	0.0004	0.02	0.0058	0.209	0.194	76.9
3192883	0.014	0.0045	0.45	0.48	0.192	0.03	17.9	0.457	0.005	0.0004	0.02	0.0058	0.210	0.194	76.7
3192883	0.014	0.0045	0.45	0.48	0.192	0.03	17.9	0.457	0.005	0.0004	0.02	0.0058	0.210	0.194	76.7
3192883	0.014	0.0045	0.45	0.48	0.192	0.03	17.9	0.457	0.005	0.0004	0.02	0.0058	0.210	0.194	76.7
3192884	0.014	0.0045	0.45	0.48	0.192	0.03	17.9	0.457	0.005	0.0004	0.02	0.0058	0.209	0.194	75.3

Appendix 2

In an attempt to identify the relationship between the various parameters, the grain size was removed. In this case, however, a rather complex relationship developed between the various parameters, which in most cases did not make metallurgical sense. The grain size was therefor kept in as a representation of the total thermal mechanical history that the alloy sees and as a parameter that can be controlled by final annealing. This fact is apparent from the correlation coefficients in the tables 4.4 and 4.5 in which the grain structure has the strongest relationship with the final cold band strip annealing temperature. The most representative model that was obtained for the normalized sag values indicates that the sag value is influenced by the grain size, final-annealing parameters, niobium content and the slab reheat temperature (Table A2.1).

Table A2.1

Model of Normalized sag versus parameters analyzed

Independent variable	**coefficient**	**std. error**	**t-value**	**sig.level**
CONSTANT	7.484716	1.814599	4.1247	0.0001
1/grainsize^2 (mm)	0.000519	0.000108	4.7963	0.0000
1/grainsize (mm)	-0.02311	0.009043	-2.5552	0.0116
Final Gauge Strip Temp. (^{o}C)	-0.0138	0.002028	-6.8022	0.0000
Final Gauge Line Speed. (m/s)	0.00688	0.002292	3.0014	0.0031
1/Slab Discharge Temp (^{o}C)	7639.729	976.3215	7.825	0.0000
Nb^2 (Mass %)	2.297238	0.310191	7.4059	0.0000
R. SQ. (ADJ.) = 0.7056				
SE = 0.285519	MAE=0.208322	DurbWat= 1.532		
157 observations fitted, forecast(s) computed for 0 missing val. of dep. var.				

Std. Error = standard error of the coefficients **t-value** = coefficient/std.error

Sig.level = probability that if no contribution was made by that variable a larger absolute t-value would occur.

In this case some of the thermo mechanical parameters are include. The most significant (from a niobium perspective) is the slab reheat temperature, which has an inverse relationship with the sag value. This indicates that as the reheat temperature increases the normalized sag value decreases. The theoretical interpretation of this is that more niobium is probably in solution as the reheat temperature increases. It

would also appear as if this relatively higher niobium content in solution persists throughout the thermal mechanical cycle and contributes to the lower sag value.

The model predicted by Statsgraphics for the normalized sag values is:
(Sag*Final Gauge^2)/13= 0.000519/grainsize^2 – 0.02311/grainsize – 0.0138* Final Gauge Strip Temp +0.00688*Final Gauge Line Speed +7639.729/ Slab Discharge Temp+2.297938* Nb^2

The mean absolute error for this model is 0.208322. The calculated MAE for the sag alone is 1.2mm for 1.5mm gauge material. The actual normalized sag values versus the calculated sag values are shown in figure A2.1.

Attempts were made at trying to remove one of these variables, particularly the grain size and niobium content, by selection of a smaller range (grain size range 0.028mm – 0.060mm (from 0.014-0.079) and niobium range 0.437-0.538 (from 0.0405 – 0.81)) of these variables. No significant model could be established with this approach although the strongest correlations were still found to be with grain size, slab reheat temperature and the final annealing parameters of the cold band material.

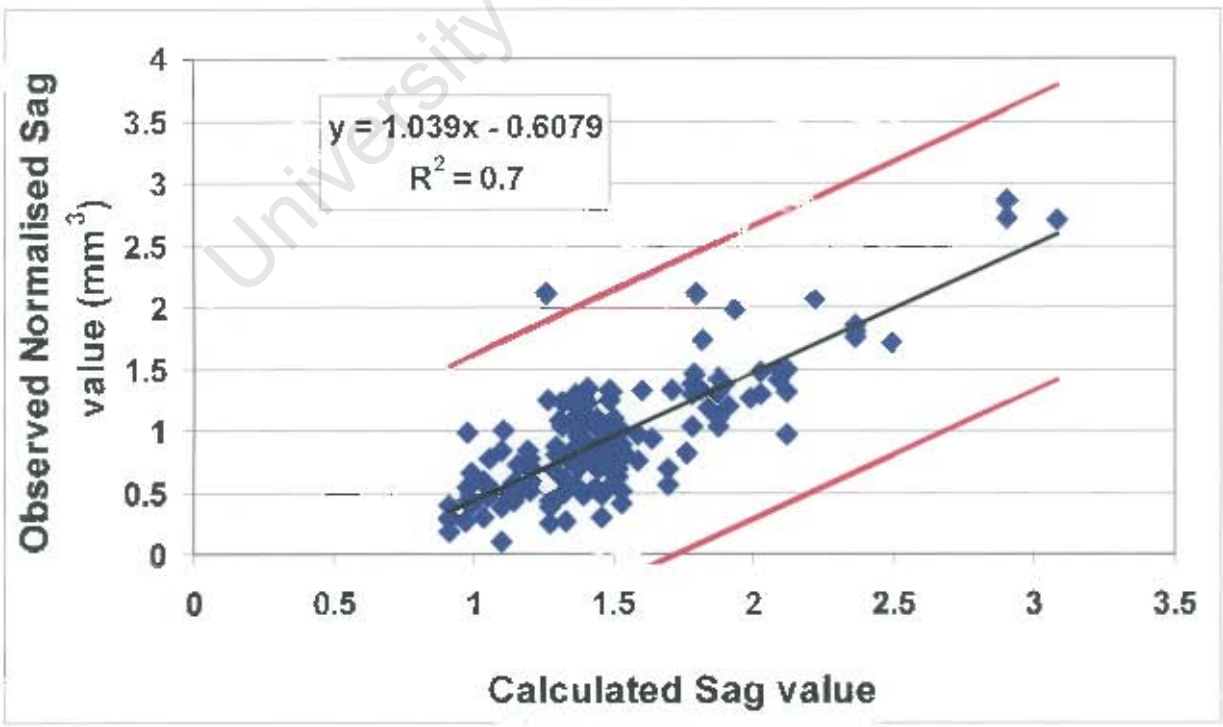

Figure A2.1: Normalized sag value versus the calculated sag value.

Appendix 3

Micrographs of cold band material annealed at various temperatures.

390 Seconds (micron marker = 100μ)

900°C

925 °C

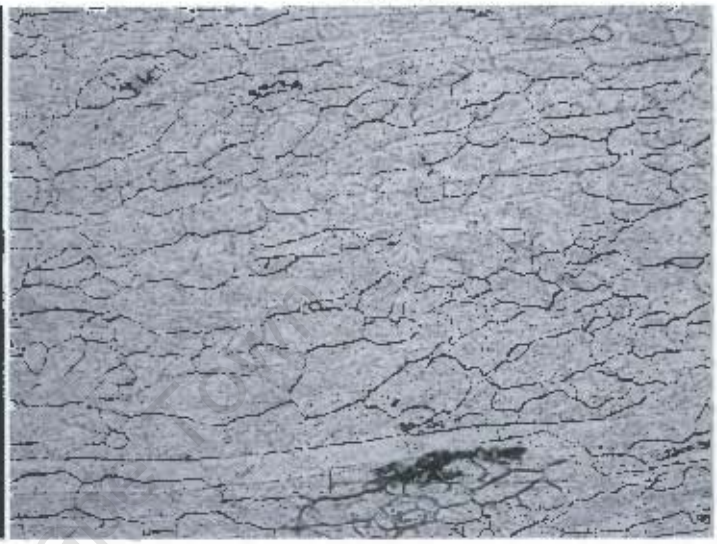

950°C

975 °C

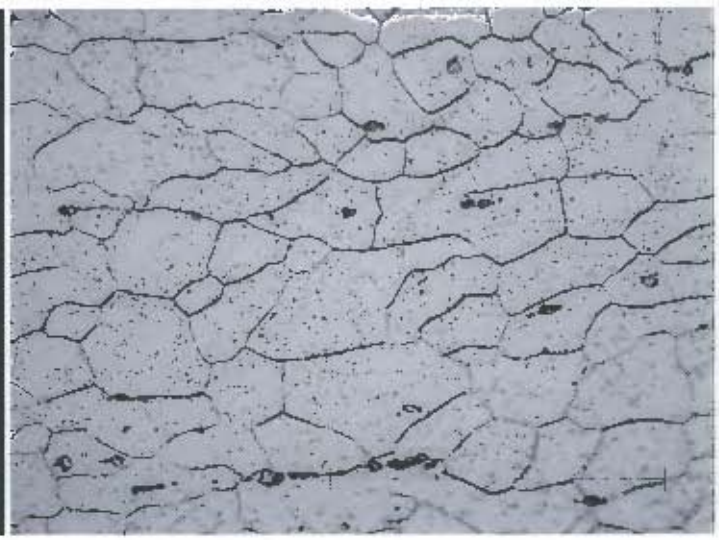

390 Seconds

1000°C

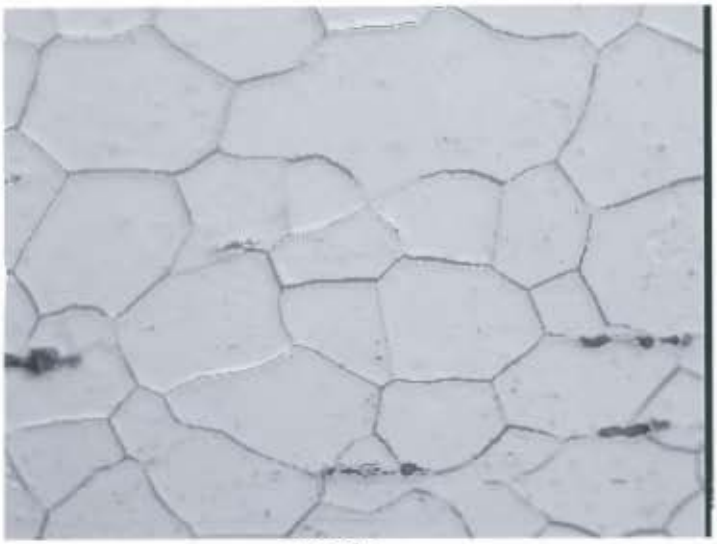

1025 °C

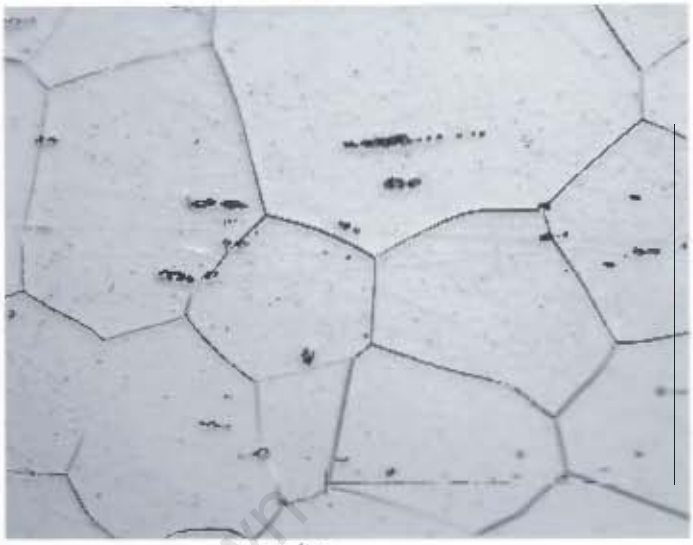

1050°C

1075 °C

1100°C

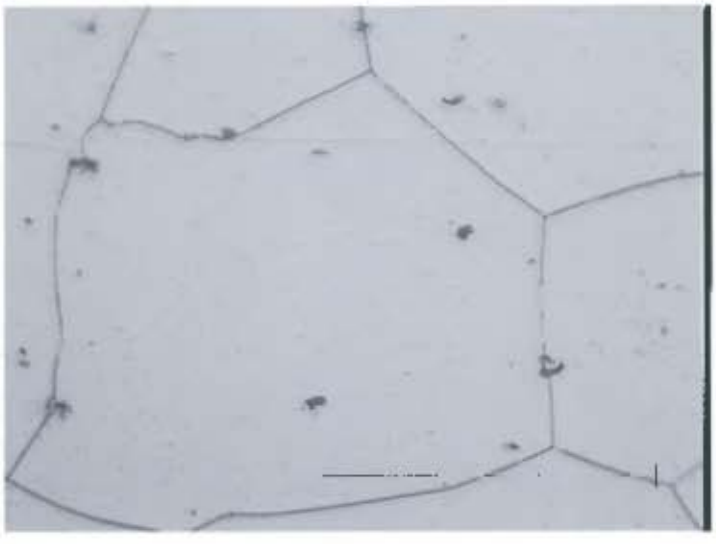

Appendix 4

Table of the grain size obtained in the experimental material. The time in seconds is the time that the sample was in the furnace. This data was used to determine the empirical relationship between the grain size and the time in the furnace.

Time	Grain size (mean intercept length (mm))							
seconds	1100°C	1075°C	1050°C	1025°C	1000°C	975°C	950°C	925°C
60	0.022	0.018						
60	0.023	0.018						
75	0.021							
75	0.021							
90	0.025	0.017						
90	0.025	0.018						
90		0.023						
105	0.032	0.026	0.022					
105	0.032	0.027	0.022					
120	0.053	0.043	0.029	0.028				
120	0.051	0.041	0.028	0.029				
120	0.040	0.037	0.040	0.021				
120	0.041	0.039	0.040	0.021				
120			0.037					
135		0.049	0.037	0.028				
135		0.049	0.037	0.028				
150			0.041	0.035				
150			0.040	0.034				
152	0.061							
152	0.061							
165				0.034				
165				0.035				
180	0.080	0.061			0.025			
180	0.086	0.065			0.025			
180					0.029			
180					0.029			
191		0.065						
191		0.067						
200			0.072					
200			0.063					
239			0.065					
239			0.063					
240			0.063	0.055	0.032			
240			0.061	0.055	0.030			
270					0.036			
270					0.035			
285					0.034			
285					0.032			

Time	Grain size (mean intercept length (mm))							
seconds	1100°C	1075°C	1050°C	1025°C	1000°C	975°C	950°C	925°C
300	0.072	0.067	0.063	0.055	0.034	0.025	0.019	0.022
300	0.077	0.067	0.063	0.057	0.032	0.025	0.018	0.023
300					0.029	0.024	0.021	0.019
300					0.031	0.025	0.021	
300					0.041			
300					0.039			
300					0.035			
300					0.032			
330	0.077	0.075	0.053	0.061	0.039	0.025	0.020	0.021
330	0.075	0.075	0.055	0.061	0.037	0.025	0.020	0.022
337				0.055		0.024		
337				0.055		0.024		
376	0.086							
376	0.083							
390	0.075	0.072	0.065	0.057	0.043	0.024	0.021	0.019
390	0.089	0.070	0.061	0.057	0.043	0.025	0.020	0.019
390						0.025	0.021	0.024
390						0.024	0.021	0.025
510				0.057	0.046	0.024	0.021	0.021
510				0.059	0.044	0.023	0.021	0.021
510						0.022		
510						0.023		
734		0.098						
734		0.092						
750						0.024	0.021	0.023
750						0.025	0.021	0.022
750							0.021	0.018
750							0.022	0.017
1180			0.072					
1180			0.080					
5050				0.089				
5050				0.080				
21600						0.051	0.049	0.025
21600							0.051	0.021
21600							0.049	0.025
21600								0.025
21600								0.023

Appendix 5

Microstructures of cold band material annealed at 1050^{O}C (140 seconds) after a hot band anneal for two hours as indicated in the micrograph title.

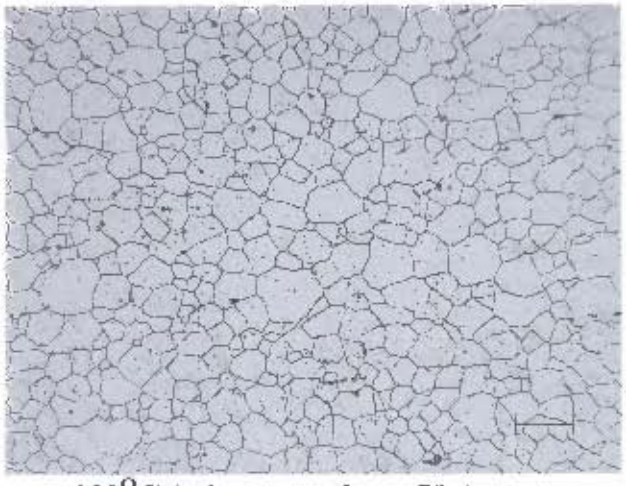

900^{O}C (micron marker =50μ)

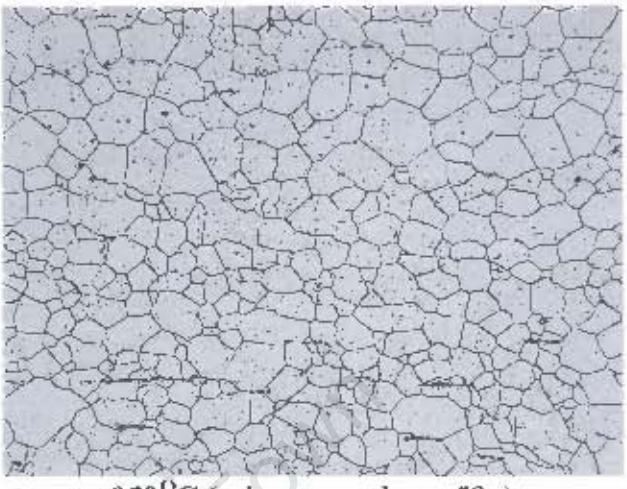

950^{O}C (micron marker =50μ)

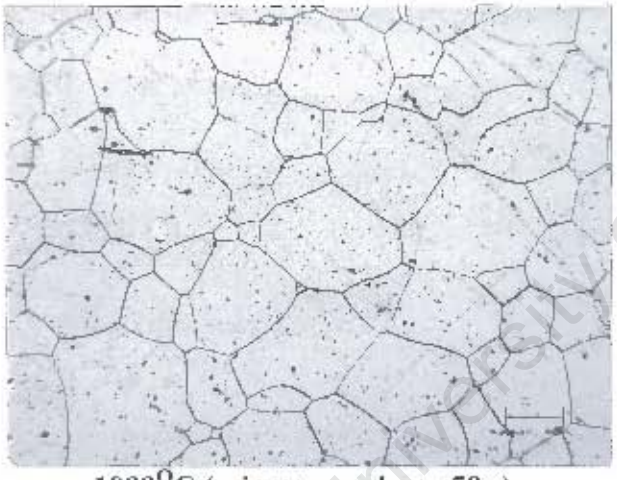

1000^{O}C (micron marker =50μ)

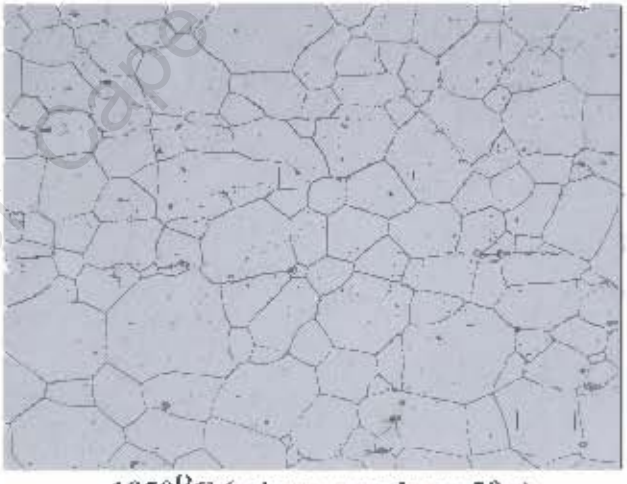

1050^{O}C (micron marker =50μ)

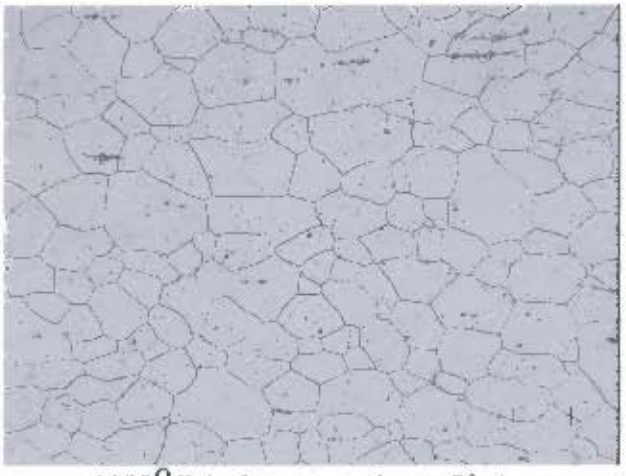

1100^{O}C (micron marker =50μ)

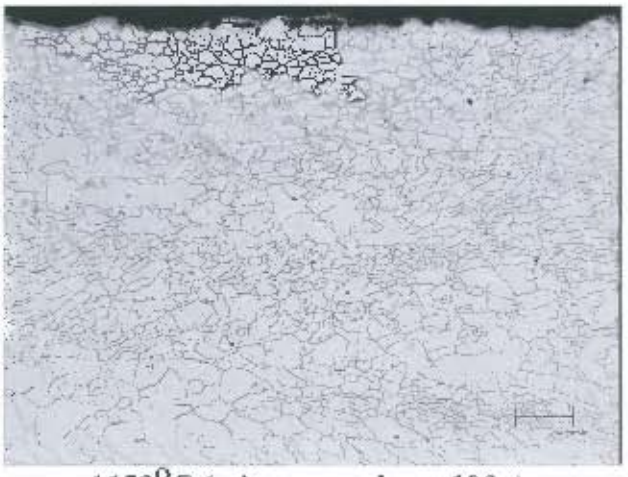

1150^{O}C (micron marker =100μ)

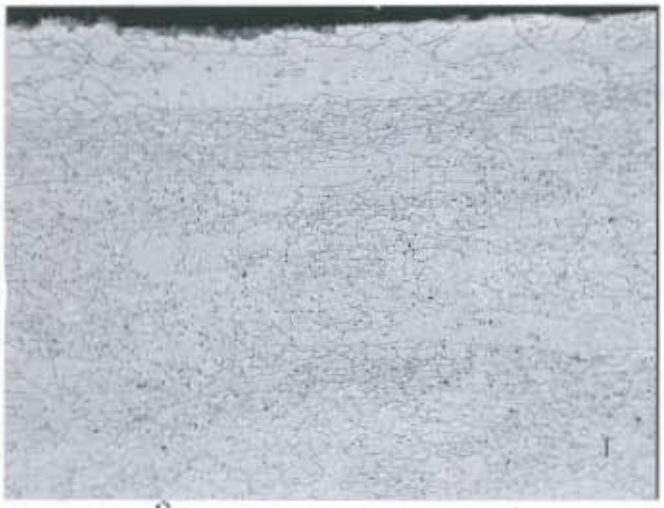

1200^{O}C (micron marker =100μ)

1250^{O}C (micron marker =100μ)

Microstructures of cold band material annealed at 1000^{O}C (264 seconds) after a hot band anneal for two hours as indicated in the micrograph title.

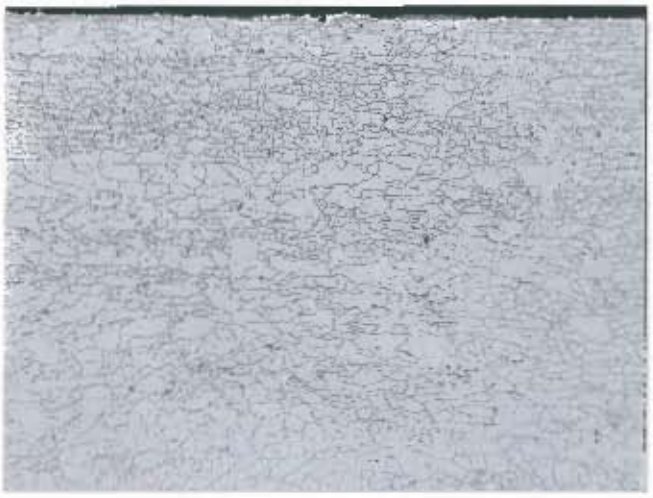

1100^{O}C (micron marker =100μ)

1150^{O}C (micron marker =100μ)

1200^{O}C (micron marker =100μ)

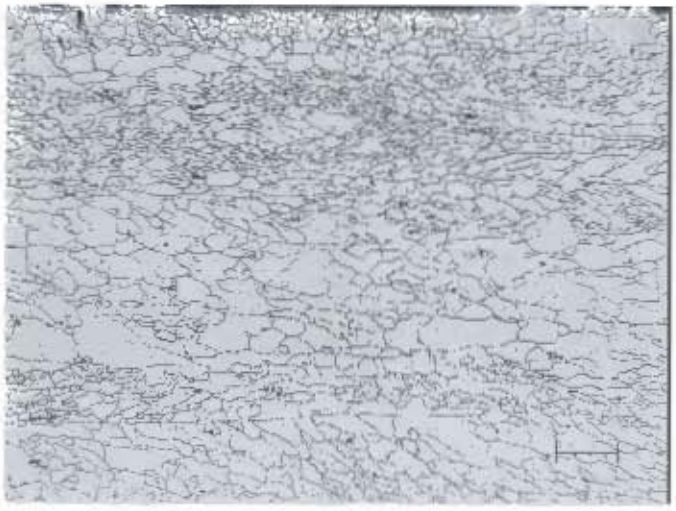

1250^{O}C (micron marker =100μ)

Microstructures of hot band material annealed for two hours at the temperatures as indicated in the micrograph title.

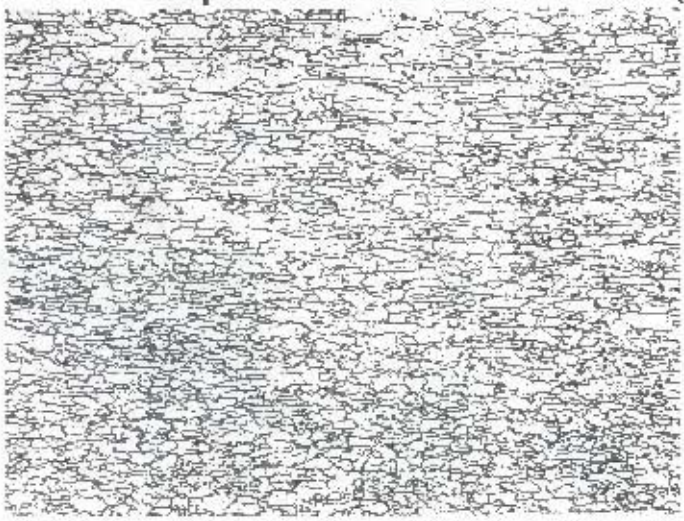

900^{O}C (micron marker =100μ)

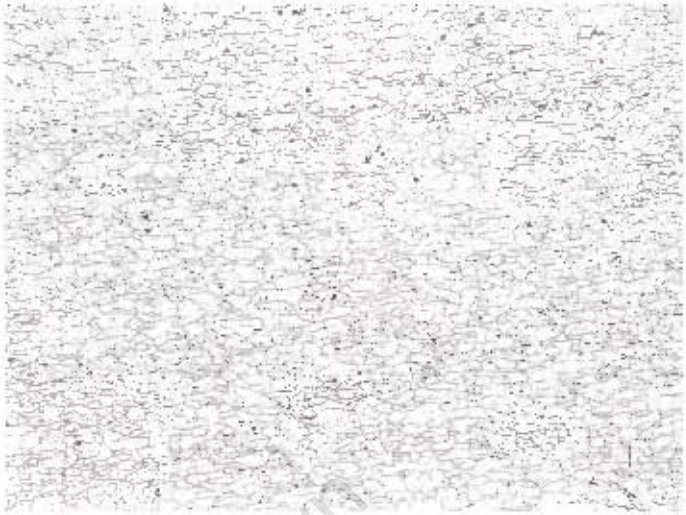

950^{O}C (micron marker =100μ)

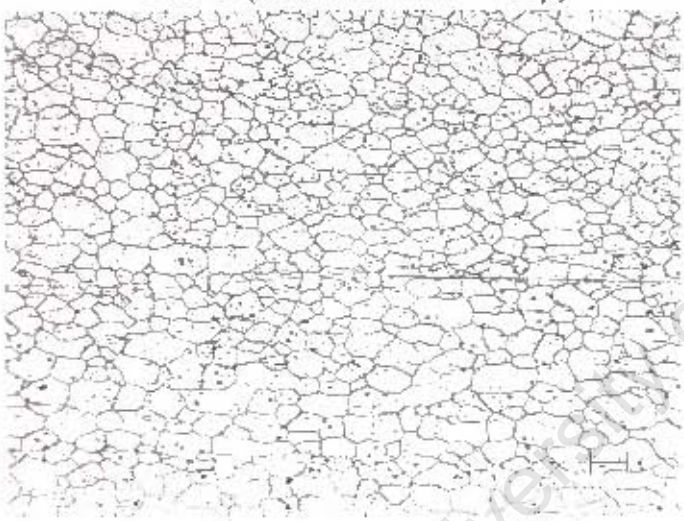

1000^{O}C (micron marker =100μ)

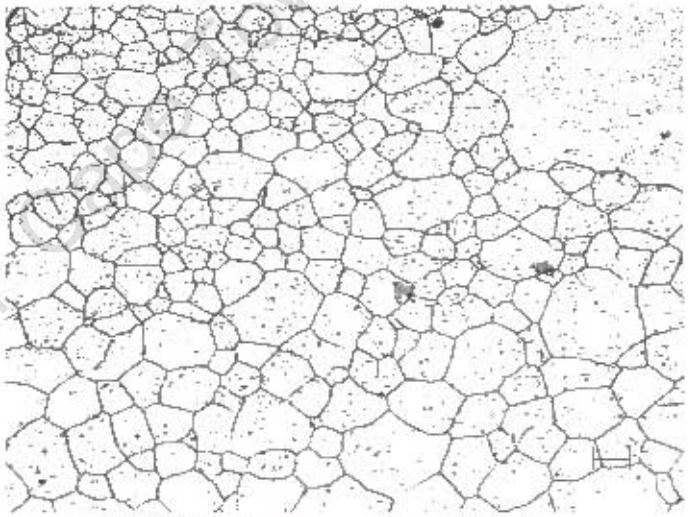

1050^{O}C (micron marker =100μ)

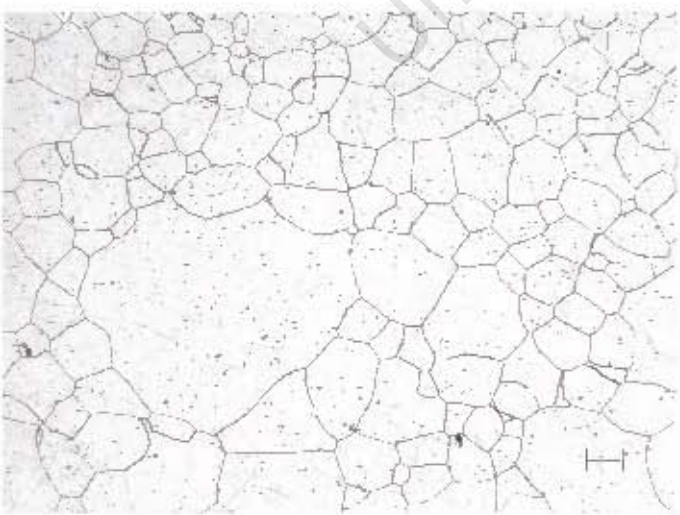

1100^{O}C (micron marker =100μ)

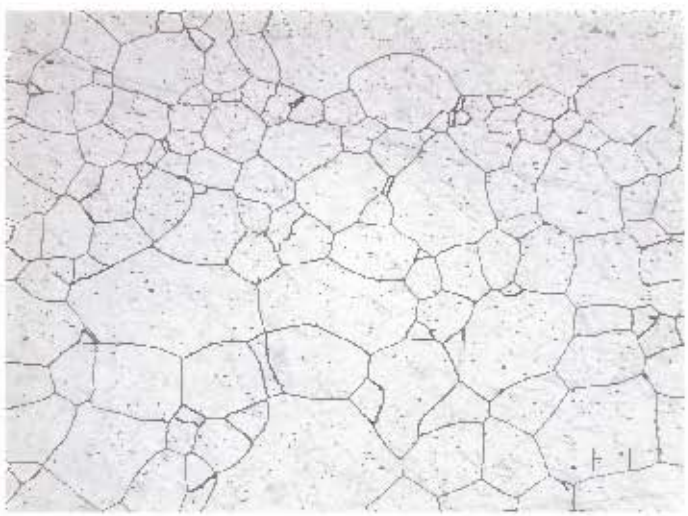

1150^{O}C (micron marker =100μ)

1200^{O}C (micron marker =100μ)

1250^{O}C(micron marker =100μ)